universität wien

MASTERARBEIT / MASTER'S THESIS

"Changes within the T-cell Receptor-CD3 Complex Quaternary Structure upon T-Cell Activation"

verfasst von / submitted by

Lisa-Maria Wurm, BSc.

angestrebter akademischer Grad / in partial fulfilment of the requirements for the degree of

Master of Science (MSc)

Wien, 2022/ Vienna, 2022

Studienkennzahl lt. Studienblatt / degree programme code as it appears on the student record sheet:	UA 066 834
Studienrichtung lt. Studienblatt / degree program as it appears on the student record sheet:	Masterstudium Molekulare Biologie
Betreut von / Supervisor:	Assoc.-Prof. Dr. Johannes Huppa

ABSTRACT

T-helper-cells are mediators of the adaptive immune response. They react to antigenic peptides that are presented to them via the Major Histocompatibility Complex (MHC) of an antigen-presenting cell (APC) in a highly sensitive and specific manner. All that while being able to tolerate “self”. Central to antigen recognition is the cells multisubunit T-cell antigen receptor (TCR)-complex. The signal, created by the TCR-complex in response to foreign antigens, modulates cellular immune response and is therefore a pivotal step in host defense. Still, mechanisms underlying TCR proximal signal transduction across the plasma membrane are yet to be determined.

This work provides evidence for intermolecular movement within the TCR-complex as a result of cognate peptide MHC binding. Extending the super-resolution microscopy method established by the lab of Johannes Huppa allowed me to temporally define the observed event as occupying the first seconds post antigen exposure and even prior to signaling protein recruitment to the complex.

We used small fluorophore conjugated single chain antibody fragment (scF_v) probes to site-specifically label the TCR subunits in a Förster Resonance Energy Transfer (FRET)-based assay. This way we were able to observe changes in inter- and intramolecular distances, when confronting live T-cells with a peptide-loaded MHC on a functionalized glass supported lipid bilayer acting as an APC surrogate. To synchronize MHC-TCR binding, we introduced a UV-cleavable caging entity to the system. This allows real-time monitoring of molecular dynamics within the target cell during TCR-MHC engagement.

To properly evaluate the findings and characterize the method used, parts of this work are devoted to uncouple the FRET signal from bystander effects as well as discussing limitations of the different imaging approaches I undertook throughout my work.

ZUSAMMENFASSUNG

T-Helfer-Zellen sind essentieller Bestandteil der adaptiven Immunantwort. Sie reagieren auf Peptidantigene die ihnen mittels Haupthistokompatibilitätskomplex (MHC) einer Antigen präsentierenden Zelle (APC) unterbreitet werden, auf hoch sensitive wie auch spezifische Art und Weise. All das während sie immernoch fähig sind Selbstantigene zu tolerieren. Eine zentrale Rolle in der Antigenerkennung spielt der aus mehreren Untereinheiten bestehende T-Zell Rezeptor (TCR)-Komplex. Das als Antwort auf Fremdantigen vom TCR-Komplex generierte Signal moduliert die zelluläre Immunantwort und gilt daher als Schlüsselpunkt in der Pathogenabwehr. Trotzdem sind die Mechanismen die der TCR proximalen Signaltransduktion durch die Plasmamembrane hindurch zugrunde liegen weitgehend ungeklärt. Diese Arbeit liefert Hinweise auf Intermolekülbewegung innerhalb des TCR-Komplexes, die aus der Konfrontation mit stimulierenden Peptiden im MHC hervorgehen. Durch Erweiterung der im Labor von Johannes Huppa etablierten Methode der Super Resolution Mikroskopie konnte ich das beobachtete Ereignis den ersten Sekunden nach Antigen-Konfrontation zuordnen und weiters der Rekrutierung sekundärer Botenstoffe voranstellen.

Um die Untereinheiten des TCR ortsspezifisch zu markieren, verwenden wir Antikörperfragment (scF_v) sondern im Zuge einer Förster- Resonanzenergietransfer (FRET) basierten Analyse. Damit könen wir inter- und intramolekulare Distanzänderungen beobachten, während lebenden T-Zellen peptidbeladene MHC Moleküle auf einer funktionalisierten glasgestützten Doppellipidschicht, welche als APC Surrogat fungiert, aussetzen. Um die TCR-MHC Bindung zu synchronisieren, erweitern wir das System mit einer Maskierungseinheit, welche durch ultraviolettes Licht abspaltbar ist. Wir können somit die molekularen Dynamiken innerhalb der Zielzelle in Echtzeit verfolgen, während TCR und MHC in Verbindung gehen.

Um diese Ergebnisse ausführlich zu evaluieren und die verwendeten Methode zu charakterisiert beziehen sich auch Teile dieser Arbeit darauf, das FRET Signal von ungewollten Nebeneffekten zu entkoppeln sowie die Limitierungen der unterschiedlichen Bildgebungsverfahren zu diskutieren.

Index

INTRODUCTION

The body's initial response to pathogens and harmed cells is the innate immune response. It is based on conserved pattern recognition and as aconsequence is very fast and effective but limited within its scope. Adaptive immunity, the second line of defense, consists of B- and T-lymphocytes as well as their products that complement their abilities. Adapdive immunity is able to react specifically, modulate inflammation and build memory based on the primary protein structure of an antigen. B-lymphocytes are able to secrete of a vast number of highly specific antibody molecules that interact with antigenic structures in order to flag them for destruction. T-cells on the other hand are responsible for modulating immune response as well as for extinction of infected or malignant somatic cells.

Adaptive Immunity

T-lymphocytes fulfill a central role in higher order vertebrate immunity, as they provide ways to adapt immune response to specifically target malignancies or pathogens. Whenever noxious or foreign agents encounter the innate immune system, the first line of defense, they become digested by phagocytic cells by which their peptide fragments are presented to T-cells in the context of a major histocompatibility complex (MHC) surface molecule. T-cells constantly scan their environment using their unique, clonotypic T-cell antigen receptors (TCRs) through which, when encountering a stimulatory antigen presented within the MHC (pMHC), they are activated. In this process, they efficiently distinguish between self and non-self in a highly sensitive way in order to respond appropriately. Activation leads to generation of memory T-cells, long-lived descendants of the responsive lymphocytes. Even though antigen recognition is a crucial step in immunity, the basis underlying antigen sensitivity and downstream signaling are not completely understood.

Because the TCR alone does not possess any signaling domains, it is non-covalently associated by the invariant subunits of the cluster of differentiation 3 (CD3) signaling complex. Consisting of a δε-, a δγ- and a ζζ-dimer, the CD3 subunits are responsible for the initiation of a kinase cascade at the cytoplasmic side of the membrane. This happens whenever the T-cell is presented with a stimulating peptide presented within the MHC of an APC. Upon productive pMHC-TCR interaction, Immunoreceptor tyrosine-based activation motives (ITAMs) of the CD3 subunits cytoplasmic domains are phosphorylated by associated kinases. This ultimately leads to the activation of the T-cell, expression of cytokines or the release of cytotoxic granules[1,2].

In the vast majority of T-cells, the TCR itself is comprised of an α and a β immunoglobulin (Ig) glycoprotein subunit. 1-2% of T-lymphocytes display the less variable γδ variant of this receptor. Those cells are primarily found in gut epithelial tissue where they recognize a small variety of non-peptide antigens. Of note, most of the γδ T-cells are lacking the CD3δ subunit. αβ T-cells, for reasons of clarity from here on referred to as T-cells, recognize peptide epitopes[2–4].

T-cells express a glycoprotein co-receptor that restricts antigen recognition to one of the two classes of MHC molecules. Conforming to this co-receptor, T-cells are divided into cluster of differentiation 4 or 8 positive ($CD4^+/CD8^+$) T-cells, that interact with MHC class II (MHC II) or MHC class I (MHC I) bound antigens

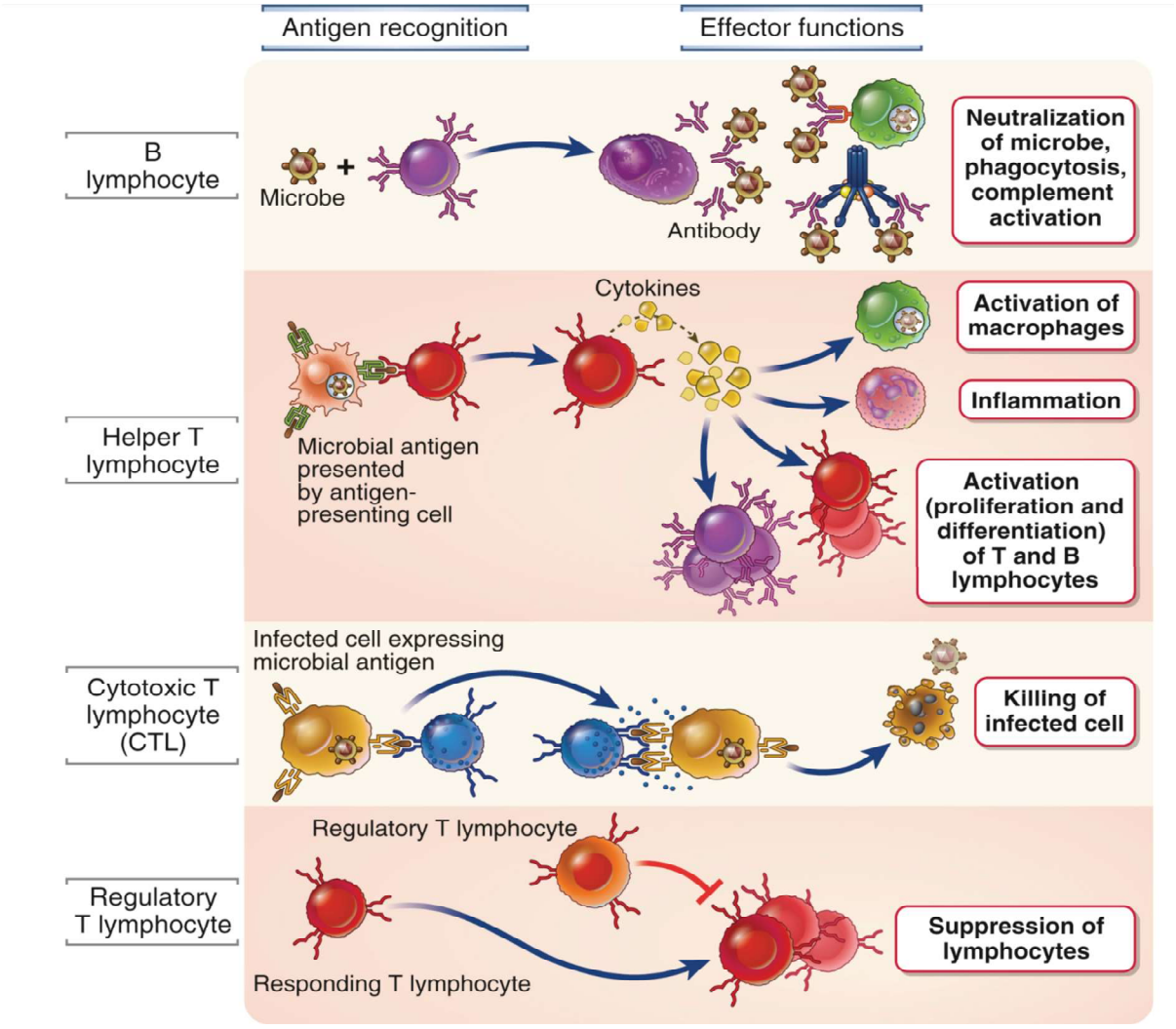

Figure 1

"B lymphocytes recognize many different types of antigens and develop into antibody-secreting cells. Helper T lymphocytes recognize antigens on the surfaces of antigen-presenting cells and secrete cytokines, which stimulate different mechanisms of immunity and inflammation. Cytotoxic T lymphocytes recognize antigens on infected cells and kill these cells. Regulatory T cells suppress immune responses (e.g., to self-antigens)." Source: Abbas, A. K., Lichtman, A. H., Pillai, S., Baker, D. L. & Baker, A. Cellular and molecular immunology. *(Elsevier, 2018); Figure 1.5*

respectively. All nucleated cells in the body are able to preset antigens via MHC I. The peptides displayed this way are 8-10 amino acids in length and have been predominantly synthesized within the cell. The MHC II complex on the other hand, is present on the surface of professional antigen presenting cells (APCs) such as macrophages, dendritic or B cells. APCs take up antigen from the cells surrounding environment and degrade them to longer fragments of about 15 to 24 amino acids in their endosomes[5,6]. This co-receptor linked mode of antigen presentation and recognition renders the cellular immune response dependent on the region of antigen encounter. An exception to this is cross presentation, where extracellular antigens are presented via MHCI to $CD8^+$ cells in the course of a viral and tumor immune response[3,7].

The MHC II molecule is composed of a non-covalently associated α- and β-chain and several isoforms of both chains exist in vertebrates. As the gene locus is expressed codominantly and hundreds of allotypes exist within several isotypes, the locus is thought to be the most polymorphic among the human population. Much like the TCR itself, each of the subunits displays a membrane-proximal Ig domain (α_2 and β_2) that anchors within the cell membrane, as well as a distal domain (α_1 and β_1) that creates a peptide binding groove [14]. During MHCII assembly in the endoplasmic reticulum (ER) the dimer is loaded with an invariant chain (Ii) which prevents binding of self-antigens and targets the complex to the late endosomal-lysosomal compartments. It is not until reaching an antigen-processing compartment with at a low pH of around 5.5, that the Ii peptide is cleaved by proteolysis to expose binding cleft for peptide uptake [6,8,9].

The MHC I molecule binding cleft is created only by its α- chain which is accompanied by a smaller, more conserved β-chain. Firstly, the MHC I molecule is expressed within the ER as an incomplete form consisting only of subunits α-1, -2 and -3, bound to Calnexin, until it fully assembles with subunit β-2. Still sheltered from interaction by chaperones, it is guided to its destination within the ER that is close to the transporter associated with antigen processing (TAP) channel of proteosome degraded foreign endogenous proteins where peptide loading takes place. Hereafter, peptide loaded MHC I travels to the cell membrane through the Golgi apparatus to present the endogenous epitope on the cell surface [6,10].

Without proper control, the actions of a machinery as powerful and specialized as the adaptive immune system can cause serious harm to its host. Fundamental processes like self-tolerance or spatial and temporal extent of inflammation are regulated thoroughly as they could otherwise lead to collateral damage of inflamed tissue or autoimmune diseases. These include diabetes mellitus type 1, chronic heart disease, chronic fatigues syndrome, multiple sclerosis, arthritis, to name only a few[11–13,14]. $CD4^+$ T-cells orchestrate the full complexity of the cellular immune response as their main role is to direct inflammation by producing cyto- and chemokines in order to guide leukocytes to the site of infection and enhance their

effector functions. Further, they interact with antigen specific B cells to drive their maturation and antibody production. These traits earned them the name CD4 $^{+}$ T-helper-cells. In contrast, CD8 $^{+}$ T-killer-cells administer targeted elimination of infected and degenerate cells and CD4 $^{+}$ Regulatory T-cells (Treg) function as inhibitors of adaptive immune response[15,16].

T-cell Development

T-cells originate in the bone marrow as a hematopoietic stem cell, but in their precursor state, they travel to the thymus for development. They each produce their very own TCR clonotype. Responsible for the great variability of the TCR repertoire, that is being estimated to contain about $1x10^{7-8}$ effective clonotypes present in each human individual[17] , is the unique somatic recombination of the TCRβ locus´s *variable (V), diversity (D)* and *joining (J)* gene segments and the TCRα locus´s *V* and *J* gene segments. These encode for the TCRs recognition domain and the rearrangement of the loci is exerted by the recombination-activating genes (RAG)-1/2 complex[2,18]. The TCRα and β subunits extracellular part is composed of a constant (C) and a variable (V) Ig domain, whereby only the V domains are subjected to somatic recombination.

Before T-cells are released to the periphery, the usefulness of their TCR is ensured by positive and negative thymic selection[19,20]. This process occurs for every progenitor T-cell. Initially cells do not to express either of the co-receptors and are therefore in their double negative stage when they enter the thymus. They then have to pass a checkpoint control of their recombined β subunit (β-selection). During following positive selection, T-cells express the complementing α chain from their rearranged α locus on the cell surface.

Allelic exclusion suppresses the unselected TCR α and β alleles so that only one species of each chain is displayed at the cell surface from this stage on[21].

The completed TCR is subsequently supposed to weakly bind a spectrum of specific self-peptides, presented exclusively by the cortical thymic epithelial cells (cTECs) in the context of an MHC molecule. The intensity of the signal generated this way is responsible for progenitor survival. Responders are given survival stimuli and non-responders, approximately 90%, die by neglect[22,23]. Following this stage, both co-receptors (CD4 and CD8, the double positive state) are present on the T-cells surface, however after a while, CD8 expression is lowered by default. Lineage commitment to one of the co-receptors is dependent on either MHCI or MHCII derived stimuli given by an APC. After lowering surface CD8, a continuous signal leads to suppression of CD8 and loss of signal to suppression of CD4 genes[24,25].

In the context of this thesis, we focus on CD4 $^{+}$ T-helper-cell fate, as all our experiments were conducted with CD4 $^{+}$ murine T-cells. The single positive progenitor thymocytes migrate further towards the medullar

cortical border where they are presented with a diverse selection of self-antigen displayed by the medullary cortical thymic epithelial cells (mTECs) to finally eliminate TCRs that interact too strongly with self-peptides in order to promote central tolerance. This process is called negative selection and requires the population of mTECs to express a diverse selection of peripheral self-transcripts[23]. This promiscuous gene transcription, restricted to mTECs, is facilitated by the transcription factor Autoimmune regulator (AIRE) aided by over 50 partner molecules[26]. As it is necessary to generate a repertoire of functional T-cells but at the same time to shield the body from ones that are self-reactive, only about 5% of the initial thymocyte population is left at the end of this procedure. Multiple models are proposed to explain how T-cells evade these strict controls in the case of autoimmunity[2].

Establishing tolerance for self is essential and other than excluding responsive T-cells, they can as well be taken advantage of. In the presence of certain stimulatory molecules such as transforming growth factor beta (TGF-β1) and interleukin (IL)-2, intermediate responders convert to regulatory T-cells[27] . Those are able to down-regulate inflammatory response whenever found related to self-antigen display (Figure 1).

Surprisingly, some features of the generated lymphocytes seem to be transient, as not only TCR and coreceptor expression but also T-cell sensitivity is altered in peripheral single positive T-cells. A variety of events, like reduced expression of voltage gates sodium channel (VGSC) or posttranscriptional downregulation of inhibitory phosphatases by the microRNA miR-181a are responsible for the conferred responsiveness to self-ligands[28–30]. In general, mature T-cells show less activation when encountering antigenic peptides than they did prior or during thymic selection[29,30].

Once T-cells are selected, they leave the thymus to peripheral secondary lymphoid organs where they circulate to encounter APCs. If these matured but naïve T-cells happen to be confronted with their nominal peptide, presented within the MHC, as well as a costimulatory molecule, they are primed. Depending on the presence of inflammatory cytokines like IL-2, IL-12 or tumor necrosis factor alpha (TNF-α), those, now antigen experienced T-cells differentiate into subsets of T-helper-cells with distinct effector functions[31]. These include macrophage activation, neutrophil recruitment or migrating into lymphoid follicles to guide B-cell isotype switching[16]. Apart from becoming effector T-cells, a small proportion of T-cells differentiate into memory T-cells which remain in an inactive state until re-encounter with their cognate antigen.

The Immunological Synapse

The communication of immune cells does not solely rely on TCR-pMHC interaction. T-cells rearrange their cytoskeleton to establish a platform for presentation and engagement of surface and signaling molecules

at the T-cell APC interface: the immunological synapse (IS). Within the IS, the two cell surfaces are facing each other, leaving a narrow cleft of 15 nm[32].

Starting out as small microclusters composed of 30 to 300 TCRs and coreceptors, T-cells soon establish a larger contact area with a defined architecture. In the course of a few minutes after engagement with its nominal pMHC, dispersed microclusters organize to gather in a central signaling area surrounded by a ring like adhesive domain composed of intercellular adhesion molecule 1 (ICAM-1) and lymphocyte function-associated antigen 1 (LFA1)[33]. This supramolecular activation cluster (SMAC) contains receptor and adhesion molecules, as well various co-receptors and phosphatases or kinases involved in signaling. When fully established after several minutes, the SMAC displays a bullseye-like pattern with a central (cSMAC), peripheral (pSMAC) and distal (dSMAC) area, all characterized by their specific set of surface and signaling molecules[34,35].

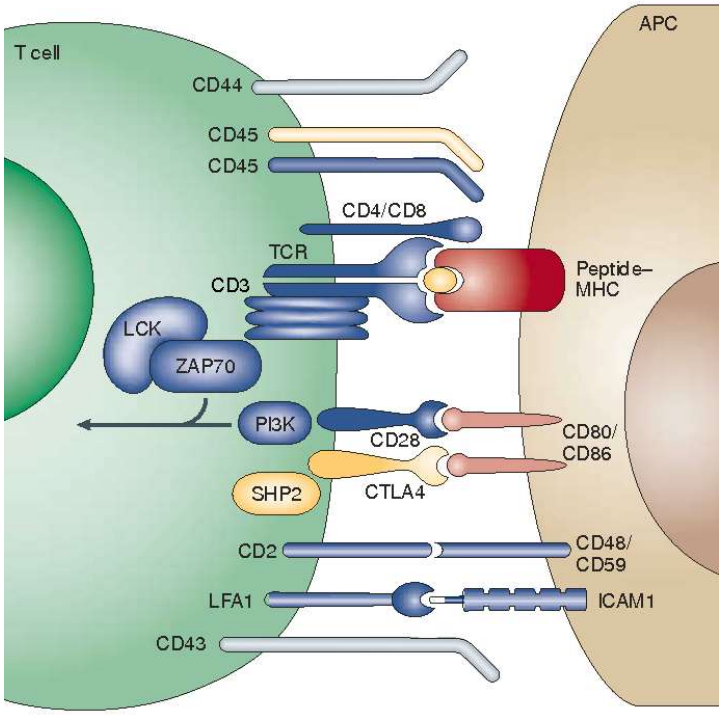

Figure 2

"Overview of a mature T-cell synapse. a | A profile view showing a selection of the key ligand pairs and signalling molecules that are involved in T-cell recognition. The stimulatory peptide–MHC molecule is shown in red, activating/co-stimulatory molecules are blue, inhibitory molecules are yellow and molecules that are not contributing to signalling are grey. The arrow indicates converging signals that lead to T-cell activation)." Source: J. Huppa, Mark M. Davis; T-cell-antigen recognition and the immunological synapse; Nature Reviews Immunology (2003), Figure 1a

Smaller molecules like TCR-CD3, coreceptor, protein kinase C- θ (PKC-θ) and costimulatory CD28, group in the central region, surrounded by integrin LFA-1 and talin enriched pSMAC, whereas molecules with the biggest extracellular domains, such as the collagen binding CD44 and the phosphatase CD45 reside in the outermost region.

Several molecules are already associated with the TCR-CD3 complex at the level of microclusters, including pivotal scaffolding and signaling molecule linker for activation of T-cells (LAT) as well as ζ-chain associated kinase of 70kDA (ZAP70) [33]. Generic activation signs such as increase of intracellular calcium levels and ζ-chain phosphorylation can be observed at this early stage.

Nonetheless, accessory kinases appear to be internalized before even reaching the cSMAC and most of the CD3 ITAMs within the cSMAC seem to be unphosphorylated. This could indicate an inhibitory function of the cSMAC, or simply relate to the fact that TCRs are internalized and recycled quite fast in this area[36]. After 3-6 minutes post stimulation, TCRs concentrate in a cytoplasmic region beneath the IS to be internalized for recycling after 7 minutes[37]. Alongside that, TCRs are released in microvesicles to be taken up by B-cells[38].

Costimulators and Adhesion Molecules

Importantly two simultaneous stimuli have to be given to result in full activation, proliferation and differentiation of a naïve T-cell. Other than the distinct interaction with the antigenic peptide presented by the MHC, a costimulatory molecule, such as CD28, must engage with the APC. The CD28 receptor is constitutively expressed on naïve T-cells and binds to B7, describing the two structurally similar isoforms of the glycoproteins B7-1 and B7-2 that are upregulated in macrophages, DCs or B-cells as a result of pathogen associated molecular pattern recognizing receptors (PAMPR) stimulation or danger signals. This ensures T-cell response only takes place in the presence of infection. Consequently, the activating PI3-kinase is recruited to the cytoplasmic tail of CD28 to trigger calcium signaling and pro-survival downstream pathways for example expression of the anti-apoptotic proteins Bcl-2 and Bcl-X_L[39].Because antigens presented in the absence of this second signal are usually self-antigens, responding T-cells are forced into anergy. In this state, they are no longer able to exert effector functions and thus grant peripheral tolerance to self-antigen. Costimulation also allows for a negative feedback loop, as the positive stimulus of CD28 can be titered out with the inhibitory cytotoxic T-lymphocyte-associated protein 4 (CTLA-4) receptor that binds to the same target i.e., B7-1 or B7-2, yet with a higher affinity. CTLA-4 is expressed in order to suppress T-cell activation post APC stimulation.

The co-receptor CD4 was found to display low affinity to its binding partner, MHCII [40] and not directly be involved in establishing the IS but more so in recruitment of adaptor proteins such as Lck to the engaged complex. CD4 blockage did not affect pMHC TCR affinity but attenuated T-cell signaling[41,42], resulting in a 10-50-fold reduction in T-cell sensitivity to antigen [43].

Signaling Cascade

The cytoplasmic tails of the CD3ε, CD3δ and CD3γ each contain one, those of the ζ chains even three immunoreceptor tyrosine-based activation motifs (ITAMs), which results in a total of 10 ITAMs that can

be the target of tyrosine-phosphorylation[44]. The TCRs ligand-binding units themselves do not possess intrinsic catalytic activity and signaling is initiated by separate intracellular non-receptor tyrosine kinases. Upon stimulatory epitope engagement, the ITAMs of the CD3 signaling complex are phosphorylated by the tyrosine kinase Fyn and the lymphocyte-specific protein kinase (Lck). LCK is introduced to the site of activation already associated to the cytoplasmic tails of the coreceptor CD4/8[45–47].

The biphosphorylated ITAMs allow the cytoplasmic protein tyrosine kinase ZAP70 to bind CD3 with their SH2-Domains thereby being activated through the action of nearby Lck. ZAP70 in turn phosphorylates the transmembrane adapter protein linker of activation (LAT) and other substrates, such as 76 kDa SLP76 and PLCγ at multiple tyrosine residues. This creates docking sites for SH2 domains of multiple downstream effectors that are responsible for initiation and maintenance of signaling pathways. The two key players Lck and ZAP70 provide different tyrosine residues for a regulatory feedback mechanisms to take place due to their potential to promote the generation of active and inactive conformations[30,47].

Three major pathways are induced by this so-termed signalosome: The Calcium -calcineurin-, the mitogen-activated protein kinase (MAPK) and the nuclear factor kB (NF-kB) pathway. All of them result in the translocation of critical transcription factors such as the nuclear factor of activated T-cells (NFAT), AP-1 and NFkB to the nucleus for gene expression[48].Ultimately T-cell activation leads to actin polymerization, proliferation, upregulation of transmembrane receptors and, depending on the $CD4^+$ subset, cytokine production.

One early effect of activation is the release of calcium ions (Ca^{2+}) from the endoplasmic reticulum (ER) into the cytoplasm as a result of Phosphoinositol (4,5) bisphosphate (PIP_2) hydrolysis by phospholipase C γ (PLCγ). When activated, PLCγ creates the second messenger Inositol (1,4,5) triphosphate (IP_3) from hydrolysis of PIP_2. IP_3 binds to its receptor on a ligand-gated Ca^{2+}-channel on the ER[33,49]. This increase in intracellular Ca^{2+} can be visualized by a calcium-sensitive, cell-permeable, fluorescent ion-indicator such as Fluo-4, Fura-2 or others [50].

Structure of the T-cell antigen receptor

The TCR-CD3 complex is composed of eight transmembrane polypeptides. One αβ heterodimeric TCR is non-covalently associated with its CD3 signaling complex consisting of a CD3εδ, a CD3εγ as well as a CD3ζζ dimer[51]. Within the TCR heterodimer, α and β subunits associate via conserved interchain disulfide bonds [16,52] . Each subunit is made up by two extracellular domains (ECD) which are, via a long linker (~20 residues, 22 for α, 16 for β) that contains the disulfide bridge, connected to the transmembrane domain (TMD) and

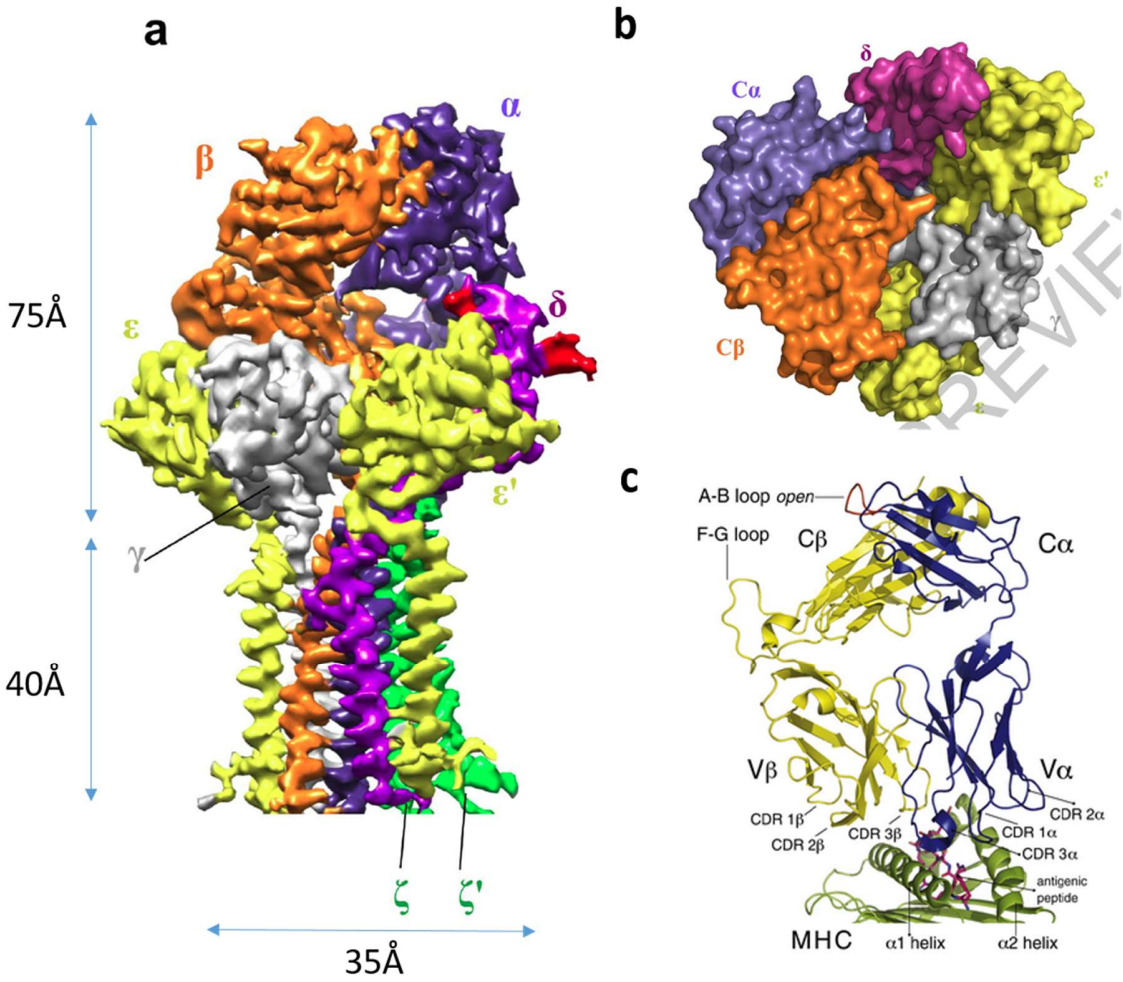

Figure 3

Structural rendering of the human TCR-CD3 complex ***a.*** *"Side view of the cryo-EM map of the human TCR-CD3 complex. Color codes for the subunits of the complex are indicated."* ***b.*** *"Top view of the ECDs of the TCR-CD3 complex shown in (…) surface representation (right). TCR Vα and Vϐ domains are not shown."* *Source: Dong, D. et al. Structural basis of assembly of the human TCR–CD3 complex. Nature; Accelerated Article Preview Published online 28 August 2019.*

c. *"Molecular Model of the αϐ T-cell antigen receptor. The ''open'' conformation of LC13 TCR in complex with HLA-B8 (PDB accession code 1MI5) (Kjer-Nielsen et al., 2002b). The MHC molecule is represented as a cartoon and colored green. The antigenic peptide is shown in stick format with the carbon atoms colored magenta. The heterodimeric TCR is colored by chain with the a chain represented in blue and the b chain in yellow. The variable and constant domains within each chain are labeled Va,Vb and Ca,Cb, respectively. The positions of the CDR loops and the F-G loop are indicated. The position of the A-B loop is indicated and highlighted in red. In this ''open'' conformation, the A-B loop projects away from the Cb domain."* *Source: Structure of the TCR Antigen Ligation Trlggers a Conformational Change within the Constant Domain of the αϐ T-cell antigen receptor; Beddoe, Travis et al.; Immunity , Volume 30 , Issue 6 , 777 – 788 (2009).*

a very short intracellular domain[53]. The ECDs consist of a variable (Vα and Vβ) and a constant domain (Cα and Cβ) respectively (, c). The VβCβ domains are connected by the prominent FG-loop[54,55], extending laterally from the TCR . All domains are part of the Ig superfamily and except Cα do adopt Ig typical folding. The site of antigen binding is a composite of both, the Vα/Vβ most distal part, which each contain three regions of hypervariability. Those complementary determining regions (CDRs) are promoting precision in

antigen recognition as CDR3α and CDR3β loops are located at the central part of the recognition site whereas CDR1 α connects to the amino-terminal and CDR1 β to the carboxyterminal ends of the antigenic peptide within the MHC (, c). Interestingly only CDR3 undergoes *V(D)J* somatic recombination as it is the product of the randomly assembled *variable (V) diversity (D*, only in the case of CDR3 β) and *joining (J)* gene segments[17] . The CDR3s were shown to be highly dynamic and according to the induced fit model of peptide recognition, binding to its nominal ligand could lead to a stabilizing mechanism[56,57]. CDR1 and CDR2 loops are germline-encoded and contact the MHC itself [1–4]. This way, they determine a certain diagonal docking geometry, which has been intensively studied to understand binding restriction towards one of the MHC classes [2,58,59].

As fusion protein studies discarded a side-by-side model of CD3δ and γ, but indicated close proximity of the two CD3ε domains[60], subunits were proposed to arrange in an asymmetric, one-way-facing model, leaving CD3εγ CD3εδ on one side and the ζ chains the other side of the TCR[61]. Further NMR studies challenged this view by identifying sites of interactions on either side of the αβ TCR ECD[57] therefore suggesting the CD3 heterodimers to assemble on opposite sides of the αβ TCR.

Since interactions of the receptors ECD with its CD3 signaling domains were found to be quite weak [57,62], recent studies focused on the TMD and showed that TCRαβ displayed highly conserved positively charged residues that connect the heterodimers in the already proposed stoichiometry. Here TM domains were stated to interact in an eight TM bundle, rendering all of the subunits within a radius of ~30 Å[63]. Each of the CD3εγ and CD3εδ subunits TM domains contain helix stretches by which they assemble to form the multimeric TCR-CD3 complex[64,65]. Within the plasma membrane, TCRα partners with CD3εδ as well as CD3ζζ and TCRβ associates with CD3εγ.

Structural data from cryo-EM (cryo-electron microscopy) could confirm those findings, but show the ECM domains of the TCR CD3 complex arranging in a triangular, tightly packed shape. Here, the CD3 dimers are all gathered on one side of the αβ TCR as they are aligning clockwise in the order CD3δ CD3ε CD3ε CD3γ (, a, b) [52]. As previously suggested, the CD3 ECDs are positioned slightly underneath rather than alongside the ECDs of the TCRαβ subunits[5,51,57].

The TCRα constant region associates with CD3εδ and TCR Cβ with CD3εγ. In more detail, molecular interactions have been identified between the DE loop of TCR Cα and CD3εδ as well as between the TCRβ FG-loop, its helix3 and helix 4-F region and CD3εγ [52,66]. TCRβ was even thought to interact with both of the CD3 heterodimers[67], but follow up NMR experiments could not confirm these findings[57].

In accordance with this, mutations in the Cα DE loop destabilizes the TCR-CD3 complex. Yet, unlike Cα C- or F-strand mutations, they do not impair IS formation[60].

Furthermore, there is evidence that CD3εγ assembly is somehow dependent on the presence of CD3εδ as interaction with the ECD of the TCR was only observed in mutual addition of both heterodimers[51,61,62].

Movement and Forces

In close relation to TCR-CD3 junctions, evidence for movement upon activation has been found for several parts of the αβ TCR heterodimer[57,67–69]. NMR shift perturbation analysis suggested a dynamic change in the H3 and H4 helices proximal to the cell membrane of the Cβ constant region, where the highly conserved residues involved, have also been proposed to interact with CD3εγ as previously stated[57]. Likewise, the CD3ζ chains have been under investigation regarding conformational change and were considered to act as an energetic switch region that diverges upon antigen recognition[70].

Newer findings revealed a highly dynamic hinge region of the TCRα transmembrane helix by NMR. That led to the assumption that the bipartite TM domain undergoes movement upon pMHC encounter that straightens the L-shaped membrane-aligned to a more membrane buried conformation, therefore pushing the TM helix associated ζ chains further away. This switch is thought to be force-induced and could be the first hint of how actual transmembrane signal transduction takes place[71].

The relay mechanism proposed features an active and an inactive state of the TCR-CD3 complex, where, in the inactive form, interactions might be sparse and cytoplasmic tails of the CD3 subunits associate lateral to the inner membrane leaflet as FRET experiments using a transgenic labeled CD3ζ chain indicated[72,73]. CD3ε and ζ are thought to reside on the inner leaflet of the membrane due to their stretch of basic residues that are able to participate in electrostatic interactions with the cytoplasmic membrane[65,71].

Our special interest concerns the function and structure of the Cβ FG-loop (Cβ G216-R227), as it was shown to be crucial not only to stabilize the rigid β unit of the dimer [74,75] but also to contribute to bond lifetime [75] and even facilitates negative selection in mammal T-cell development[76].

Presenting as a candidate for only moderate interaction in NMR analysis, the FG-loop displayed major movement upon applying forces with the use of optical tweezers [55,75]. Those experiments showed that lifetime of the pMHC-TCR bond is stabilized by the loop and even suggests an 8-15nm conformational transition linked to its existence[75]. Because of its geometry it is thought that the Cβ FG-loop close to the CD3ε of the CD3εγ heterodimer, acts as a lever converting mechanical energy into a biochemical signal[55]. Furthermore, the geometry of the complex and direction of the applied force were shown to be of importance since the activating agent had to be „pushed“ in a diagonal rather than perpendicular way. However, recent cryo-EM analysis of the ECM could not detect major conformational changes within the

TCRαβ ECDs when comparing the structures of free versus pMHC engaged receptors[52]. Rearrangement of the subunits or short-lived transient states could not be excluded in this study.

On the other side of the membrane, intracellular domains of the CD3ε units are thought to undergo reversible conformational change in conjunction with ligand binding which results in the display of a proline rich sequence (PRS) domain in each of the subunits. Recruitment of the adapter protein NCK to this PRS is observed during T-cell activation [77,78] and an intracellular switch detected connected to its existence might regulate TCR expression and promote CD3ζ phosphorylation[79]. This switch could be regulated by the cholesterol environment of the TCR itself[77,80,81].

Kinetic measurements using an optical force clamp assay that allows for only two dimensions of freedom in order to reflect *in situ* constraints of the IS were conducted by Cheng Zhu et.al. and showed catch-bond like kinetical hallmarks, namely that mechanical force acted out on the productive pMHC-TCR bond, amplified its lifetime[82] whereas antagonist peptide did not show this behavior[82,83]. This phenomenon could be detected in adhesion molecules like p-selectin[84] hence whenever interactions have to take place in increased velocity medium.

Higher Order Structures

Higher order TCR structures, conglomerates or even multimers of TCRs upon stimulation have been repeatedly been in focus of attention and is still being discussed [20,61,85]

Monovalent soluble agents binding the TCR were not able to induce T-cell activation, whereas multivalent antibodies against CD3 as well as tetrameric pMHC and membrane associated pMHC were[81]. From this finding, two opposing mechanistic models can be constructed. One being that signaling only occurs when TCRs are clustered by a multimeric ligand, or two, that the force acted out onto the receptor by a rigid binding partner is responsible for T-cell activation.

There is evidence for the existence of higher order or dimeric arrangement derived from electron microscopy of immunogold-labeled T-cell surfaces and small-angle X-ray scattering [5,86] but recent single molecule FRET studies render it more likely that monomeric TCRs drive antigen recognition. Outcomes of latter experiments used FRET bases live-cell microscopy and even indicated that MHC molecules were further separated when engaged with microclustered TCRs[20]. Still, microdomains seem to exist [36,41,87,88] and are arguable in their cooperative behavior[41,89,90].

Kinetics of TCR-pMHC Interactions

When using surface plasmon resonance (SPR) to determine TCR and pMHC affinities, both molecules are free rotate in all directions. Affinities measured by this method can therefore be described as three dimensional (3D). Those, with a K_d of around 1-100 µM, are remarkably low between TCR and cognate pMHC [18,41,83]. Even though TCRs display a higher affinity and a faster off-rate for stimulating peptides in contrast to non-stimulating ones, the line to distinguish nominal and irrelevant peptide kinetics is blurry and thresholds differ greatly between $CD4^+$ and $CD8^+$ cells[18,41,83].

Analyzing TCR-pMHC binding kinetics using live T-cells that interact with pMHC on a lipid bilayer restricts the movement of the interaction partners to two dimensions (2D) to simulate an *in vivo* scenario. Single molecule tracking experiments on a functionalized bilayer showed an intermediate interaction duration ($t_{1/2}$) of 1.68s at room temperature (RT) and as little as 100ms at 37°C for the 5C.C7 TCR recognizing I-E^k/MCC[41]. When identifying the binding kinetics between the interaction partners with FRET, both association and dissociation were highly accelerated using bilayer-associated ligands (2D) as compared to soluble ones (3D).The dissociation constants were found to be up to 100-fold increased with destabilizing forces presumed to reside in the actin cytoskeleton[41]. However, because single molecule FRET is highly sensitive in term of the spacial arrangement of the FRET partners, small intramolecular movements result in a change of signal that could be misinterpreted for unbdinging events. Data obtained in similar setups led to conflicting results. For the same TCR bound to its ligand, the lifetime of binding, tau_{off}, was calculated to be 7,2s in single molecule tracking experiments [91]. Here on the other hand a detection window of > 500ms and indirect measurement of binding does not allow for exact assumptions and cannot exclude fast multiple engagement of TCR and pMHC as this would result in overestimation of dwell time.

The majority of measured bond lifetimes show strong negative dependence on temperature and positive dependence on interaction motif. Mutation of one single amino acid in a weak 5C.C7 TCR agonist, MCC (T102S), for example shortened the interation duration by half [1,2,92].

Additionally forces play a role in bond-lifetime. Optical tweezers together with a DNA tether spacer allows to apply force onto the TCR-MHC binding. The intermediate interaction duration of 4.3s was evaluated and showed catch-bond criteria. Introduction of the antigen-binding fragment (Fab) H57 that binds the TCRβ led to a major stabilizing effect that resulted in a 10-fold elongated timespan until bond rupture[75]. Nevertheless, the extent of T-cell activation is not only correlated to affinity and fast k_{on} rates. On the contrary, when testing selected agonist peptides gained from a yeast library, affinity poorly corresponded to activation levels[93]. In general, the immunoglobulin domain receptor displayed only about a fourth of

the binding affinity of an antibody. Other than that, sustained or serial interactions play an important role for proximal and distal signaling outcome [18,41] as cytokine release was only detected after several hours of sustained APC-T-cell interaction [94]

Taken together, we can state, that the existence of stimulatory potent monomeric TCR-CD3 complex seems to be still in question and that pMHC TCR kinetics cannot yet describe the high degree of specificity displayed by T-lymphocytes. Defining the orientation of the binding partners could be responsible for permitting mechanotransduction and conformational change or structural reorientation of the complex upon activation. Despite of that, the geometry of the immunological synapse acts as a signaling tuning machinery itself as it defines the spatial arrangement of the participating key players. For example, by excluding phosphatases from the pSMAC and recruiting Lck as a first messenger.

Total Internal Reflection Microscopy

The response of an optical imaging system to a detected signal is called its point spread function and the minimum distance between two separate signals of the specimen is defined as the systems resolution (R). R is physically limited by the Abbe diffraction limit and described by

$$R = \lambda / 2n(\sin(\theta))$$

Figure 4
Total internal reflection seen as the black area surrounding the Snell´s window (with crocodile) as observed from under water credit: Luis Javier Sandoval /Nikon D7000 / Tulum, Riviera Maya, Mexico/ Instagram: @luisjaviersandoval

where R is resolution the separation distance, λ is the illumination wavelength, and n(sin(θ) the numerical aperture of an objective with n= medium refractive index and θ = one-half of the objective angular aperture. Achieving this resolution with a light microscope is challenged by aberrations of the microscope. A Factor that greatly influences the quality of an image acquired from a live cell sample is the scattered light and fluorescence emitted from out of-focus areas of the sample sine they contribute to a low signal to noise ratio [95]. To minimize the excitation of fluorescent entities that are out of the focus plane, one can take advantage of Total Internal Reflection (TIR)[96]. This reflection of a light beam occurs, when light hits the surface of a medium with a

different refractive index (n) than the one it has been traveling in, in an angle that is ≥ the critical angle θ_c. Whereas all angles smaller than θ_c lead to refraction, every angle beyond θ_c will result in reflection. This can occur when light from inside a body of water (n=1.33) hits the air surface (n=1) to be reflected back into the water, as well as to a laser beam traveling through a glass coverslip (n=1.52), hitting the surface of a liquid sample (n=1.33) to be reflected back into the coverslip. If the angle of incidence is greater than the critical angle, light rays undergo total internal reflection as described by Snell's law:

$$\theta_c = \sin^{-1}(n_1/n_2)$$

n1 and n2 are the refractive indices of the media in between which refraction and reflection occurs[97]. θ_c is the critical angle off the surface normal for the incident wave = angle of incidence.

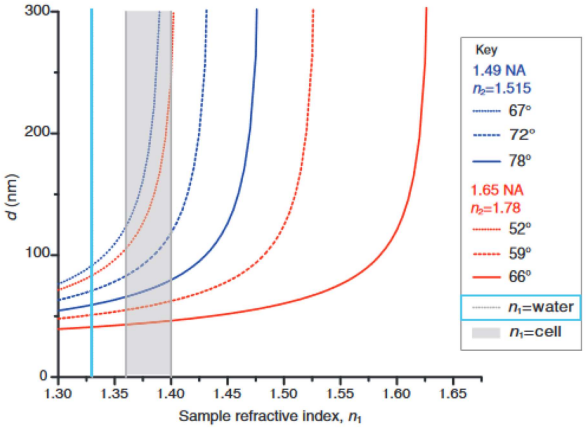

Figure 5

"The depth of the evanescent field depends on the refractive index of the sample. The depth of the evanescent field (d) is a function of the index of refraction of the sample (n_1). Incidence angles were chosen as 1.5 ° less than the maximum incidence angle (solid lines). As the angle of incidence is increased, the sensitivity of d to the sample refractive index decreases in the range for cells. The 1.65 NA objective has a larger range with lower sensitivity to sample refractive indices than the 1.49 NA objective." n_1 of water as in our case indicated in light blue, adapted from Source: Mattheyses, A. L., Simon, S. M. & Rappoport, J. Z. *Imaging with total internal reflection fluorescence microscopy for the cell biologist.* J. Cell Sci. ***123***, *3621–3628 (2010).*

The critical angle needed for TIRF illumination also acts as a bottleneck in instrumental setup. There are two common solutions to this. A prism based TIRF arrangement or an objective TIRM design. In our lab, we use the latter. In order to achieve an incident angle of the laser beam, great enough to be totally reflected upon hitting the same interface, an objective lens with a great numerical aperture (NA) is needed. This also is an advantage in emission detection, considering the widespread emission pattern of a fluorophore that could be missed using a smaller lens. At the same time, a high NA also bares the risk of illuminating light sources to scatter inside of the objective, which can contribute to an increase of illumination depth[98] . In order to obtain a collimated laser beam that emerges from the objective lens in a steep angle to hit the sample plain in TIR, it must pass the back focal plane of the objective focused, but radially translocated off the axis[98–100].

The energy that is exciting the fluorophore within the sample is transmitted orthogonally to the interphase in a wave. This evanescent field decays exponentially with penetration depth. The magnitude of the incidence angle here is inversely proportional to the depth of the evanescent field. For a nominal TIRF

angle of 66° the evanescent field on a glass and water interface, depth of the evanescent field lies slightly underneath 100nm[97,101]. New TIRF objectives with numerical aperture of 1.65 allows for angles that result in field depths as narrow as 50nm but need the use of special immersion oil and flint glass slides. Super-resolution techniques like stochastic optical reconstruction microscopy (STORM), photoactivation localization microscopy (PALM) or structured illumination microscopy (SIM) are able to bypass diffraction-limited detection by reconstructing an image from sparse, far spread signals and reach lateral resolution of some ten nanometers. Still, they all rely on the acquisition of a multitude of hundreds of images which mostly requires fixed samples and is not well suited for live cell imaging, although there are novel approaches to solve that problem [102–104].

Förster Resonance Energy Transfer

Förster Resonance Energy Transfer (FRET) takes place when an excited donor chromophore nonradiatively transfers energy to a close proximity acceptor chromophore. This can only occur when the emission spectrum of the lower wavelength donor fluorophore overlaps with the excitation spectrum of the higher wavelength acceptor. When excited, the donor transfers a certain amount of energy to the acceptor by dipole-dipole coupling. This does not only quench its own emission but also causes the acceptor to emit in its own wavelength. The efficiency (*E*) of this phenomenon is extremely sensitive to distance, namely inversely proportional to its sixth power, resulting in a very accurate tool to optically measure distance in the nm range[105]. The effective area of FRET differs between FRET pairs and is described as the Förster radius R_0, the distance where half of the input energy is transferred via FRET (Figure 6). It can be calculated as follows:

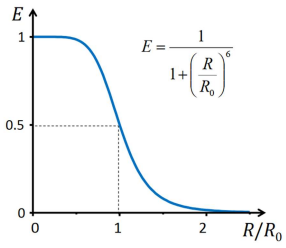

Figure 6
Förster resonance energy transfer efficiency as a function of the Förster radius (R_0) to radius (R) ratio between the FRET pair

$$R_0^6 = 8.8 \times 10^{23}\ \kappa^2\ n^{-4}\ QYD_0\ J$$

with κ being the orientation factor of the fluorophores, n being the refractive index of the medium and QYD_0 the donor quantum efficiency (www.thermofisher.com).

FRET efficiency (*E*) is defined as

$$E = \frac{k\mathrm{ET}}{\sum k},$$

where k_{ET} is the energy transfer rate and $\sum k'$ the sum of all depletion rates of donor-excited stage. Discrete FRET efficiency for a single donor acceptor pair can only be measured passively by single-molecule donor recovery after acceptor photobleaching (DRAAPB) or time-correlated single-photon counting (TCSPC). Bulk, or apparent FRET obtained from DRAAPB therefore resembles the average FRET state of all participating molecules in an ensemble[106]. Indirect measurements of FRET via sensitized emission (SEm) calculates a FRET index from donor emission resulting from donor excitation. This value must be carefully corrected for crosstalk within the fluorophores such as donor bleed through and acceptor cross excitation. Chromatic aberrations within the microscope that interfere with in-focus detection of more than one fluorophore simultaneously can be corrected for by using an apochromatic lens system.

MATERIALS AND METHODS

Experimental Setup

FRET analysis to understand live T-cell dynamics cannot be carried out on live cells in solution as the movement of the floating cells would complicate in-focus acquisition. The use of a planar lipid bilayer a surrogate for the APC restricts the formation of the synapse to one plane. This has several advantages:

1) The synaptic environment during T-cell stimulation can be reconstituted in a quantitative fashion.
2) TIRF microscopy can be performed as the nascent immunological synapse is formed right at the glass slide that serves as the interface for total internal reflection.
3) Low intensity signals obtained from single molecule fluorophores that lie beyond light microscopy diffraction limit can be acquired.

The method is minimally invasive, as it does not require any kind of fixation or lysis. TIRF microscopy enables us to not only dramatically reduce background fluorescence due to the shallow penetration depth of laser illumination but also to image live cells throughout a certain time without seriously damaging the cell because of radiation. Combining TIRFM with the highly sensitive FRET, dynamic information can be obtained from two specifically labeled sites in real time.

By using a glass supported lipid bilayer (SLB) as a surrogate for the APC, the 3D receptor-ligand encounter is restricted to a 2D interaction site at the SLB surface. We can therefore reduce the dimensions of the problem and bring the IS as close as possible to the refracting area. Because of the differences in refractive indices between the different wavelength lasers (Chromatic aberration due to dispersion), slight abbreviations of the critical incidence angle occur and in theory emission of both ends of the spectrum could never be detected in focus at the same time, on the same z-plane. As our experiments require simultaneous imaging of multiple wavelength fluorophores, we use a three-color apochromatic lens to correct for this phenomenon.

To study the relative movements of the TCR subunits in situ, we labeled murine T-cell blasts with fluorescent probes consisting of a fluorophore, covalently linked to an antibody single chain fragment (scFv) with a known epitope. An antibody single chain fragment is a truncated, monovalent version of an antibody. The constant (Fc) region of the IgG heavy and light chain is missing and only the two variable regions remain, interconnected with an artificial linker. The scFvs size is thus reduced to approximately 25kDa, 6-fold smaller than a 150kDa IgG, still displaying a full antigen-binding region. This decreased size

and monovalent binding cleft is crucial for studying live cell interactions since bivalent probes would trigger T-cell response and bigger molecules could interfere with receptor recognition. Lacking free cysteine residues, single amino acids like Serine can be mutated to a cysteine for site-specific labeling with maleimide dyes to maintain stoichiometry in FRET assays. ScFvs were expressed from pET21 in Escherichia coli (E. coli) BL21 (DE3). Lacking cell compartments that are needed to provide the chemical environment for proper folding, those proteins remain completely denatured and water insoluble in the form of inclusion bodies (IB). They can be isolated from cell lysates by vigorous vortexing and application of mild detergents and enzymes like DNase and repeated centrifugation. Refolding in oxidizing conditions allows disulfide bonds to establishing between thiol groups of the proteins. The single chain fragments of H57 and KT3 are derived from the monoclonal antibody (mAb) H57-597 and mAb KT3-1-1 respectively. H57-scFv attaches to the TCRβs C regionFG-loop[107–109], whereas KT3-scFv is directed to the CD3ε and suggested to have more affinity towards the γ-associated subunit[110]. Both scFvs were shown not to interfere with pMHC binding [20] when bound to the receptor. Single mononucleotide substitutions have been introduced to H57-scFv and KT3-scFv, in order to generate different mutants for site-specific labeling using maleimide conjugated fluorophores.

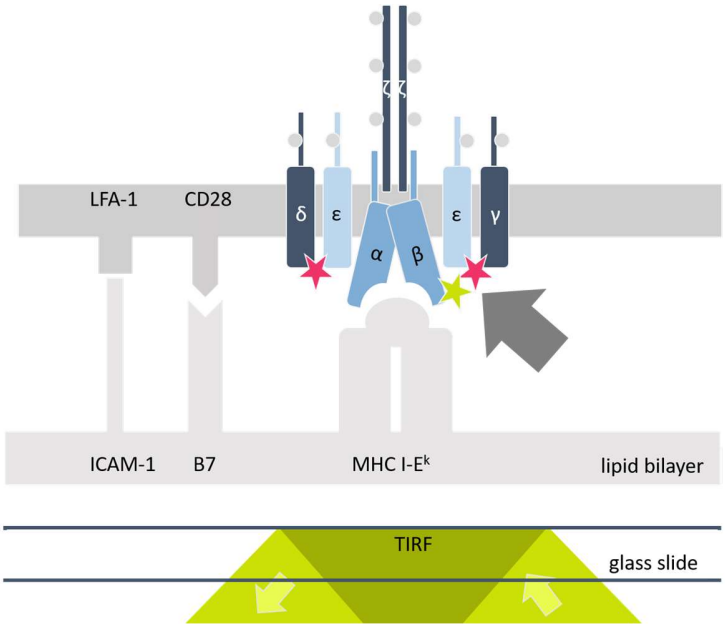

Figure 7
Illustration of a TCR-CD3 complex on a T-cell membrane (top) facing the stimulatory lipid bilayer platform. Laser TIR illumination is applied onto the sample with an inverted microscope. Donor fluorophore AF555 conjugated to H57-scF$_v$ and acceptor fluorophores AF647 conjugated to KT3-scF$_v$ indicated with stars of respective color

Imaging Techniques

Two approaches to evaluate the efficiency of energy transfer between the FRET partners were undertaken; Donor Recovery after Acceptor Photobleaching and Sensitized Emission Imaging.

I used the FRET pair Alexa Fluor (AF) 555 and AF647. According to structural data obtained by crystallography and computational modelling, the Förster radius (R_0) of 51Å is sufficient to cover the

distance between the TCRβ and CD3ε which we probed in order to study movement within the receptor[20,50,63] In all conducted experiments AF555 linked to H57-scF$_v$ acts as the FRET donor, whereas AF647 linked to KT3-scF$_v$ binding both of the CD3ε subunits is situated within R_0 range to act as the FRET acceptor. Apparent FRET values obtained by this method can be correlated to movements taking place within the complex. However, a second FRET-probe like H57- scF$_v$ binding to a single target, such as KJ25-scF$_v$ binding TCR Vβ, must be introduced to be able to measure quantitative FRET values that can be directly translated into nanometers.

We challenged live, antigen experienced, labeled effector T-cell blasts with either a stimulatory or a non-stimulatory bilayer and evaluated FRET via Donor Recovery After Acceptor Photobleaching or Sensitized Emission Imaging.

Donor Recover after Acceptor Photobleaching Imaging

In DRAAPB, the apparent FRET efficiency is calculated from the increase of donor fluorophore intensity after depleting the acceptor with a laser pulse as compared to the quenched "before image"(Figure 8) Intrinsically this limits the method to one single measurement per region of interest (ROI).

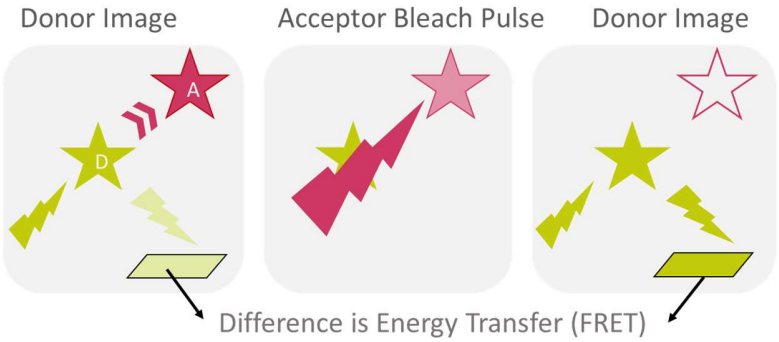

Figure 8
Schematic representation of DRAAPB imaging; left: Donor excitation, quenched donor image, middle: Acceptor bleach pulse, right: Donor excitation, unquenched donor image

Sensitized Emission Imaging

When using sensitized emission, FRET efficiency is directly calculated from the FRET emission channel after donor excitation with the use of a dichroic wedge. As this method does not involve a bleaching step, the same cell can be observed for an extended period allowing tracking movements between the FRET partners. The FRET image, acquired in the acceptor channel of the donor excitation image, must be corrected for acceptor cross excitation (ACE) and donor bleed through (DBT). Those values can be

obtained from donor only and acceptor only excitation controls of the same experiment. This makes acquisition and calculation more complex, but allows for a higher framerate.
The calculated value is described as nFRET, an index that varies with fluorophore concentration and cannot be quantitatively used directly. The SEm FRET index is calculated as follows:

$$nF = F^{exD;emA} - \alpha F^{exA;emA} - \beta F^{exD;emD}$$

$$\text{with } \beta = \frac{FD^{exD;emA}}{F^{exD;emD}} \text{ and } \alpha = \frac{FA^{exD;emA}}{FA^{exA;emA}}$$

F= Intensity of the selected area, corrected for background noise. β refers to donor bleed-through acquired in a donor only sample and α to acceptor cross excitation factor depending on the amount of acceptor.

ScF_v from an IgG Specific Hybridoma B-cell Line

To further evaluate changes in quaternary structure of the TCR upon activation in a quantitative fashion, an additional monovalent FRET probe was developed from an IgG specific Hybridoma cell line.
The Armenian Hamster (*Cricetulus migratorius*) Antibody KJ25 recognizes the murine αβ T-cell antigen receptor (5c.c7 TCR) Vβ chain at its CDRs [111], thus inhibiting interactions with its nominal peptide leading to impaired T-cell activation. As, besides receptor engagement, activation of T-cells can be induced by providing counter-force onto the receptor[112], this scF_v can alternatively be anchored onto the SLB to trigger TCR response.
Using KJ25-scF_v gives rise to the possibility of testing force dependent activation detached from TCR-pMHC interaction. The soluble variant of the FRET probe can be used to actively titer out productive receptor interaction, whereas the SLB conjugated variant would trigger T-cell activation. By site-specifically attaching a fluorophore to the KJ25-scF_v, quantitative FRET measurements can be conducted. Introducing this additional FRET partner to the already existing H57-scF_v KT3-scF_v dyad in a triple-FRET assay could provide three-dimensional information about TCR-CD3 movement.
To this end, an antibody single chain fragment was created from a hybridoma B-cell line. Since the organization of mature IgG mRNA follows *5´V-J-C-3´* and only the *J*- and *C*-segments of the antibody is known, a template switch- 5´RACE (rapid amplification of cDNA Ends with polymerase chain reaction) was carried out.

Tissue Culture

Monoclonal KJ25 antibody producing BALB/c hybridoma B-cells were thawed and kept in culture using Dulbecco`s modified Eagle`s medium (DMEM, Sigma) supplemented with 0.1 units/ml of penicillin, 0.1mg/ml streptomycin, 2 mM L-glutamine + 10% (v/v) fetal calf serum (FCS, Sigma) in a 5% CO_2 atmosphere for at least 46 hrs. (two divisions).

Rapid epitope blockade assay:

KJ25 antibody expression was verified by using the tissue culture supernatant in a quick blockade assay. In comparison to untreated cells, immunostaining efficiency of a purchased, labeled KJ25 mAB is reduced if the epitope is blocked by unlabeled antibodies that are present in the Hybridoma culture supernatant.

- Block 100 000 spleenocytes with 2 µl CD16/CD32 Rat Anti-Mouse (BD Pharmingen, 0.5 µg/µl) for 20 minutes on ice.
- Add 1 µl of CD4 mAb pacific blue Rat Anti-Mouse (BD Pharmingen, 0.5 µg/µl).
- Add 1ml of hybridoma cell supernatant for 30 minutes on ice.
- Wash cells 2x with FACS buffer.
- Stain with AFo488 labeled KJ25 full antibody for 30minutes on ice.
- Flow cytometric analysis (FACS) on BD™ LSR II (FACSDiva software).

FACS data were analyzed using FlowJo®

<u>FACS buffer</u>

PBS, 1%BSA, 0.02% NaAz

5´Rapid Amplification of CDNA Ends (RACE)

In this approach, I took advantage of the fact that Maloney Murine Leukemia Virus Reverse Transcriptase (M-MLV RT) adds 2-5 additional Cytosine residues to the 3´end of the newly synthesized cDNA. The gene specific primer to start with was created in antisense direction stretching from *J*- to the beginning of the *C*-segment. After the M-MLV RT incorporated the Cytosines, I introduced a primer that starts with a self-chosen sequence and ends with a poly-G sequence in order to hybridize with the cDNA synthesized in the first round of reverse transcription. In order to avoid misannealing of the primer, I performed a step

out PCR subsequently (Figure 9). The template created from sequencing results obtained by Eurofins® was ordered from iDT DNA to be cloned into an expression vector in two variations with the use of different restriction enzymes. One variant with the addition of a C-terminal polyhistidine tag (KJ25-scF$_v$-His$_{12}$) for anchoring it into the lipid bilayer and one without that tag (KJ25-scF$_v$).

A minimum 5 x 10^6 cells were harvested by centrifugation and RNA was extracted following the TRIzol RNA extraction protocol by ThermoFischer. The RNA pellet was washed using 70% Ethanol after which it was air-dried and dissolved in diethylpyrocarbonate (DEPC) treated water. Directly after extraction, rapid amplification of cDNA ends (RACE) was performed for both the heavy and the light chain mRNA, using the template switch (TS-RACE) approach inspired by Pinto and Lindblad (2010)[113], Matz(1999)[114] and Bower (2010)[115]. A separate reaction was performed for each mRNA template.

The gene specific primer 1 (GSP1) was obtained from the respective Fc-region *C*-segment in antisense direction. The template switch oligo (TSO) consists of a step out segment that is absent in the template transcriptome and ends with a poly G at its 3´terminus. In the step out part of the reaction, three more

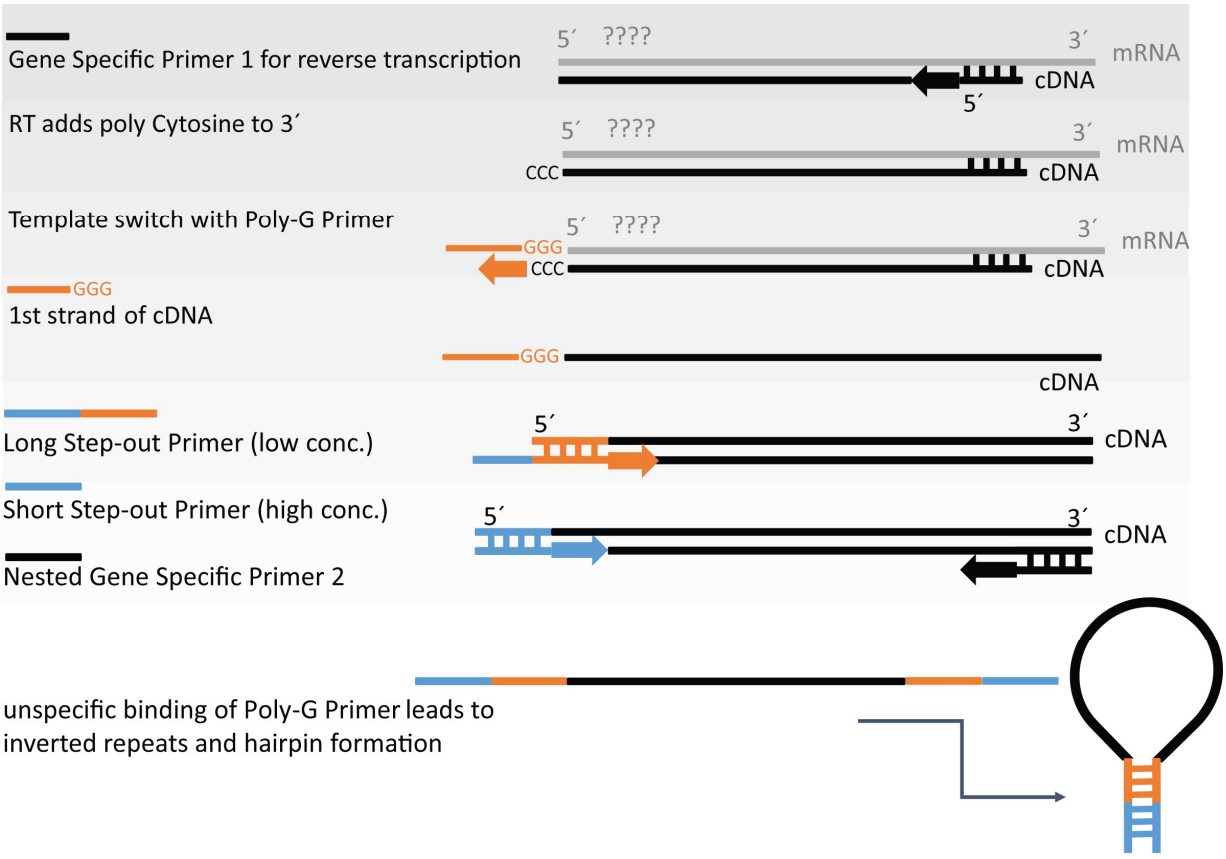

Figure 9
Schematic representation of the 5´RACE Step-out PCR approach. Grey color depicts mRNA, black color, cDNA.

primers were introduced. A gene specific primer 2 (GSP2) likewise antisense to the template *C*-segment but more upstream, stretching from the *J*- to the beginning of the *C*-segment and a step-out primer mix with two other primers. A long step out primer (SOP_long) which 3´end is identical to the 5´end of the TSO and a SOP_short, which is identical to the 5´end of the SOP_long (Figure 9).

In order to increase efficiency of template switching step, the procedure was undertaken with an alternative TSO and UPM primers separately for every extraction (see table below)

Denaturation Mix

GSP1 Primer (10 µM final= 0.002 µM), dNTP (Invitrogen) (10 µM final= 0.004 µM) RNA (1-3 µg/µl)

Elongation Mix

First Strand Buffer 5X, $MgCl_2$ (Sigma) (25 mM final= 2 mM), SuperScript2 Reverse Transcriptase (Invitrogen) (200 U/µl final volume= 0.5 µl), DTT (0.1M final= 0.01M) H_2O DEPC

Template switch Mix

$MgCl_2$ (25 mM final= 2 mM) $MnCl_2$ (100 mM final= 8 mM) SSII RT (200 U/µl), TSO (10 µM)

Step-out PCR Mix

10 µl of 5x Q5 Reaction Buffer, 0.2 mM dNTPs (Quiagen), 0.02 U/µl, 0.5 mM GSP2, 0.12 mM SOP_long and 0.02 mM SOP_short. Reaction volume: 50 µl

	standard primer	**alternative primer**
GSP1_hc (heavy chain)	5´GTGCTGGAAGGTACAGTCACTGAGCTGCTGAGG 3´	5´CTGTCTGAGCTGTCTTGTCTTCTACGTTGTTCAC ATACCAGTTG 3´
GSP2_hc (heavy chain)	5´TGGTCAGGGCTCCAGAGTTCCAGCTTACGGTC 3´	-
GSP1_lc (light chain)	5´CGCCATCTCGTTTTTCACTGCCATCTACTTTCCACTTG 3´	-
GSP2_lc (light chain)	5´GATGGTGGGAAGATGGAGACGGTTGGCTTAGC 3´	-
TSO	5´GTCGCAC GGTCCATCGCAGCAGTCACAGGGGG 3´	5´GTCGCACGCTCATCGCAGCAACGCATGGGGG 3´
UPM_long (step-out primer long)	5´ACGCTGACGCTGAGCCTACCTGACGTCGCACGGTCCATC GCAGCAGTC 3´	5´ACTGACGCTGCGTCGATGGTTGACGTCGCACG TCCATCGCAGCAACG 3´
UPM_short (step-out primer short)	5´ACGCTGACGCTGAGCCTACCTGAC 3´	5´ACTGACGCTGCGTCGATGGTTGAC 3´

Sequences from the Armenian Hamster γ-heavy chain (U17166) and κ-light chain (U17165) were taken from www.imgt.org/ligmdb/. T_m and ΔG of the primers secondary structures were calculated from www.idtdna.com, where none of the secondary structures exhibited a ΔG<-9 kcal/mol.
Primers were obtained from Sigma-Aldrich.
All master mixes for the step-out template-switch RACE were prepared and kept on ice.

- Pipet 6 µl Denaturation master mix onto 1 µl of fresh RNA (1-3 mg/ml) on ice
- Denature for five minutes at 65°C
- Chill sample on ice for two minutes before addition of 7.5 µl of DNA Elongation mix
- Allow first strand cDNA synthesis for 60 minutes at 50°C
- Add 10 µl of the Template switch master mix to reaction and allow template switching for 90 minutes at 42°C
- Add 80 µl of 2.3 mM EDTA (Ethylenediaminetetraacetic acid; Roth) to sample and inhibit reverse transcriptase for 10 minutes at 70°C

We verified the RACE-PCR fragments predicted length of 596 bp for the heavy chain fragment and 483 bp for the light chain fragment on a polyacrylamide gel.

Template-Switch, Step-Out PCR and Cloning

After denaturation, first strand synthesis and template switch, 3 µl of the reaction was used for the step-out PCR using a low concentration of long step-out primer and a high concentration of short step-out primer. The reaction volume for the Q5 polymerase PCR was 50 µl. PCR profile was set up as displayed in Figure 10.

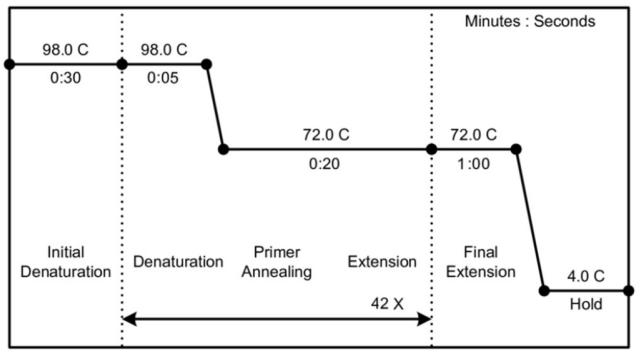

Figure 10
Step-out PCR profile

The PCR reactions were loaded on a 1% agarose gel containing SYBR®green in a ratio of 1:20 000 and the relevant bands subsequently cleaned up using the Wizard® SC Gel and PCR Cleanup System by Promega.

Sequencing was carried out by Eurofins Genomics Germany GmbH, Europe. A template without leader peptides (predicted at phobius.sbc.su.se) was generated where the sequences were joined using an inter domain linker adopted from Huppa et al. (2010)[41] and partially codon optimized using http://www.idtdna.com/CodonOpt. The final gene was synthesized by IDT© and after PCR amplification via the 5´NdeI site and 3´BamIII (or 3´ HindIII in case of the His-tagged fragment) cloned into pET21 harboring a bio-3c-his cassette (EMB, USA) under control of the T7 promoter. Cleaving in front of the integrated stop codons using BamHI, allows for expression of the construct followed by the pet21 originated 12x His-tag (Figure *11*).

KJ25- single chain fragment

T7 Promoter, **NdeI**,START, Heavy Chain, Linker, Light Chain, **BamHI**, stop, stop, **HindIII**, T7 Terminator

TAATACGACTCACTATAGGG**a**catATG
CAGGTGCAGCTGAAGGAGTCAGGACCTGGCCTGGTGCAGCCCTCACAAACCCTGTCTCTGACCTGCAC
TGTCTCTGGGTTCGCATTAACTGACCATGCTGTACACTGGGTCCGCCAGCCTTCAGGAAAAGGTCTGG
AGTGGATGGGAATAATATGGAGTGATGGAAGCACTGATTATAATTCACCTCTGAAATCCCGTGTCACC
ATCAGCCGTGACACCTCCATGAGCCAAGTTTCCTTAAAACTGAACAATCTGCAAACCGAGGACACAGC
CATGTATTACTGTGCCCGTCGTCATAGCGGATATCGTTACTTCGATTTCTGGGGCCAGGGGACCCAGG
TCACCGTCTCCTCAGCCGGTGGAGGCGGTTCTGGTGGCGGAGGTTCTGGAGGTGGCGGTTCTGACATC
ATGATGACCCAGTCTCCATCAAGCCTGAGTGTGTCAGCAGGAGAGAAAGCCACTATTACTTGCAAGTC
CAGTCAGAGTCTTTTCCACAGTAACACCAACAAGAACTACCTGAACTGGTACCTGCAGAAGCCAGGCC
AGTCTCCTAAACTGCTGATCTATTATGCATCCACTCGTCATAATGGCGTCCCTGATCGCTTCATAGGC
AGTGGATCTGGGACAGATTTCACTCTGACCATCAGCAGTGTCCAGGAGGAAGACCTGGCAGATTATTA
CTGTCAGCAGTGGCATACCTACCCATACACGTTCGGAGGTGGCACCAAACTGGAGATCAAACGGGCT**g**
gatcctaataaaagcttACCGCTGAGCAATAACTAGC

Figure 11
KJ25-scF$_v$ final gene as inserted into pET 21 via NdeI and HindIII, the heavy chain is followed by a GGGS-linker domain and the light chain, alternative cleavage at BamHI before insertion gives rise to a His tagged variant of the scF$_v$.

Enzymatic restriction reactions

1	µg	DNA
5	µl	10X Cutsmart Buffer
1	µl	NdeI
1	µl	Bam HI

to 50 µl w ddH_2O
incubate at 37°C for 60 minutes

Vector: pet21 (EMB, USA) + cloning cassette + vector backbone = 6143bp

Insert: 750bp

Inserts and the lower band were cleaned up by Wizard Kit® (Promega) and two ligations with a vector insert ratio of 1:3 and 1:10 were performed o/n at 16°C and subsequently kept at 65°C for 10 minutes to inactivate the enzyme.

Ligations were transformed into *E. coli* DH5α. Three colonies were picked for sequencing. One clone that showed 100% sequence identity with the template and was picked for plasmid preparation and subsequent retransformation into *E. coli* BL21 for scF_v expression as inclusion bodies.

Protein Expression and Inclusion Body Preparation

20ml of preculture was grown in selective Lysogeny Broth (LB) medium (100 µg/ml Ampicillin) over night at 28°C while shaking to be inoculated into 1l of selective lysogeny broth (LB)-Medium for incubation in the shaker at 37°C the next day.

When cultures reached an OD_{600} of 0.5, we induced expression by adding 1 mM IPTG (Thermo Scientific). Cells were harvested 4 hours hereafter by centrifugation for 15 minutes at 8525rcf. The bacterial pellets were resuspended in 5ml per liter of culture resuspension buffer by vortexing.

After up to six sonication steps for 30 seconds on ice using a SH70G sonde (Bandelin), 1mg/ml Lysozyme (Sigma) and 0.5mg/ml DNAseI (Sigma) was added and digestion was performed for 30 minutes at 37°C.

Using a spatula and a pipette, pelleted inclusion bodies were repeatedly centrifuged and subsequently resuspended in detergent buffer and wash buffer I until the pellet appeared chalky white. The pellet was then washed in wash buffer II and finally in ddH_2O. Pellets obtained were stored at -20°C. For usage the pellet was dissolved in 6M Guanidinium-hydrochloride (GuHCl; AppliChem).

All centrifugation steps were carried out at 4°C for 10 minutes with 11000rcf.

Resuspension buffer: 50 mM TRIS (tris(hydroxymethyl)aminomethane buffer; Roth) (pH=8.0), 25% sucrose (Sigma), 5 mM $MgCl_2$ and 0.02% sodium azide

Detergent buffer: 50 mM TRIS (pH= 8.0), 200 mM NaCl (Sigma), 2 mM EDTA, 1% deoxycholic acid (Sigma) and 1% Triton X-100 (Sigma)

Wash buffer I: 50 mM TRIS (pH= 8.0), 200 mM NaCl (Sigma), 2 mM EDTA and 1% Triton X-100 (Sigma)

Wash buffer II: 50 mM TRIS (pH= 8.0), 200 mM NaCl (Sigma), 2 mM

In Vitro Refolding Reaction

10mg of soluble denatured KJ25-scF_v (kept in 6M GuHCl (pH=8 at 4°C)) was dialyzed (molecular weight cutoff, MWCO= 12kD) for seven days against a series of TRIS based refolding buffers differing in their concentration of GuHCl as described in more detail[41]. The concentration of GuHCl in the buffer solution

decreases to zero in the course of a stepwise dialysis to allow slow refolding, while gradually introducing oxidizing reagent in the form of glutathione disulfide (GSSG, Thermo Scientific)[116] .
Oxidizing conditions and a pH higher than 6.5 result in the free thiol groups of the immunoglobulin lysins to form disulfide bonds. Additional presence of L-Arginine was shown to increase yields as it suppresses protein aggregation[117,118]. Notably pH must be adjusted after addition of Arginine.

Sample buffer
50 mM TRIS (pH=8.0 at 4C°), 200 mM NaCl, 10mM β-Mercaptoethanol, 1 mM EDTA

Refolding buffer
50 mM TRIS (pH=8.0 at 4C°), 200 mM NaCl, 1 mM EDTA

Sequence
Day 1) 1 liter of refolding buffer

Day 2) 1 liter of refolding buffer +3 M GuHCl

Day 3) 1 liter of refolding buffer +2 M GuHCl

Day 4) 1 liter of refolding buffer +1 M GuHCl +400 mM L-Arginine +375 µM GSSG

Day 5) 1 liter of refolding buffer +0.5 M GuHCl +200 mM L-Arginine +187.5 µM GSSG

Day 6) 2 liters of PBS

Hereafter the dialysate was spun at 5500g to pellet misfolded or aggregated material and concentrated in the presence of 25 µM tris(2-carboxyethyl) phosphine hydrochloride (TCEP) using stir- as well as spin-concentrators (Amicon®) with a molecular weight cutoff of 10kDA. Whereby a concentration of 3mg/ml was not exceeded. Subsequently the proteins were sterilely filtered (0.2 µm) and loaded onto a Superdex 200 10/300 GL (S200) column for size exclusion fast protein liquid chromatography (FPLC). Fractions 16ml to 18ml were collected.

Fluorophore conjugation

After gel filtration, the collected fractions were pooled and concentrated to 950 µl of 0.69mg/ml for N-Hydroxysuccinimidester (NHS- ester) labeling. Using a 2-fold molecular excess of dye, for 277 µg of KJ25-scF_v, 25.4 µg AlexaFluor647-NHS was incubated together with 40 µl of $NaHCO_3$ (1M) at pH =8.0 for 2 hours at RT in the dark. Subsequent Superdex 75 10/300 (S75) gel filtration and collection of fractions 11.5ml to 14ml yielded 148.2 µg with a degree of labeling (DOL) of 1.54.

Maleimide conjugated dyes can be irreversibly coupled to sulfhydryl groups at pH= 6.5 to 7.5, resulting in a thioether linkage. Single cysteines were incorporated into the scF_v sequence for stoichiometric and site-specific fluorophore conjugation at either one of the positions depicted in Figure 12.

H57- J5/J3 single chain fragment

start, Heavy Chain, Linker, Light Chain, stop,

```
60  atg tct gaa gtt tac ctg gtg gag tca ggg gga gat tta gtg cag cct gga agt tcc ctg
     M   S   E   V   Y   L   V   E   S   G   G   D   L   V   Q   P   G   S   S   L
120 aaa gtc tcc tgt gca gcc tct gga ttc acc ttc*agt*gac ttc tgg atg tac tgg gtc cgc
     K   V   S   C   A   A   S   G   F   T   F   C   D   F   W   M   Y   W   V   R
180 cag gct cca ggg aag ggg ctg gag tgg gtt ggt aga att aaa aac ata cct aat aat tat
     Q   A   P   G   K   G   L   E   W   V   G   R   I   K   N   I   P   N   N   Y
240 gca aca gaa tat gcg gat tcc gtg aga ggc aga ttc acc atc tca aga gac gac tca aga
     A   T   E   Y   A   D   S   V   R   G   R   F   T   I   S   R   D   D   S   R
300 aac agc atc tat ctg caa atg aat agg tta aga gtc gat gac aca gcc att tat tac tgt
     N   S   I   Y   L   Q   M   N   R   L   R   V   D   D   T   A   I   Y   Y   C
360 act aga gcc ggg agg ttc gac cac ttc gat tac tgg ggc caa gga acc atg gtc acc gtc
     T   R   A   G   R   F   D   H   F   D   Y   W   G   Q   G   T   M   V   T   V
420 tcc*tgt*gcc ggc gga ggc gga tcc ggt ggt ggc gga tct gga ggt ggc gga agc tat gag
     S   C   A   G   G   G   G   S   G   G   G   G   S   G   G   G   G   S   Y   E
480 ctg atc caa cca tct tca gca tca gtc act gta gga gag acg gtc aaa atc act tgc tct
     L   I   Q   P   S   S   A   S   V   T   V   G   E   T   V   K   I   T   C   S
540 ggg gac cag ttg cca aaa aat ttt gct tat tgg ttt cag caa aag tca gac aag aac att
     G   D   Q   L   P   K   N   F   A   Y   W   F   Q   Q   K   S   D   K   N   I
600 tta cta cta ata tac atg gat aat aag cga cca tca ggg atc cca gaa cga ttc tgt ggg
     L   L   L   I   Y   M   D   N   K   R   P   S   G   I   P   E   R   F   C   G
660 tcc act tca ggt aca aca gcc acc ttg acc atc agt gga gcc cag cct gag gat gag gct
     S   T   S   G   T   T   A   T   L   T   I   S   G   A   Q   P   E   D   E   A
720 gcc tat tac tgt ttg tct tca tat ggt gat aat aac gat tta gtt ttt ggc agc gga acc
     A   Y   Y   C   L   S   S   Y   G   D   N   N   D   L   V   F   G   S   G   T
780 cag ctc acc gtc cta cgt gga taa
     Q   L   T   V   L   R   G   -
```

KT3- J5/J1/J4 single chain fragment

start, Heavy Chain, Linker, Light Chain, stop,

```
60  atg gag gtg tac ctg gta gag tct ggg ggc ggt tta gtg cag cct ggc ggg tcc gtg aaa
     M   E   V   Y   L   V   E   S   G   G   G   L   V   Q   P   G   G   S   V   K
120 ctc tcc tgt tca gcc tca gga ttc act ttc*tgt*acc ttt cca atg gcc tgg gtc cgc cag
     L   S   C   S   A   S   G   F   T   F   C   T   F   P   M   A   W   V   R   Q
180 gct cca acg cag ggt ctg cag tgg gtc gca acc ctt agt cct agt ggt gat agc act tac
     A   P   T   Q   G   L   Q   W   V   A   T   L   S   P   S   G   D   S   T   Y
240 tat cgc gat tcc gtg aag ggc cgc ttc act atc tcc cgc gat aat gta ctg aac acc ctg
     Y   R   D   S   V   K   G   R   F   T   I   S   R   D   N   V   L   N   T   L
300 tac ctc cac atg gac att ctg cgc tct gag gac acg gcc act tat tac tgt aca aaa gtc
     Y   L   H   M   D   I   L   R   S   E   D   T   A   T   Y   Y   C   T   K   V
360 gga ttt acc acc ttc tat ttt gat tcc tgg ggc caa gga gtc atg gtc gca gtc tcc tca
     G   F   T   T   F   Y   F   D   S   W   G   Q   G   V   M   V   A   V   S   S
420 gct ggt gga ggc ggt tct ggt ggc gga ggt tct gga ggt ggc ggt tct gac atc cag atg
     A   G   G   G   G   S   G   G   G   G   S   G   G   G   G   S   D   I   Q   M
480 acc cag tct cct tca ttc ctg tct gca tct gtg gga gac cgc gta act atc aac tgc aaa
     T   Q   S   P   S   F   L   S   A   S   V   G   D   R   V   T   I   N   C   K
540 gca agt cag aat att aac aag tac ttg gac tgg tat cag caa aag ttt ggt gag act ccg
     A   S   Q   N   I   N   K   Y   L   D   W   Y   Q   Q   K   F   G   E   T   P
600 aaa ctc ctg atc tat aat att aac aat ttg cat tca gga gtc cca tca cgc ttc agt ggc
     K   L   L   I   Y   N   I   N   N   L   H   S   G   V   P   S   R   F   S   G
620 agt gga*tgt*ggt cct gat ttc aca ctt acc atc agc agc ctg cag cct gaa gat gtt gcc
     S   G   C   G   P   D   F   T   L   T   I   S   S   L   Q   P   E   D   V   A
680 aca tat ttc tgc ctt caa cat cgc act ggg tgg acg ttc ggt gga ggc acc aag gtg gaa
     T   Y   F   C   L   Q   H   R   T   G   W   T   F   G   G   G   T   K   V   E
740 ttg cgt cgc gct*tgt*taa
     L   R   R   A   C   -
```

Figure 12

H57- and KT3-scF_v- nucleotide sequence (upper) and amino acid sequence (lower), heavy chain followed by a GGGS linker domain and the light chain, Mutations leading to J1, J3, J4 and J5 respectively indicated with asterisk Positions of the mutations within the structure of the scFv, derived from a H57 Fab fragment (PDB ID: 1NFD) displayed in Figure 15, b. cysteine positions of KT3-scFv were chosen to match the respective position on H57scFv.

Cysteine residues harboring mutants of the scF_vs H57 and KT3 were labeled for 3hrs on RT with AF555- or AF647-malemide in the presence of 50 µM TCEP. TCEP in comparison to other reducing agents like dithiothreitol (DTT) and β-mercaptoethanol does not contain sulfhydryl groups that would compete with the dye for maleimide conjugation.

To calculate the DOL the molecular extinction coefficient at absorption maximum ($\varepsilon \lambda_{max}$) of both the dye and the protein must be taken into account for as well as the dye specific correction factor (CF) at 280nm.

$$DOL = \frac{E(dye) \times \varepsilon(protein)}{E(protein) \times \varepsilon(dye)}$$

$\varepsilon\lambda_{max}$ *of AF647= 239 000* $cm^{-1}M^{-1}$

$\varepsilon\lambda_{max}$ *of KJ25-*scF_v*= 52 620* $cm^{-1}M^{-1}$

E(protein) correction: E(280)-(E(dye at λ_{max}*)x* CF_{280nm}*)*

CF_{280nm} *for AF647= 0.03*

KJ25-scF_v *labeling parameters and specificity*

We performed an *in vitro* epitope saturation assay to determine the amount of scF_v needed to label TCR-epitopes on 100 000 primed murine 5C.C7 T-cells. Therefore, a dilution series of AF647 labeled KJ25-scF_v was incubated on ice and in the dark for 30 minutes. The labeling reaction volume was 20 µl. Hereafter the samples were incubated in a 25°C water bath for varying time in order to determine bond lifetime in a flow cytometry assay.

To verify conservation of KJ25 specificity, I conducted an epitope blocking assay using murine spleenocytes. Therefore, cells were blocked and labeled with CD4+ T-cell specific marker and the KJ25 epitope was saturated with unlabeled mAb KJ25. Hereafter cells were incubated with the AF647 conjugated KJ25-scF_v to determine non-specific binding

- Blocking Agent CD16/ CD32 -20min on ice
- Add CD4 mAb (AF488), KJ25 mAb (unlabeled) -20min on ice (dark)
- Add KJ25-scF_v (AF647) -20min on ice (dark)
- Flow cytometric analysis

pMHC-NVOC Expression

The MCC peptide was ordered from Intavis Bioanalytical Instruments with the protective NVOC group derivatized onto its Lys99 residue, as is most crucial for 5Cc.C7 TCR recognition (ANERADLIAYL**K**QATK, K99 in bold). The peptide was purified by reverse-phase high performance liquid chromatography (HPLC). Fractions were eluted with a gradient from polar buffer A (H_2O, 0.1% Trifluoroacetic acid (TFA)) to less polar buffer B (90% Acetonitrile, 9.9% H_2O, 0.1% TFA) and the presence of the caging entity was evaluated using TOFMS (calculated MW 2043.04 Da with NVOC and 1802.85 Da without NVOC group) (Figure 18). TFA and solvent was removed by overnight lyophilization. MHC I-E^k α-12 and a β-0 immunoglobulin domain subunit have already been cloned into expression vectors whereby the transmembrane domain of the β-0 subunit had been removed completely and theone of the α-12 subunits had been substituted by a His_{12} extension on the C-terminus for bilayer conjugation. Both chains were expressed as inclusion bodies separately. After IB cleanup as described, they were denatured in 6M GuHCl, a chaotropic salt and exposed to ambient oxygen for oxidation for three days. The molecules were refolded in the presence of MCC 3-Amino-3-(2-nitrophenyl)propionic acid (MCC-ANP) for two weeks in 4000ml of I-E^k refolding buffer.

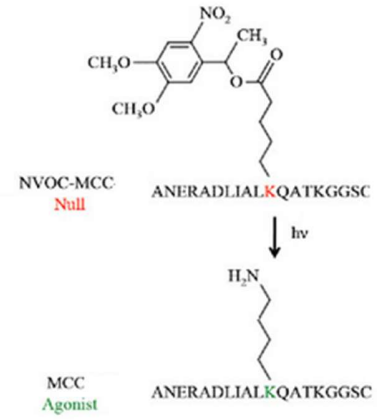

Figure 13
NVOC-protected MCC cleaved by UV pulse to agonist peptide, figure adapted from source: Klein, L. Imaging initial events in T cell activation: ligand binding and signaling, PhD Diss. Interdepartmental Program in Biophysics Stanford University (2010)

Using a Pall tangential flow filtrator with a 10kDa cutoff, the chelating agent EDTA was diluted to a maximal concentration of 0.5 mM (hereby not exceeding a pressure of two Pascal) to allow subsequent purification via Ni-NTA chromatography. The column was eluted with a 0.02M to 0.5M imidazole gradient and fractions were analyzed for the presence of MHC via photospectrometry. Aliquots were shock frozen in liquid nitrogen. Peptide exchange to MCC-NVOC was conducted as follows:

- 200 µl of PBS with a pMHC concentration of 1 µg/µl
- add 100 µl MCC-NVOC in PBS in at least 10-fold surplus

I-E^k refolding buffer		
4000	ml	I-E^k refolding buffer
25	%	glycerol
40	mM	Na_2HPO_4 $7H_2O$
10	mM	$NaH2PO_4$ $2H_2O$
2	mM	EDTA
5	mM	GSH red
0.5	mM	GSH ox
0.1	mM	PMSF
10	µM	ANP-peptide
2	µM	I-E^k α-12
2	µM	I-E^k β-0
0.05	%	sodium azide

- add 60 µl citric acid buffer (pH=5.2)
- incubate at RT for 1h before centrifugation (16000g for 1 min)
- incubate at RT for 1-3 days
- filter (MWCO= 10kDA) and purify via FPLC

After exchange, MHC I-E^k was purified via gel filtration (S200) in the dark. (Figure 18, b, c, d).
Remaining steps and bilayer preparation for NVOC experiments as well as imaging were conducted in the dark to avoid spontaneous UV-uncaging of the protected epitope.

Retroviral Transfection of ZAP70-GFP

The ζ chain associated protein kinase 70 (ZAP70) is recruited to the tyrosine-phosphorylated TCR-CD3 complex via its SH-domains as a result of activation and is one of the first messengers involved in signaling. We aim to visualize its recruitment simultaneous to measuring FRET in order to place the event of movement in the TCR/CD3 complex within the cascade. For this purpose, a ZAP70-GFP fusion gene was created to be transduced into our target 5C.C7 TCR transgenic murine spleenocytes.
For the generation of an isotropic murine retrovirus, we used a Phoenix-Eco cell line that already possesses the *env* as well as the *gag-pol* gene segments [119] needed for retrovirus production. Transfection with a ZAP70-GFP construct that is preceded by a ψ packaging signal was conducted using calcium phosphate precipitation. Because the introduced DNA plasmid harboring the gene of interest is lacking a transport signal, the plasmid can only properly reach the nucleus during mitosis. Hence, one must be careful to grow the cells up to a confluency of a 75% where division rates are high [119]. Chloroquine was added five minutes prior to transfection to inhibit DNase digestion of the plasmids in the lysosome as the weak base is increasing the pH when taken up into the vesicle[120]. Because of its toxicity, cells must be carefully washed after successful uptake of the construct. Coprecipitation with calcium phosphate facilitates DNA uptake into the cell and helps to protect the nucleic acid from intracellular nucleases. The two parameters critical for efficiency are pH and crystal size. As precipitation is strongly dependent on the pH of the Hank's Balanced Salt Solution (HBSS, Gibco) and only allows for a narrow window of around seven, it is necessary to evaluate the optimum by titration. Likewise, vigorous vortexing could result in a lowered transfection efficiency, most likely due to breakage of the crystals[121].
After the virus particles are released into the supernatant, it is used for infection of primed transgenic murine T-cells. Uptake is facilitated by the addition of polybrene (Hexadimethrine bromide) as it is acting

as an agent to minimize the repulsion between the charges of the cell membrane and the virus particle envelope.

Infection of humans by ectotropic murine retroviridae is impaired by the virus´ specificity to its receptor on mouse cells [122]. Nevertheless, after transfection, the T-cells were treated in a safety level two facility until two division cycles and at least two washing steps to make sure that infectious particles had been titered out of the supernatant. As *gag, pol* and *env* genes do not possess a preceding ψ packaging signal, the virus particles do not contain information to produce a replicating virus. Only the gene of interest, in this case *ZAP70-GFP*, is transfected into the target cell. Transgenic ZAP70-GFP T-cells were used for experiments for a maximum of seven days post infection.

Tissue culture

Primary T-cells were isolated from the spleens of rag2$^{+/+}$, 5C.C7 TCR transgenic mice and kept in culture using T-cell medium supplemented with 50U/ml murine IL-2 and 1 µM of the TCRs nominal peptide derived from the moth cytochrome C protein (MCC 88-103) for T-cell priming for at least five and maximally 10 days. The MCC peptide with the sequence, ANERADLIAYLKQATK (binding epitope underlined) was purified in advance using C18 reversed-phase HPLC.

Even though the endogenous TCR locus has not been silenced, the use of rag+ mice is appropriate as the transgene encoded TCR is expressed much faster than the endogenous one, inhibiting recombination of the genomic TCR genes. In rag+ mice, the proportion of cells harboring a TCR other than 5C.C7 is less than 10% [123] .

T-cell medium

RPMI (Gibco) supplemented with

10	%	FCS
2	mM	L-glutamine (Gibco)
100	U/ml	penicillin-streptomycin (Gibco)
50	µM	β-Mercaptoethanol (Sigma)

Retroviral transduction

To generate an ecotropic retrovirus, 2x10^6 Phoenix cells (adenovirus E1A transformed packaging Human Embryonic Kidney 293T-cell line) were freshly thawed, seeded into a 10cm cell culture dish and grown to a confluency of about 75% using DMEM 10%FCS supplemented with 100 units/mL of penicillin and 100 µg/mL streptomycin as well as 2 mM glutamine (PSG).

Day 0

1) Treat cells with 25 µM chloroquine for 5 minutes.
2) Perform calcium coprecipitation by mixing 8 µg Ψ helper plasmid and 17 µg of ZAP70-GFP DNA in 125 µl 2M $CaCl_2$, filling it up to 1 ml with H_2O and dropwise adding 1ml 2XHBSS (ph=6.95) while vortexing.
3) Add the coprecipitate on top of the cells homogenously.
4) Incubate the transfected cells for 4 hours at 37°C before washing them and transfer to a safety level 2 facility. Keep in culture using T-cell medium for another 48 hours.

On day 0, spleenocytes of a 5C.C7 αβ TCR transgenic T-cells are harvested and supplemented with MCC peptide (2 µM) for priming.

Day 1

add 50 units per ml IL-2 to the spleenocytes.

Day 2

1) Harvest virus particle together with supernatant of the Phoenix cells by filtration through a 0.45 µm syringe filter.
2) Seed $5x10^5$ primed murine T-cells (spleenocytes) per well into a 24-well plate and add 2ml of virus particle supernatant as well as hexadimethrine bromide (Polybrene) to a final concentration of 8 µg/ml.
3) Spin cells at 1000rpm and 37°C for 90 minutes.
4) Change medium to T-cell medium before two days incubation at 37°C.

Day 3

Add blacticidine (20 µg/ml) to the culture in order to select for infected T-cells.

Day 4

Change the medium again. Cells can be transferred to tissue culture for ficolling. Use cells for experiments on day 5, 6 and 7 post transduction (Day 2). ZAP70 recruitment to the membrane was detected in the 532nm channel in TIR using 488nm laser excitation.

Super-Resolution Imaging

SLB formation

Glass-supported lipid bilayers were prepared from vesicles consisting of 1-palmitoyl-2-oleoyl-sn-glycero-3-phosphocholine (POPC) containing 2% 1,2-dioleoyl-sn-glycero-3-(N(5-amino-1-carboxypenyl) iminodiacetic acid) succinyl nickel salt (Ni-DOGS NTA; Avanti Polar Lipids) stored in inert atmosphere at 4°C. POPC as the predominant lipid gives rise to fluid lipid bilayers at room temperature (RT) whereas Nickel DOGSs NTA, a synthetic lipid with a chelating head group, is present for functionalization. It is able to bind the histidine tagged extracellular domains of the proteins ICAM-1, B7-1 as well as pMHC with which we decorated the bilayer prior to imaging. Those were shown to successfully promote activation of T-cells and is further described as a „stimulatory bilayer“[41,124] (Figure 7

Illustration of a TCR-CD3 complex on a T-cell membrane (top) facing the stimulatory lipid bilayer platform. Laser TIR illumination is applied onto the sample with an inverted microscope. Donor fluorophore AF555 conjugated to H57-scFv and acceptor fluorophores AF647 conjugated to KT3-scFv indicated with stars of respective color. In contrast, the same constitutions, missing the pMHC refers to a „non-stimulatory bilayer“.

The lipid bilayer was generated from small lipid vesicles [125] on top of a cover slide, which must be freshly cleaned in a bath of Peroxomonosulfatic acid (piranha solution) in order for the bilayer to form properly. Because the acid solution hydroxylates the glass surface, a phospholipid bilayer spreads on top of a thin water surface when added in the form of unilaminar vesicles. This glass-supported lipid bilayer was then incubated with recombinant membrane proteins of interest. Throughout the procedure that involves several washing steps, avoiding air contact of the bilayer is crucial.

Mobility of the bilayers can be witnessed by signal recovery after bleaching a defined area of labeled membrane bound proteins. We assayed the stimulatory potency of the decorated bilayer using the fluorescent Ca^{2+} indicator dye Fluo-4. Calcium flux as evidence for T-cell activation took place seconds after cells, carefully pipetted into the chamber, made bilayer contact.

For a detailed protocol of unilamellar vesicle generation, please refer to the Handbook “The immune synapse: methods and protocols. (Humana Press, 2017).”

Imaging buffer

HBSS supplemented with 1%FCS, 2 mM $Ca^{2+}Mg^{2+}$

In the chemical hood:

1) Clean a N°1.5 (0.17x 24 x 60 mm) Menzel glass slide (refractive index of 1.52) in Peroxomonosulfatic acid (piranha solution, H_2SO_4 and 30% H_2O_2 in a ratio of 1:1) for 30 minutes.
2) Rinse carefully with ddH_2O from top to bottom, only touching the edges with the tweezers
3) Let the slide dry and attach an 8-well Lab-Tek™ chamber (Thermo Scientific) to the glass slide using dental silicone putty (Picodent twinsil 22; Picodent).

In the incubator:

4) Incubate at 37°C shed from dust until set for 15 minutes.

On the bench

5) Cut away excessive Picodent on the bottom of the glass slide in order to provide an even bearing surface for imaging
6) Dilute Lipids 1:10 in PBS and sterile filter (0.22 µm)
7) Add 200 µl of diluted lipids per Lab-Tek well and let the bilayer form for 10 minutes.
8) Wash each well 2 x with 15ml PBS using a 30ml pipette on low exhaust speed.
9) Remove surplus with a 1000 µl pipette tip and aspirate additional 350 µl to not expose the bilayer to air.
10) Add proteins in 50 µl of PBS and carefully mix before incubating for 60 minutes.
11) Wash as indicated in step (8).
12) Aspirate to minimum as indicated in step (9).
13) Shortly before imaging, exchange the PBS buffer with imaging buffer prewarmed to the desired temperature.

Concentration of histidine tagged extracellular domains of the bilayer attached molecules:

ICAM-1: 80ng giving rise to about 500 mol/μm^2

B7-1: 24ng giving rise to about 500 mol/μm^2

$I\text{-}E^k$/MCC or MCC-NVOC: 250ng giving rise to about 2000 mol/μm^2

The stimulatory potency of the bilayer was verified by adding 2.5 µM of the fluorescent Ca^{2+}-ion indicator dye Fluo-4 to $1x10^5$ T-cells 15 minutes before measuring calcium flux as a means of activation. Increased fluorescence was detected at 488nm seconds after T-cells have been carefully placed onto the functionalized surface using a piston pipette.

Setup and Programs

Imaging was performed on a Nikon Eclipse TiE inverted microscope equipped with a 100x N.A=1.49 TIR Plan-Apochromatic objective (Nikon) operated on Metamorph software (Universal Imaging). Excitation was applied using laser light sources (640nm, 488nm, 405nm; Toptica and 532nm; OBIS). All images were acquired on an electron multiplying CCD-camera (Andor iXon Ultra 897) after passing a dichroic longpass mirror (H 643 LPXR superflat; AHF) additionally equipped with a 575 +/-25nm bandpass and a 640 longpass filter (ET575/50m and 640dcxr; Chroma). A mobile neutral density =1 was used for 532nm exposure.

<u>DRAAPB protocol</u>

streamed Multi-Dimensional Acquisition (MDA), exposure time= 30ms

640nm image, 532nm image, 4x 540nm bleaching pulse (5kW/cm^2), 532nm image, 640nm image

<u>SEm protocol</u>

Time-lapse acquisition for 40 seconds (timepoint every second) or 7 minutes (timepoint every 10 seconds), exposure time= 30ms

532nm and 488nm image every timepoint, 647nm image every third timepoint

Uncaging pulse (200ms) last event of timepoint 8, power of bleaching pulse was chosen to bleach 10% of the acceptor fluorophores

Separate images were recorded from acceptor only and donor only samples to calculate acceptor bleed through and cross excitation. Cross excitation correction was calculated for every third timepoint and applied for the following two images. FRET index was calculated as follows:

$$SEM\ index = \frac{F^{ex\ ;emA} - \alpha F^{exA;emA} - \beta F^{exD;emD}}{F^{exD;emD}}$$

where *F* depicts mean fluorescent intensity in the ROI, background corrected.

The superscript indicates excitation wavelength (ex) and emission channel (em) of either donor (D) or acceptor (A) fluorophore.

α is the acceptor cross excitation factor multiplied with acceptor image intensity and β, the donor bleed through factor. Those factors can be obtained by calculating:

$$\beta = \frac{FD^{\mathrm{exD;emA}}}{F^{\mathrm{ex\ ;emD}}}\ ;\ \alpha = \frac{FA^{\mathrm{exD;emA}}}{FA^{\mathrm{exA;emA}}}$$

All experiments shown were carried out at 25°C unless stated otherwise.

Cells were kept on ice and in the dark during labeling and until they were exposed to the PBS buffered SLB by careful pipetting. Imaging took place as for 15 minutes maximally for each group of spotted cells. All images except for brightfield images were acquired in TIR. The UV uncaging pulse was conducted in epifluorecence illumination.

To calculate AF555 MFI fold increase, SEm images of the 532nm donor channel were corrected for camera background and multiplied with a threshold binary mask designed to show whole cell or high intensity (microclustered) areas. Subsequently Z-axis profiles were obtained for the timeline image stack in ImageJ and mean intensity was corrected for the percent of signal area. Fold-increase was normalized to the mean of images before UV uncaging pulse and first image after uncaging. This could be easily automated for further experiments.

RESULTS

ScF_v from an IgG Specific Hybridoma B-cell Line

To generate a tool that would allow to either to activate T-cells independently of pMHC interaction or to inhibit pMHC binding completely, I sought to devise two scF_vs derived from the KJ25 mAb, targeting the TCR 5C.C7 β subunit. KJ25-scF_v for impaired T-cell activation by blocking the antigen binding cleft and KJ25-scF_v-His_{12} for force dependent T-cell activation.

In order to verify KJ25-IgG expression in two B-cell hybridoma cell line candidates, cell line supernatants were tested in a blocking assay. Blocking T-Cells with the supernatant of clone number two completely inhibited epitope specific cell staining, indicating IgG expression (Figure 14, a). After extracting the full RNA from the sample, I obtained the sequence of the V_L and V_H encoding gene segments by performing rapid amplification of 5´ cDNA ends (5´RACE) followed by a step-out PCR. A separate reaction was performed for each mRNA query. I estimated fragments lengths according to published sequences of the Armenian hamster Ig heavy and Ig κ-light chain, derived from IMGT, the international ImMunoGeneTics information system. Around 596 bp in case of the heavy chain and approximately 483 bp in case of the light chain could be confirmed on a 1% agarose gel (Figure 14, b). After receiving concurring sequencing results from four independent reactions for both cDNA fragments from Eurofins®, I proceeded to create a construct that could serve as an expression template for both KJ25-scF_v and the KJ25-scF_v-His_{12} (Figure 14, c, d). The gene template was synthesized by IDT© and both variants were cloned via NdeI and BamHI/HindIII respectively into pET21 (EMB, USA). I expressed KJ25-scF_v without the His-tag via inclusion bodies in *E. coli* BL21. Together with samples taken during expression, purified inclusion bodies where denatured and analyzed on a 10% Sodiumdodecylsulfate Polyacrylamidegel (SDS-PAGE), where the estimated size of around 25kDa could be confirmed (Figure 15, a). I carried out *in vitro* refolding using stepwise dialysis and thereafter size-exclusion FPLC using a S200 column based on the procedure used for H57- and KT3-scF_v. Fractions pooled corresponded to 16ml to 18ml as indicated in Figure 15, b and were analyzed for the presence of the scF_v on a PAGE. Expression yielded 82.5 µg of purified scF_v per 10mg of denatured unpurified scF_v.

The single chain fragment was stochastically labeled for two hours using N-hydroxysuccinimide ester (NHS ester) derivatization, and again purified via an S-75 column (11.5ml to 14ml) (Figure 15, b). Labeling resulted in 148.2 µg with a DOL of 1.54.

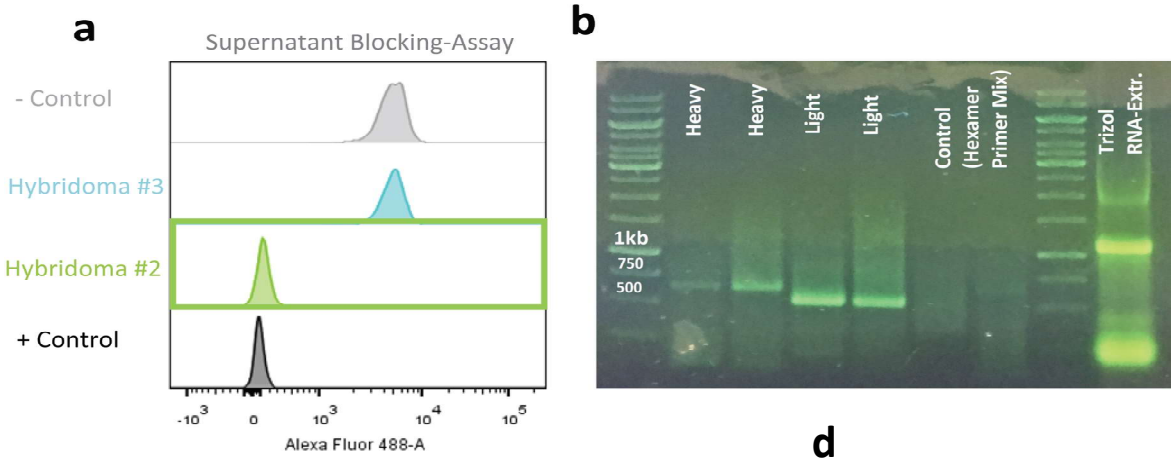

c

Sequencing Results KJ25 IgG Heavy Chain:

signal peptide, variable (and joining) region, constant region

```
0atggctgtcctggtgctgctcctctgcctggtgactttgccaagctgtgtcctgtcacag
  M  A  V  L  V  L  L  L  L  C  L  V  T  L  P  S  C  V  L  S  Q
60gtgcagctgaaggagtcaggacctggcctggtgcagccctcacaaaccctgtctctcacc
  V  Q  L  K  E  S  G  P  G  L  V  Q  P  S  Q  T  L  S  L  T
120tgcactgtctctgggttcgcattaactgaccatgctgtacactgggtccgccagccttca
  C  T  V  S  G  F  A  L  T  D  H  A  V  H  W  V  R  Q  P  S
180ggaaaaggtctggagtggatgggaataatatggagtgatggaagcactgattataattca
  G  K  G  L  E  W  M  G  I  I  W  S  D  G  S  T  D  Y  N  S
240cctctcaaatcccgagtcaccatcagcagggacacctccatgagccaagtttccttaaaa
  P  L  K  S  R  V  T  I  S  R  D  T  S  M  S  Q  V  S  L  K
300ctgaacaatctgcaaaccgaggacacagccatgtattactgtgccagacgtcatagcgga
  L  N  N  L  Q  T  E  D  T  A  M  Y  Y  C  A  R  R  H  S  G
360tataggtacttcgatttctggggccagggacccaggtcaccgtctcctcagccacaaca
  Y  R  Y  F  D  F  W  G  Q  G  T  Q  V  T  V  S  S  A  T  T
420acagccccatctgtctatcccttggcccctgcctgtgacagcacaaccagcacc…
  T  A  P  S  V  Y  P  L  A  P  A  C  D  S  T  T  S  T …
```

Sequencing Results KJ25 IgG kappa Light Chain:

signal peptide variable (and joining) region, constant region

```
0atggaatcacatatccatgtcttcatgtccttgttcctttgggtgtctggttcctgtgca
  M  E  S  H  I  H  V  F  M  S  L  F  L  W  V  S  G  S  C  A
60gacatcatgatgacccagtctccatcatccctgagtgtgtcagcaggagagaaagccact
  D  I  M  M  T  Q  S  P  S  S  L  S  V  S  A  G  E  K  A  T
120attacttgcaagtccagtcagagtcttttccacagtaacaccaacaagaactacttgaac
  I  T  C  K  S  S  Q  S  L  F  H  S  N  T  N  K  N  Y  L  N
180tggtacctgcagaagccagggcagtctcctaaactgctgatctattatgcatccactagg
  W  Y  L  Q  K  P  G  Q  S  P  K  L  L  I  Y  Y  A  S  T  R
240cataatggggtccctgatcgcttcataggcagtggatctgggacagatttcactctcacc
  H  N  G  V  P  D  R  F  I  G  S  G  S  G  T  D  F  T  L  T
300atcagcagtgtccaggaggaagacctggcagattattactgtcagcagtggcatacctac
  I  S  S  V  Q  E  E  D  L  A  D  Y  Y  C  Q  Q  W  H  T  Y
360ccatacacgttcggaggtgggaccaaactggagatcaaacggctgatgctaagccaacc
  P  Y  T  F  G  G  G  T  K  L  E  I  K  R  A  D  A  K  P  T
```

d

KJ25-scF$_v$ nucleotide sequence

T7 Promoter; **NdeI**, start, Heavy Chain, Linker, Light Chain, **BamHI**, stop, stop, **HindIII**, T7 Terminator

```
TAATACGACTCACTATAGgga catATG
CAGGTGCAGCTGAAGGAGTCAGGACCTGGCCTGGT
GCAGCCCTCACAAACCCTGTCTCTGACCTGCACTG
TCTCTGGGTTCGCATTAACTGACCATGCTGTACAC
TGGGTCCGCCAGCCTTCAGGAAAAGGTCTGGAGTG
GATGGGAATAATATGGAGTGATGGAAGCACTGATT
ATAATTCACCTCTGAAATCCCGTGTCACCATCAGC
CGTGACACCTCCATGAGCCAAGTTTCCTTAAAACT
GAACAATCTGCAAACCGAGGACACAGCCATGTATT
ACTGTGCCCGTCGTCATAGCGGATATCGTTACTTC
GATTTCTGGGGCCAGGGGACCCAGGTCACCGTCTC
CTCAGCCGGTGGAGGCGGTTCTGGTGGCGGAGGTT
CTGGAGGTGGCGGTTCTGACATCATGATGACCCAG
TCTCCATCAAGCCTGAGTGTGTCAGCAGGAGAGAA
AGCCACTATTACTTGCAAGTCCAGTCAGAGTCTTT
TCCACAGTAACACCAACAAGAACTACCTGAACTGG
TACCTGCAGAAGCCAGGCCAGTCTCCTAAACTGCT
GATCTATTATGCATCCACTCGTCATAATGGCGTCC
CTGATCGCTTCATAGGCAGTGGATCTGGGACAGAT
TTCACTCTGACCATCAGCAGTGTCCAGGAGGAAGA
CCTGGCAGATTATTACTGTCAGCAGTGGCATACCT
ACCCATACACGTTCGGAGGTGGCACCAAACTGGAG
ATCAAACGGGCT
ggatcctaataaaagcttACCGCTGAGCAATAACT
AGC
```

KJ25-scF$_v$ amino acid sequence

```
(M)QVQLKESGPGLVQPSQTLSLTCTVSGFALTDH
AVHWVRQPSGKGLEWMGIIWSDGSTDYNSPLKSRV
TISRDTSMSQVSLKLNNLQTEDTAMYYCARRHSGY
RYFDFWGQGTQVTVSSAGGGGSGGGGSGGGGSDIM
MTQSPSSLSVSAGEKATITCKSSQSLFHSNTNKNY
LNWYLQKPGQSPKLLIYYASTRHNGVPDRFIGSGS
GTDFTLTISSVQEEDLADYYCQQWHTYPYTFGGGT
KLEIKRA(GS)
```

Figure 14

a. *FACS analysis of hybridoma supernatant blocking assay. The reagents used for blocking prior to KJ25-Fab (AF488) epitope staining: - Control: without blocking; Hybridoma #3: supernatant of hybridoma clone number 3 or (Hybridoma #2) 2 respectively; + Control: unlabeled KJ25 mAb* ***b.*** *1% (w/v) Agarose gel, 1:17 000 SERVA green, bands from right to left: TRIzol extraction of 7,5x10^6 KJ25 B-cell hybridoma cells; 5 µl RACE step-out PCR product using the primers: random hexamer primers as a control, two alternative light chain primers, two alternative heavy chain primers (see methods), (calculated length heavy chain: 596 bp; light chain: 483 bp)* ***c.*** *Sequencing results of KJ25 igG heavy and light chain RACE products. Consensus sequence from four different experiments. Signal peptide highlighted in grey, start of the constant region in black letters.* ***d.*** *KJ25-scF$_v$ gene templet as cloned into pET21, codon optimized for expression in E.coli and corresponding amino acid sequence*

Specificity of the KJ25-scF$_v$

To analyze the properties of the labeled KJ25-scF$_v$, I stained a sample of freshly isolated naïve mouse-spleenocytes as well as antigen experienced murine CD4 $^+$ T-cells from a 5C.C7 TCR transgenic mouse. Half-life ($t_{1/2}$) at room temperature was determined to be 15 minutes and the amount of scF$_v$ required to saturate the epitopes of 100 000 T-cells was 2 µg in a reaction volume of 20 µl (Figure 15, c) . To evaluate

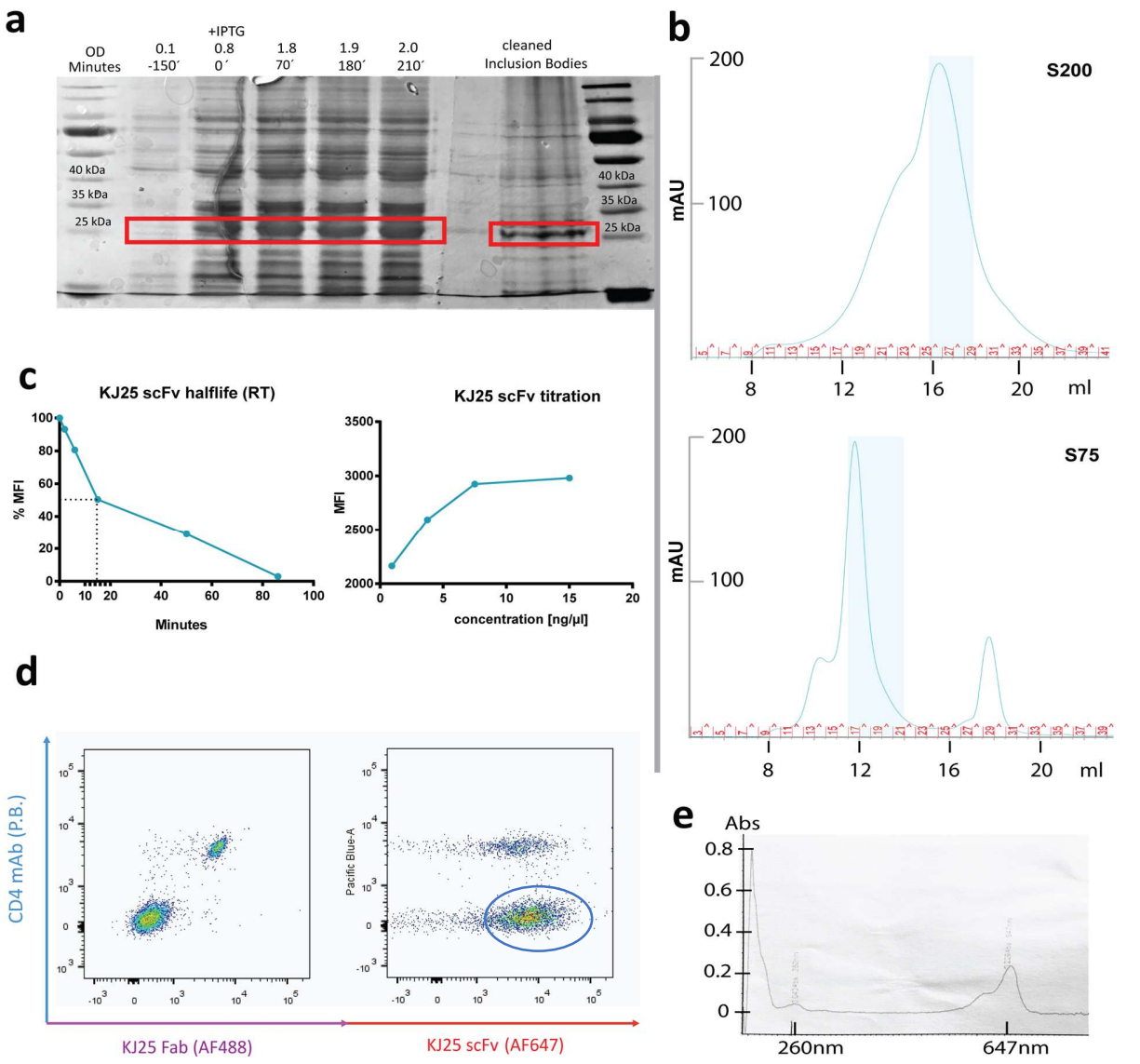

Figure 15

a. *SDS PAGE under non-reducing conditions of whole cell lysate of E.coli BL21 expressing KJ25-scF$_v$ before and after 70, 130 and 220 minutes post IPTG induction and isolated inclusion bodies after purification (see methods)* ***b.*** *FPLC purification profile of H57 mean Arbitrary Units (mAU) of UV-absorption* ***(top)*** *of the unlabeled KJ25-scF$_v$ on an S 200 column,* ***(below)*** *post NHS-labeling on an S75 column; pooled fractions highlighted in blue, peak to the left refers to multimeric aggregates, peak to the right (lower panel) refers to unbound fluorophores* ***c.*** *KJ25-scF$_v$ binding half-life on RT and KJ25-scF$_v$ titration to saturate 10 000 T-cell epitopes in a volume of 20 µl* ***d.*** *FACS analysis of 5C.C7 TCR transgenic spleenocytes labeled with CD4-mAb (Pacific Blue), KJ25 Fab (AF488) and KJ25-scF$_v$ (AF647) unspecific binding indicated with blue circle* ***e.*** *UV/VIS absorption spectrum post unspecific NHS-labeling with AF647 (DOL=1.5)*

its specificity, the scF_v was incubated to bind to a sample of spleenocytes consisting of a variety of leukocytes. Results indicated that the specificity for the KJ25-scF_v binding epitope was lost during the process. Compared to the Fab fragment of KJ25 that had retained its features, the single chain fragment adhered to an additional, unknown population of cells that were CD4 negative (Figure 13, d).

H57-scF_v and KT3-scF_v Generation

For site-specific labeling, I transformed plasmids containing the gene of the single chain fragment harboring the respective mono-cysteine substitution into *E. coli* BL21. I expressed two variants of H57-scF_v (J3 and J5) as well as three variants of KT3-scF_v (J1, J4 and J5) (see methods and Figure 17, b) and refolded them from inclusion bodies, as described for KJ25-scF_v. Fluorophores were introduced by conjugating a thiol-reactive dye to the implemented cysteine residue. The DOL after a minimum of two hours of labeling at RT was in the range of 1.30 to 0.94 for all probes used. Single chain fragments with a DOL of more than one were shown to stay in solution, unable to adhere to their target and can thus be neglected in small amounts when staining with an 8-fold molar excess[20].

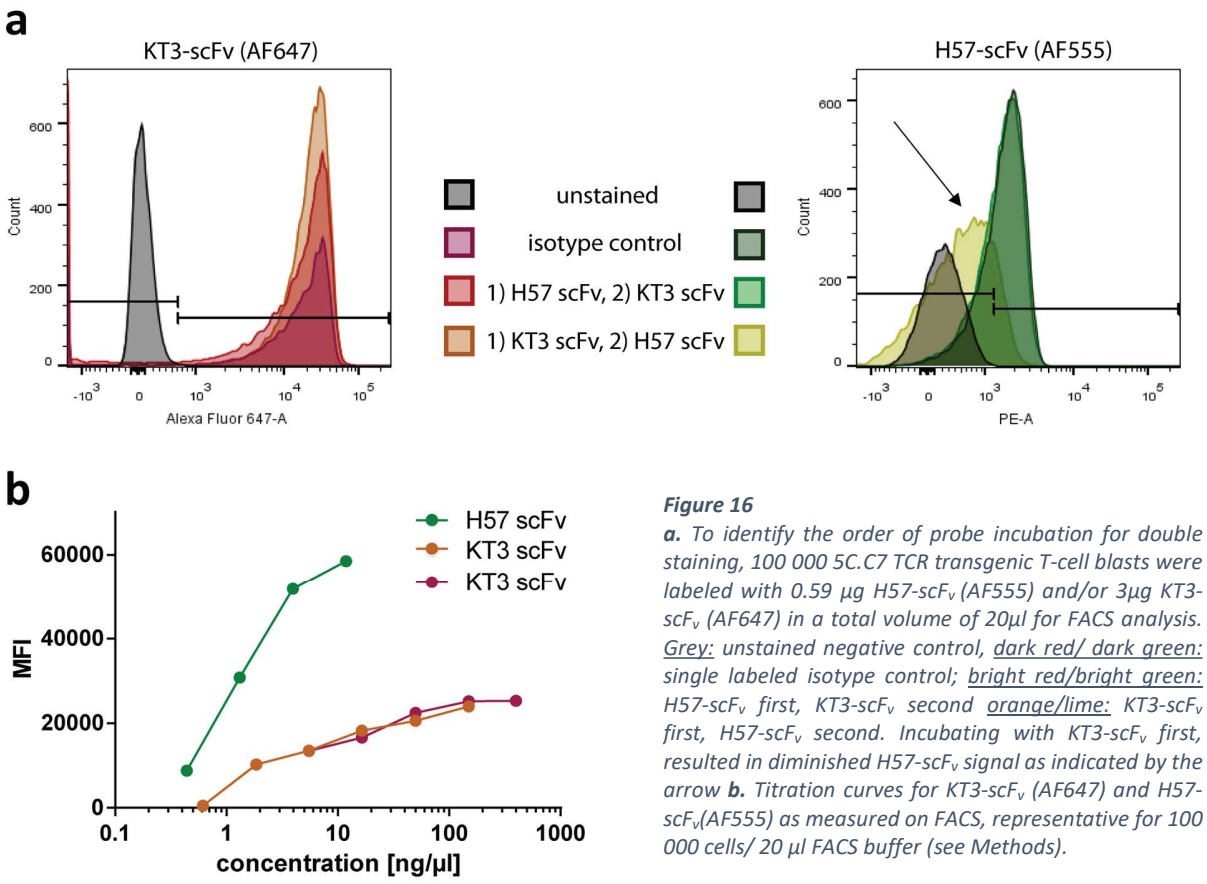

Figure 16
a. *To identify the order of probe incubation for double staining, 100 000 5C.C7 TCR transgenic T-cell blasts were labeled with 0.59 µg H57-scF_v (AF555) and/or 3µg KT3-scF_v (AF647) in a total volume of 20µl for FACS analysis. Grey: unstained negative control, dark red/ dark green: single labeled isotype control; bright red/bright green: H57-scF_v first, KT3-scF_v second orange/lime: KT3-scF_v first, H57-scF_v second. Incubating with KT3-scF_v first, resulted in diminished H57-scF_v signal as indicated by the arrow* ***b.*** *Titration curves for KT3-scF_v (AF647) and H57-scF_v(AF555) as measured on FACS, representative for 100 000 cells/ 20 µl FACS buffer (see Methods).*

Primary T-cells were isolated from the spleen of a moth cytochrome C peptide MCC 88-103 (MCC) specific, I-E^k restricted 5C.C7 TCR αβ transgenic mouse and expanded for five to seven days (see methods). In order to measure FRET within the TCR-CD3 complex upon confrontation with pMHC in a live-cell FRET imaging assay, I probed TCRβ and CD3ε subunits with the scF$_v$ FRET donor H57-scF$_v$ (AF555) and acceptor KT3-scF$_v$ (AF647) respectively. Interestingly FACS analysis of the co-stained T-cells showed a clear asymmetry in

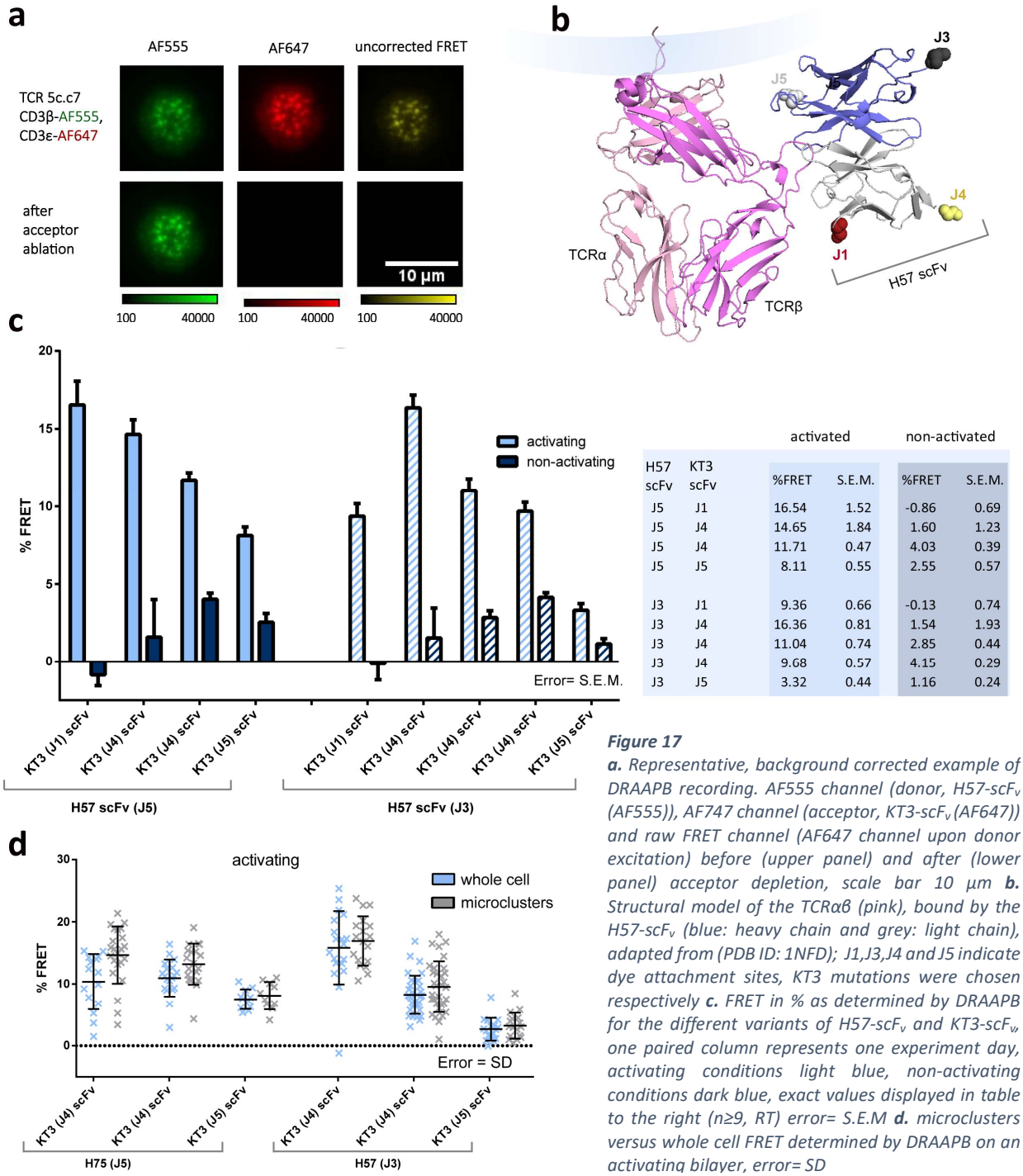

		activated		non-activated	
H57 scFv	KT3 scFv	%FRET	S.E.M.	%FRET	S.E.M.
J5	J1	16.54	1.52	-0.86	0.69
J5	J4	14.65	1.84	1.60	1.23
J5	J4	11.71	0.47	4.03	0.39
J5	J5	8.11	0.55	2.55	0.57
J3	J1	9.36	0.66	-0.13	0.74
J3	J4	16.36	0.81	1.54	1.93
J3	J4	11.04	0.74	2.85	0.44
J3	J4	9.68	0.57	4.15	0.29
J3	J5	3.32	0.44	1.16	0.24

Figure 17

a. *Representative, background corrected example of DRAAPB recording. AF555 channel (donor, H57-scF$_v$ (AF555)), AF747 channel (acceptor, KT3-scF$_v$ (AF647)) and raw FRET channel (AF647 channel upon donor excitation) before (upper panel) and after (lower panel) acceptor depletion, scale bar 10 µm* ***b.*** *Structural model of the TCRαβ (pink), bound by the H57-scF$_v$ (blue: heavy chain and grey: light chain), adapted from (PDB ID: 1NFD); J1,J3,J4 and J5 indicate dye attachment sites, KT3 mutations were chosen respectively* ***c.*** *FRET in % as determined by DRAAPB for the different variants of H57-scF$_v$ and KT3-scF$_v$, one paired column represents one experiment day, activating conditions light blue, non-activating conditions dark blue, exact values displayed in table to the right (n≥9, RT) error= S.E.M* ***d.*** *microclusters versus whole cell FRET determined by DRAAPB on an activating bilayer, error= SD*

binding efficiency between the single chain fragments, as the H57-scF$_v$ epitope had to be occupied prior to binding of KT3-scF$_v$, suggesting steric hindering (Figure 16, a). Consequently, all probes were incubated with H57-scF$_v$ alone prior to KT3-scF$_v$ addition. This resulted in 100% labeling efficiency of both fluorescent probes.

FRET Efficiency Differs between Activated and Non-Activated Conditions

Looking into T-cell recognition with the help of FRET allows us to detect molecular movements in the range of nanometers. We probed the TCR-CD3 complex with a donor and an acceptor fluorophore to see whether productive pMHC interaction would lead to differences in distance between the subunits.

Labeled T-cell blasts were presented with a functionalized glass supported lipid bilayer system, which mimics the APC surface, as it is decorated with MHC I-E^k loaded with the nominal MCC peptide as well as costimulatory molecule B7-1 and adhesion molecule ICAM-1. A similar SLB, lacking the stimulatory pMHC functioned as a negative control. DRAAPB was carried out at RT and complete acceptor ablation was verified for every image (Figure 17, a). I observed a significant increase of apparent FRET signal between the H57-scF$_v$ and KT3-scF$_v$ FRET probes in ensemble measurements, when exposing the labeled cells to their nominal pMHC as compared to the baseline FRET that occurred when cells adhered to a non-stimulatory bilayer.

The variety of fluorophore attachment positions as displayed in Figure 17, b and their combination led to different donor recovery values for every pair and I evaluated the most efficient partners.

H57(J3)-scF$_v$ together with KT3(J1)-scF$_v$ (9.36% activated versus 0.66% non-activated) or KT3(J4)-scF$_v$ (16.36% activated versus 0.81% non-activated) were used for further experiments because the KT3(J5)-scF$_v$ mutant, which displayed even higher FRET efficiencies (16.54% activated versus -0.86% non-activated) had very low expression yields throughout. Nevertheless, all combinations clearly linked the presence of stimulatory peptide MHC to an increased apparent TCRβ -CD3ε FRET value (Figure 17, c).

KT3 (J1)-scF$_v$ on both CD3ε units was outside of H57(J3)-scF$_v$s Förster radius in the non-activated, but not in the activated state of the T-cell. Controls with omitted bleach step showed a negligible median FRET of around 1-2%.

Image acquisition took place within 15 minutes after exposing the labeled cells to HBSS buffered bilayer at RT in respect of the experimentally evaluated range of $t_{1/2}$ for the scF$_v$s. No time bias could be detected when comparing first and last samples.

Most of the activated cells already displayed typical formation of high intensity areas that have been described as TCR-microclusters. These areas of first contact migrate to the cell center to build up the cSMAC after several minutes of productive pMHC-TCR interaction. Donor recovery values obtained for selectively chosen region of interests that featured microclustered TCRs were slightly higher than whole cell FRET for the respective cell (Figure 17, d).

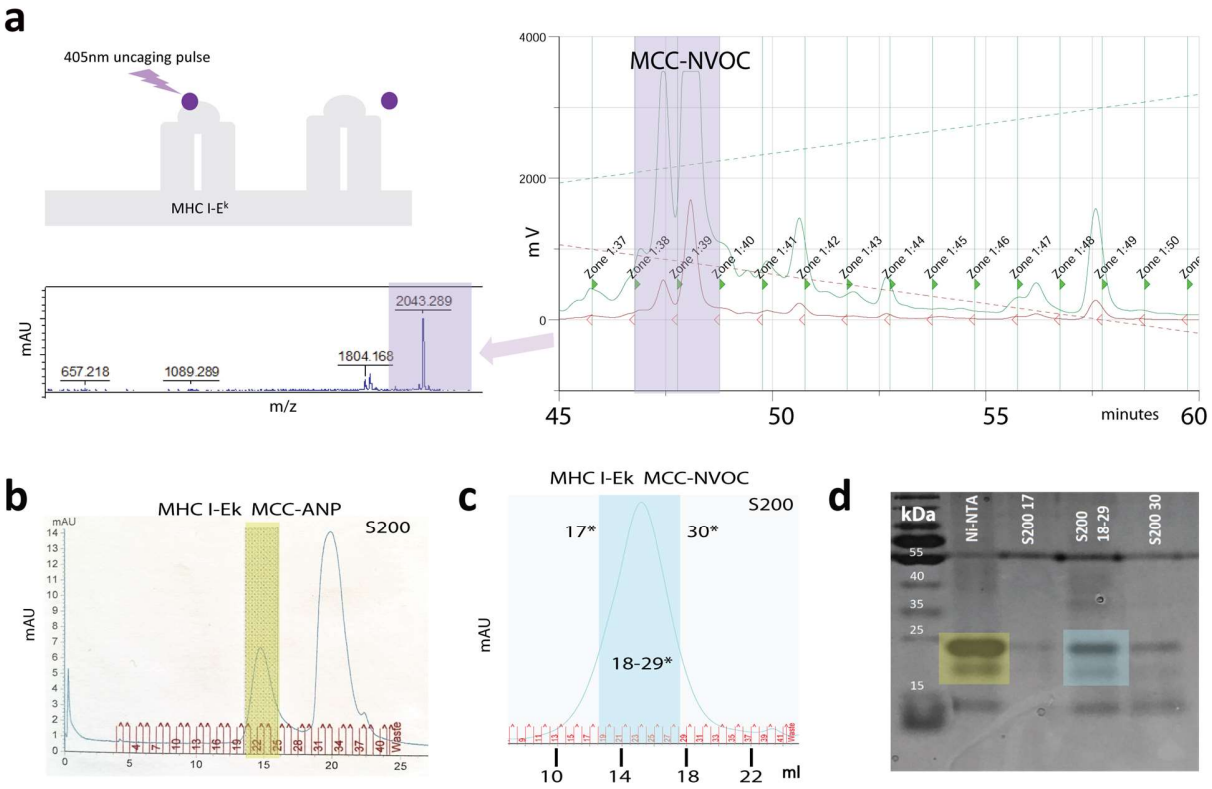

Figure 18
a. (top left) *schematic representation of the UV pulse uncaging the NVOC covered binding epitope of MHC I-Ek upon UV-pulse and* ***(top right)*** *reversed-phased HPLC chromatogram of MCC-NVOC peptide, 5ml fractions of indicated areas were analyzed via* ***(bottom left)*** *TOFMS, chosen fraction displaying the greatest MCC-NVOC (calculated MW=2043.04 Da) to MCC unmodified (1804 m/z) ratio* ***b.*** *FPLC (S200) purification of MHC I-E^k MCC-ANP refolded from its subunits MHC I-E^k α-12 and a β-0 after Ni-NTA column purification* ***c.*** *FPLC (S200) purification of I-E^k MCC-NVOC after exchange reaction* ***d.*** *corresponding SDS-PAGE under non-denaturating conditions. The double band indicates the presence of a smaller fraction of non-associated subunits. The band at 55kDa is a result of buffer contamination.*

Synchronizing Antigen Recognition by photouncaging of NVOC

As the lifetime of TCR-pMHC interactions at RT is approximated to be around one second for the 5C.C7 TCR, ensemble measurements only reflect the integrated signal of all TCRs facing the lipid bilayer. An ensemble of TCRs being in different states of interaction, as pre-bound, bound and post-bound reflected

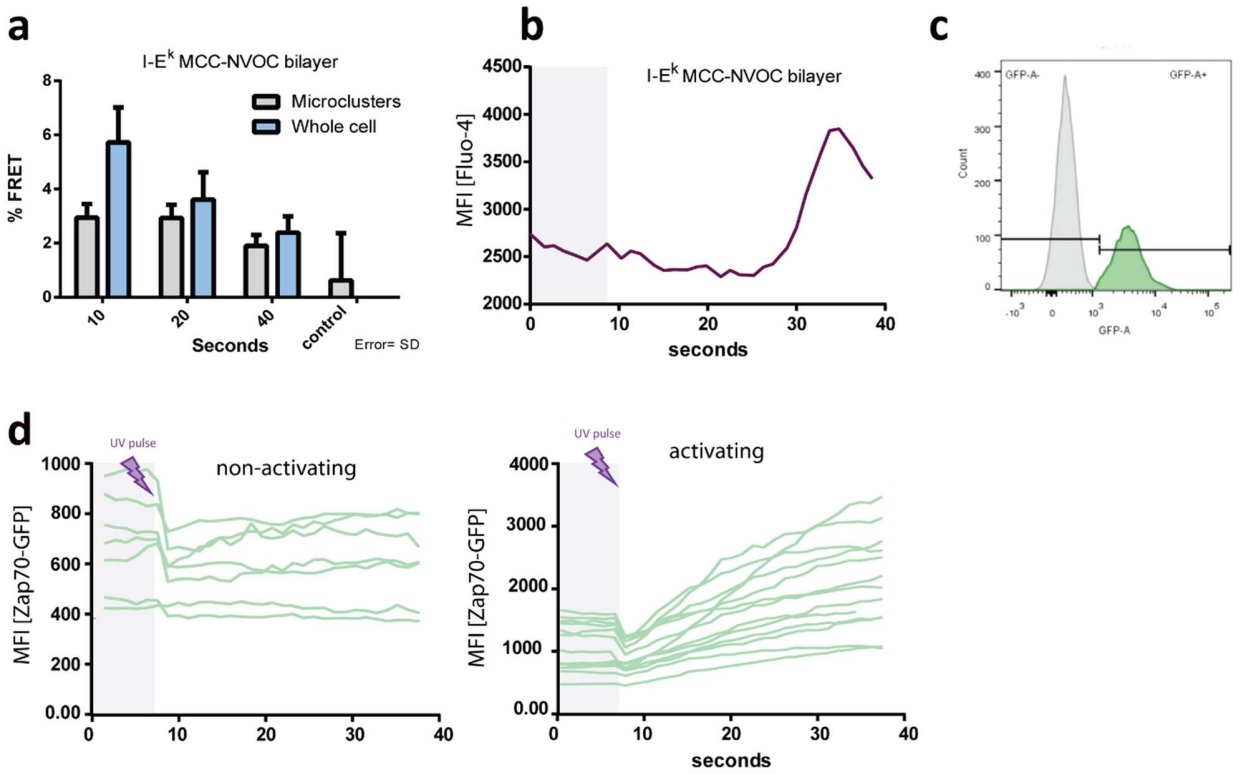

Figure 19

a. *FRET (in%) derived from DRAAPB on an I-E^k MCC-NVOC (MHC-NVOC) bilayer 10,20 and 40 seconds after UV uncaging pulse (n≥9, error=SD), control on non-activating bilayer (n=6, error=SD)* ***b.*** *Sensitized emission imaging (SEm) derived fluo-4 MFI (mean fluorescent intensity)I (representing cytoplasmic Ca^{2+} concentration) of a cell presented with an MCC-NVOC bilayer. UV-pulse was applied at timepoint 8.67 seconds as indicated by the grey area.* ***c.*** *FACS plot displaying the cell count of (green) ZAP70-GFP transfected as compared to (grey) an unselected control, transfection efficiency: 50%,* ***d.*** *SEm derived MFI of 488nm channel for ZAP70-GFP transfected T-cell blasts (every line represents one cell) on a* ***(left)*** *non-activating and* ***(right)*** *MCC-NVOC bilayer, UV uncaging pulse indicated*

by one single apparent FRET value. Hence, no conclusions could be drawn on whether the observed increase in FRET resulted from the initial binding events or later on, after recruitment of accessory activation factors. To synchronize TCR binding, I introduced a photo-cleavable caging entity into the system. 6-Nitroveratryloxycarbonyl (NVOC) attached to the 5C.C7 TCRs nominal peptide (further depicted as MCC-NVOC) inhibits interaction until the moiety is cleaved by applying a near UV-light pulse. This allowed me to instantaneously expose thousands of binding sites for TCR encounter after the cells already adhered to the bilayer.

The MCC-NVOC peptide was purified via HPLC and its integrity was confirmed using Time-of-flight mass spectrometry (TOFMS) (Figure 18, a). MHC I-E^k equipped with a His-tag was refolded from its subunits in presence of a placeholder (MCC-ANP) peptide and purified via a Ni-NTA column (Figure 18, b, d). Hereafter, MCC-ANP within the binding cleft was exchanged for MCC-NVOC. This was followed by purification via FPLC in the dark as well as PAGE (Figure 18, e). In order to test the MCC-NVOC bilayers ability to activate cells via an UV uncaging pulse, Fluo-4 stained cells were confronted with the platform and calcium flux

was measured via the GFP channel (488nm emission) (Figure 19, b). I conducted DRAAPB experiments on T-cells exposed to an I-E^k/MCC-NVOC, ICAM-1 and B7-1 containing bilayer (for simplicity depicted as NVOC bilayer) at the time points 10, 20 or 40 seconds after I applied an uncaging UV pulse. Even though FRET was increased after 10 seconds post uncaging, I did observe a decrease in apparent FRET after 40 seconds. Overall FRET values were considerably lower than the ones observed for the previously used activating I-E^k/MCC bilayer (Figure 19, a). However, similar to as previously reported for this FRET pair, not applying an uncaging pulse as well as applying one under non-activating conditions led to even less FRET efficiency.

Increase of FRET is Faster than ZAP70 Recruitment

These results indicated a dynamic shift in different FRET generating states of the TCR-CD3 complex. I therefore used sensitized emission imaging (SEm) which allowed me to monitor cells over a timespan of

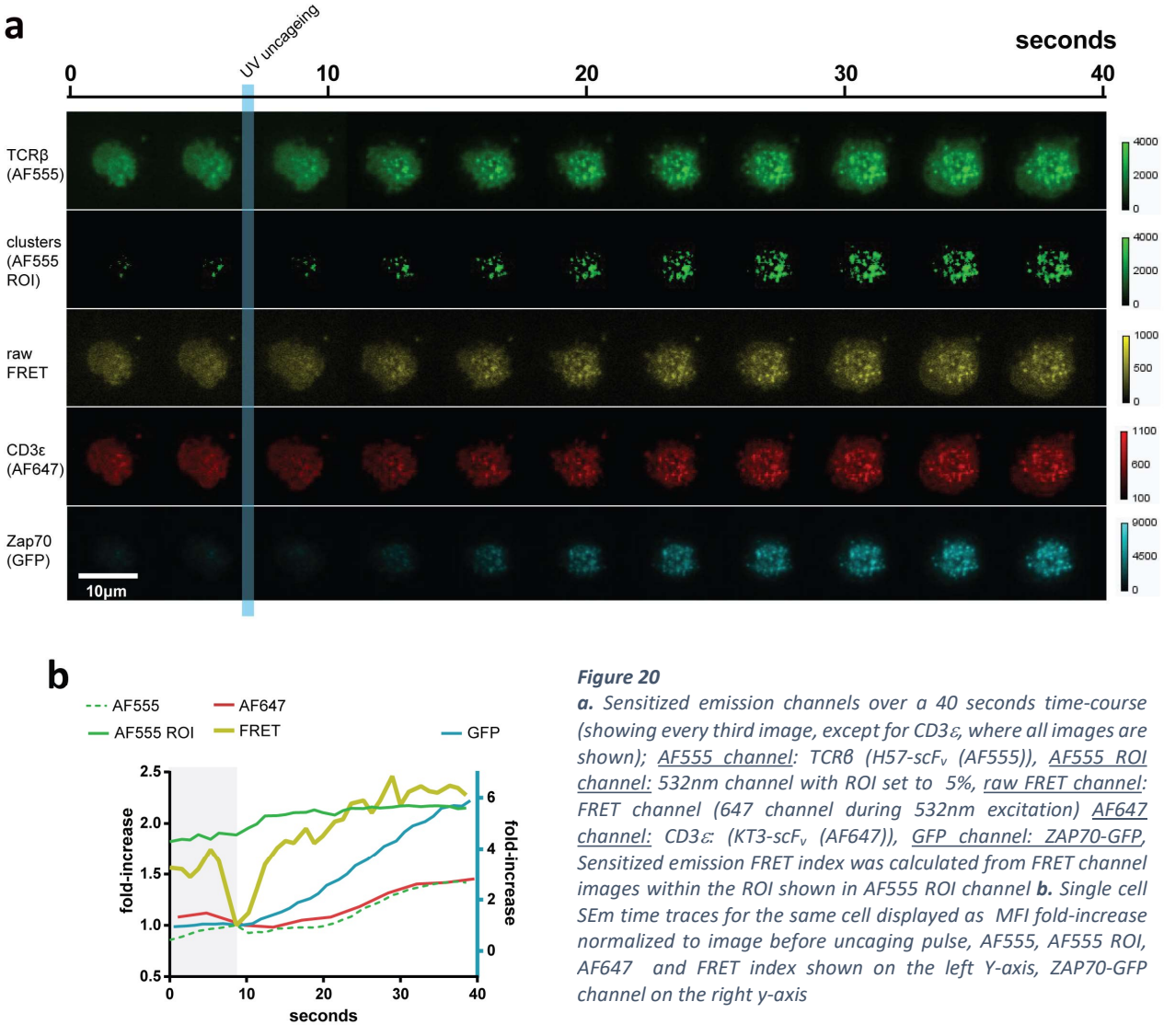

Figure 20

a. *Sensitized emission channels over a 40 seconds time-course (showing every third image, except for CD3ε, where all images are shown); AF555 channel: TCRβ (H57-scF$_v$ (AF555)), AF555 ROI channel: 532nm channel with ROI set to 5%, raw FRET channel: FRET channel (647 channel during 532nm excitation) AF647 channel: CD3ε: (KT3-scF$_v$ (AF647)), GFP channel: ZAP70-GFP, Sensitized emission FRET index was calculated from FRET channel images within the ROI shown in AF555 ROI channel* ***b.*** *Single cell SEm time traces for the same cell displayed as MFI fold-increase normalized to image before uncaging pulse, AF555, AF555 ROI, AF647 and FRET index shown on the left Y-axis, ZAP70-GFP channel on the right y-axis*

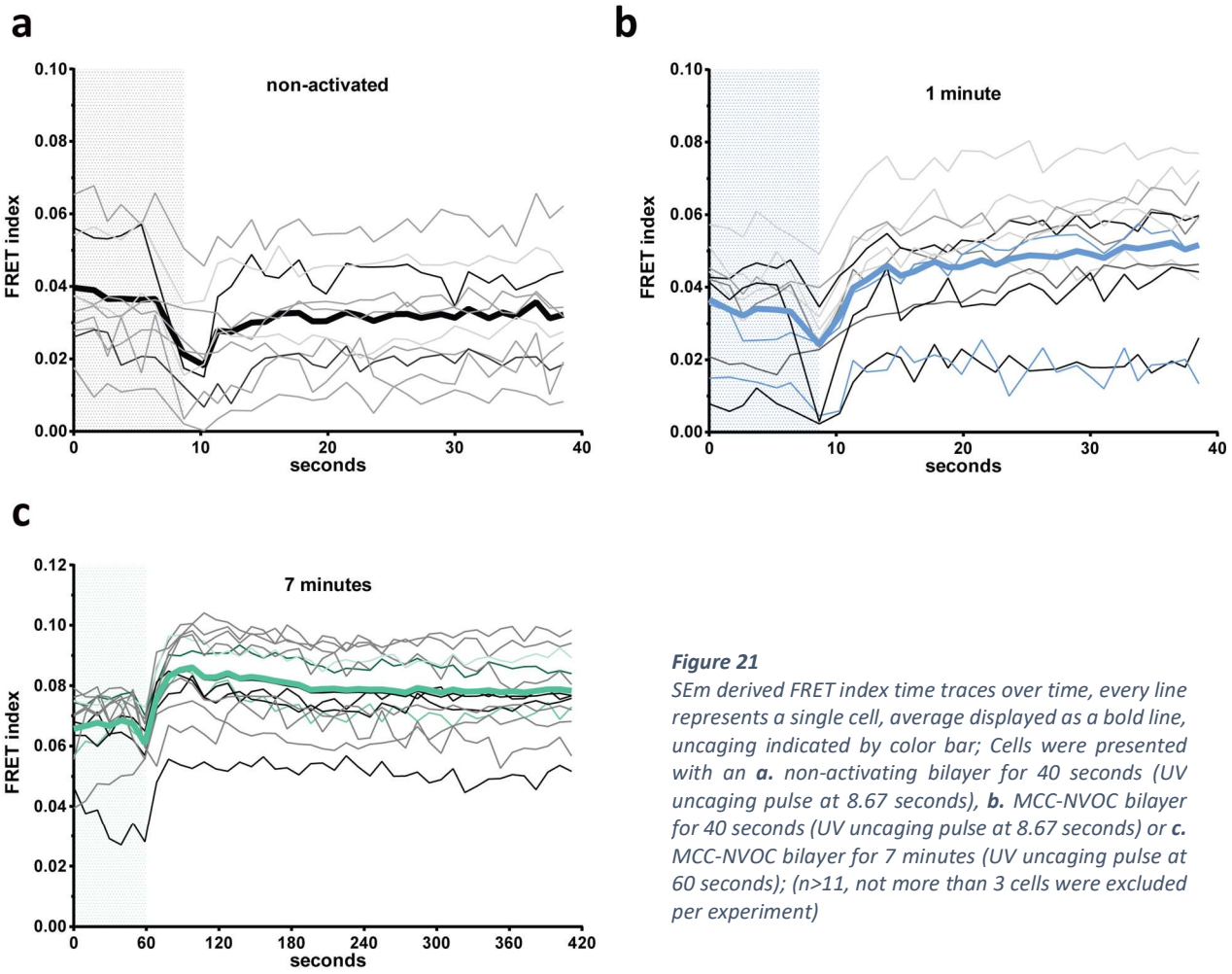

Figure 21
*SEm derived FRET index time traces over time, every line represents a single cell, average displayed as a bold line, uncaging indicated by color bar; Cells were presented with an **a.** non-activating bilayer for 40 seconds (UV uncaging pulse at 8.67 seconds), **b.** MCC-NVOC bilayer for 40 seconds (UV uncaging pulse at 8.67 seconds) or **c.** MCC-NVOC bilayer for 7 minutes (UV uncaging pulse at 60 seconds); (n>11, not more than 3 cells were excluded per experiment)*

seconds and even minutes by using of a low excitation laser power combined with longer exposure times. An example of all channels acquired throughout a time-course of 40 seconds is given in Figure 20,a.

SEm derived FRET index and MFI fold-increase for the same cell are displayed in Figure 20, b. Acceptor cross excitation, donor bleed-through and camera background was measured by acquisition of two additional controls for every experiment and taken into account when calculating apparent FRET using a custom made Matlab plugin (see Methods). Output of the program is one averaged FRET value for each given time point within a region of interest. The ROI was selected by excluding lower intensity values such as the background from calculation. Setting this ROI turned out to have a major effect on the FRET value, as I could only receive a positive FRET index when choosing the top 20% of highest intensity values of the images as a threshold for calculation. Those areas can be interpreted as TCR enriched regions, the so-called microclusters. Sensitized emission channels using a 5% threshold as shown in Figure 20, showed a mean FRET index increase of around 2% within the first 10 seconds after NVOC uncaging (Figure 21, a-c). These values remained elevated throughout the time span of 7 minutes even when cSMAC formed was observed

(Figure 21, c). Even though this effect could be observed at 37°C as well, faster molecular movement and unbinding of scF_v probes at this temperature complicated long measurements (data not shown).

To be able to monitor T-cell activation most TCR proximally, I transduced the transgenic murine T-cells with a ZAP70-GFP construct. This way, by using 488nm laser excitation in TIR mode, I aimed to observe recruitment of the tyrosine-kinase throughout the whole time of acquisition. Four days after ZAP70-GFP retrovirus transfection, comparison of cells expressing the functional fusion protein with a non-selected control showed a transfection efficiency of 27% (first batch) first and 50% (second batch) (Figure 19, c). GFP positive T-cells were selected manually using low intensity 488nm laser exposure. ZAP70-GFP transfected cells were presented with an NVOC SLB and the sensitized emission protocol was adapted in a way that FRET and ZAP70 recruitment could be evaluated for every time point (Figure 19, d).

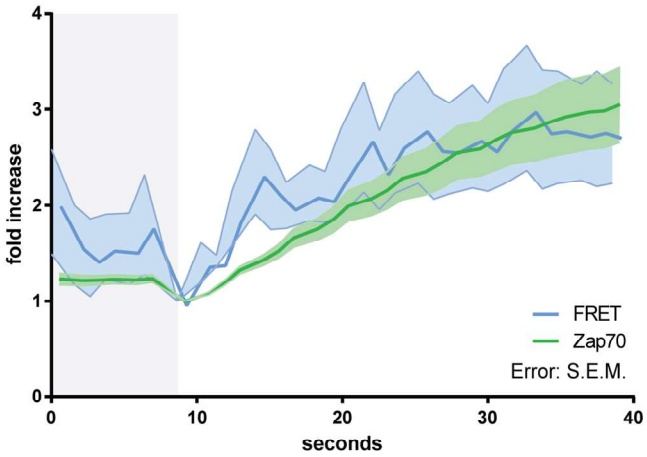

Figure 22
SEm derived FRET index (corrected FRET channel) and ZAP70 recruitment (GFP channel) for the same cell sample over a time course of 40 seconds, uncaging indicated by grey bar, values normalized to first image after UV uncaging pulse;(n=10, error=S.E.M.)

In order to rank the reorientation of the TCR-CD3 as reflected by an increased FRET index within the cellular signaling cascade, I compared the fold increase of FRET index post activation to the recruitment of the kinase to the cell surface. The data showed that FRET increase occurred slightly faster than ZAP70 recruitment (Figure 22). Unlike the FRET signal, which plateaued within the first 10 seconds, the ZAP70 signal continued to increase throughout the measurement (Figure 19, d).

Correlation of TCR density and FRET efficiency

One question that remains to be solved before interpreting this data is whether the FRET increase arose from movement within the subunits of the TCR-CD3 complex, or if it is the sole result of neighboring acceptors brought into close proximity due to elevated TCR concentration on activated T-cells. To tackle this problem, I took advantage of the fact that H57-scF_v (AF555) as a monovalent fluorescent probe for the TCRβ subunit can be used to calculate TCR surface densities in TIRF microscopy. TCR surface concentration is linearly correlated to fluorophore intensity[20,41].

To spatially dissect FRET from TCR density I generated FRET heatmaps from DRAABP images. Because of the fast molecular movement, the pixelwise values are not an accurate representation of the actual FRET efficiency, however, the overall pattern reflects the areas of high and low FRET activity. Cell areas of high

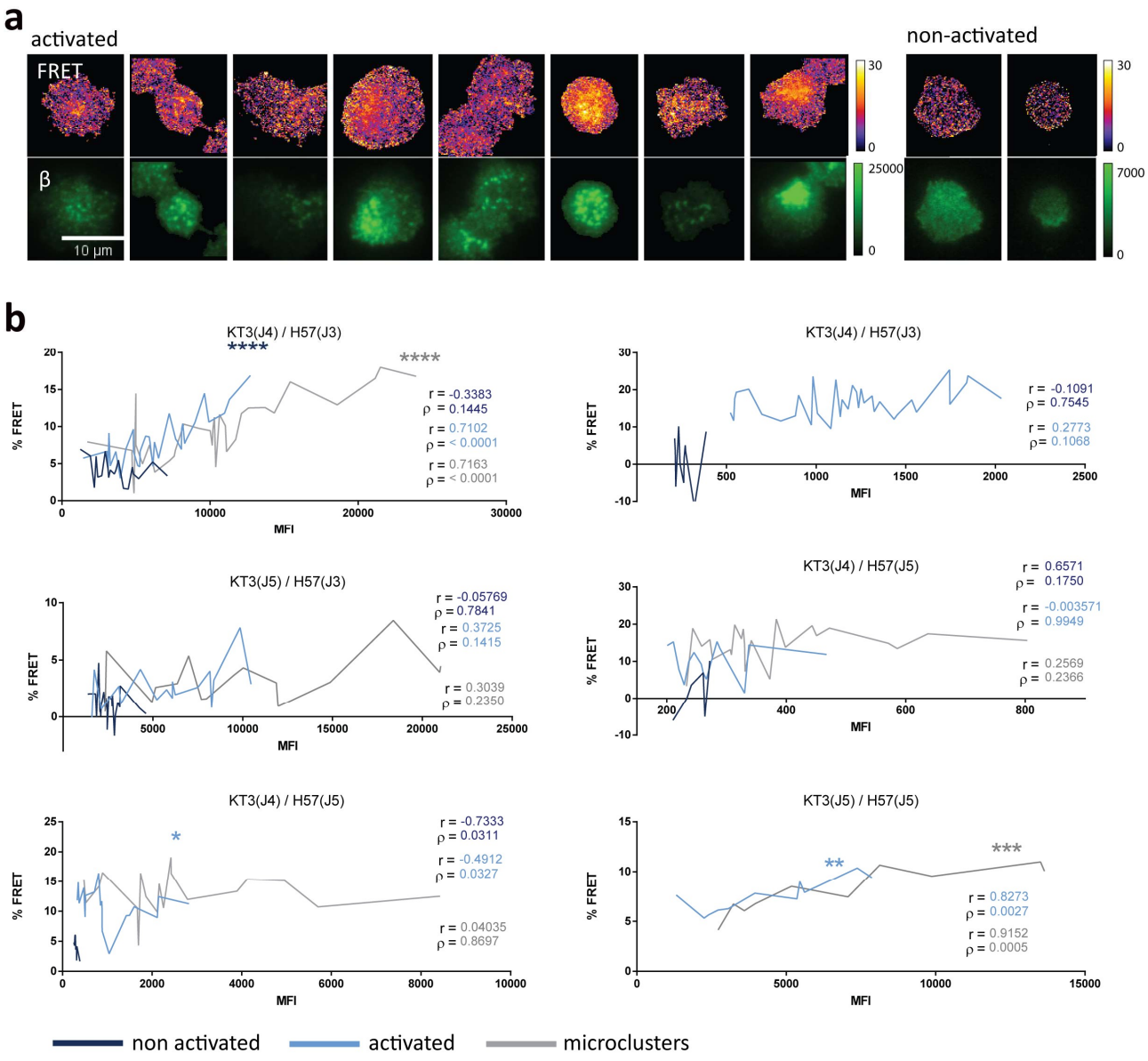

Figure 23

a. *FRET heatmaps from pixelwise DRAAPB calculation (upper panel) and corresponding cell in AF555 channel (TCRβ) on an activating (left) or a non-activating (right) bilayer, calibration bar 10 µm* ***b.*** *Apparent FRET values from DRAAPB , ranked according to the cells respective MFI of the unquenched donor image(AF555, post bleach image), each panel represents one experiment, different scF_v variants indicated, Spearman correlation stated for all graphs, significant correlation annotated with asteriks*

H57-scF$_v$ (AF555) intensity correlated with a high percentage apparent FRET (Figure 23, a) but seem to display slight aberrations in certain areas. No quantitative image correlation was performed.

I further ranked apparent FRET values of activated and non-activated cells according to their respective MFI of the unquenched donor image (TCRβ, AF555 channel) that directly correlates to TCR abundance. In two out of six experiments, positive Spearman correlation between TCR abundance and FRET was observed for both, whole cell and microclustered FRET. In four experiments, no positive correlation could be detected and one curve of the four residual experiments showed slight negative correlation. Overall, FRET efficiency seemed to be disconnected from mean TCR density in four out of six experiments in microclustered and whole cell areas (Figure 23, b). Non-activated cells (Figure 23, b, dark blue subset) do not recruit TCRs within microclusters that can be observed as high intensity donor areas and therefore barely result in MFIs similar to those of activated cells.

Finally, I tried to differentiate the signals on a temporal basis. To display the evolution of the signals in single cell sensitized emission, I normalized the MFI of each channel to its value prior to NVOC uncaging pulse at timepoint 7 (at 8.67 seconds). The MFI of the 532nm channel high-intensity areas (532nm ROI, representing microclusters) displayed after activation was normalized to the mean MFI before activation. Data from single molecule intensity measurements obtained in our lab indicated a surface density of 75 ± 24 molecules/μm^2 on the plasma membrane of living 5C.C7 specific T-cells [20] and a fold increase in of around 2-3 in microclustered areas. Both 40 seconds as well as 7-minute SEm time traces did not display more than 2-fold 532nm intensity increase (40 seconds n=8; 7 minutes n=13). The single cell time traces demonstrate that other than the rapid increase in SEm FRET index observed within the first few seconds, intensity values of both β and ε channels steadily rise throughout the measurement (Figure 24). However, none of the experiments conducted on SLBs decorated with an NVOC caged I-E^k could replicate the high FRET values observed when activating the T-cells with an uncaged molecule.

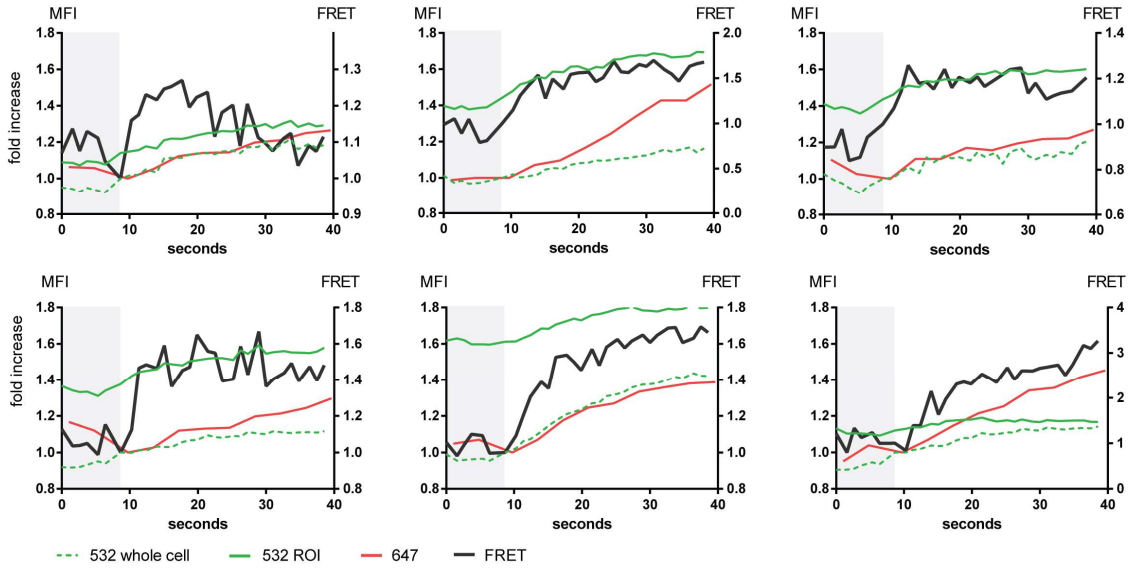

Figure 24

Single cell SEm time traces over a 40 seconds time-course for six example cells, MFI values normalized to last image before uncaging pulse, MFI index for AF555 channel (TCRβ), AF555 ROI channel (microclusters) and AF647 channel (CD3ε) shown on left y-axis, FRET index from SEm shown on the right y-axis, UV uncaging pulse indicated by grey bar

DISCUSSION

The High Specificity- Low Affinity Paradox

After decades of research focused on TCR mediated signaling, the question of how the T-cell distinguishes between irrelevant and nominal peptide in a matter of seconds despite low TCR-pMHC affinities remains. Several mechanisms including force-related, dimerization-based or affinity-associated models were suggested from observations under artificial condition. Most of the models proposed were focusing only on parts of the machinery. A stepping stone in terms of structural and functional analysis of the TCR complex is the complexity of the receptor itself, which consists of multiple transmembrane domains bearing subunits as well as additional coreceptors and cofactors that all seem to be part of the bigger picture. Structural analysis is complicated by the fact that the complex´s residence in the plasma membrane of a living cell is tied to the its function.

When a T-cell encounters an antigenic peptide presented in the context of a MHC molecule, the T-cell antigen receptor, together with costimulatory molecules interact to initiate the formation of an immunological synapse. When monitoring this process, we aim to create an environment that mimics the physiological scenario and are therefore bound to its natural constraints. Molecular imaging is minimally invasive and appears very well suited for this task especially when using very small probes for a live cell FRET assay. A multivalent probe such as a monoclonal antibody would lead to unwanted unspecific activation of the cell. This is why we opted to work with single chain antibodies derived from them.

Observations

We labeled TCR transgenic CD4 $^{+}$ T-cell blasts with scF_vs binding to the TCRβ and CD3ε subunits to assess FRET between the subunits. Our experiments show a three- to four-fold increase of the FRET signal when cells were activated by a SLB decorated with nominal peptide MHC. This can be interpreted as an integrated decrease of distance between the CD3ε units towards the TCRβ unit. Such behavior was observed in case of all fluorophore positions on our probes, tested with a Förster radius of 51Å.

To make further sense of these observations, we aimed to add a temporal component. Sensitized emission allows sub-second imaging of spatiotemporal dynamics within subunits of the T-cell antigen receptor of living T-cells. Using site-specifically labeled scF_v FRET probes together with TIR acquisition yield high spatial resolution whereas temporal resolution is mainly dependent on camera and microscope speed. This makes the method a powerful tool to monitor molecular movement in real time. We induced synchronized

antigen exposure by implementing a functionalized bilayer that can change its stimulatory properties with as little as a UV-pulse. Using SEm, we could assign the increase in FRET to the first seconds after pMHC encounter. The quantity of signal-generating TCRs after activation reached its equilibrium after 10 seconds and the effect did not recede even when cells displayed full cSMAC formation after seven minutes. Our FRET pair of choice did not yield apparent FRET in DRAAPB on non-activated cells but displayed a mean FRET of 9.4% on activated cells.

To establish an order of events in terms of the signaling machinery, we transfected CD4 $^{+}$ T-cells with a ZAP70-GFP construct. This way, recruitment of the first messenger to the membrane could be monitored during the experiment. The intracellular protein kinase ZAP70 is recruited to the TCR when it is given the chance to bind to biphosphorylated ITAMs of CD3εδ, CD3εγ and the CD3ζζ dimer to facilitate downstream signaling. We observed an almost similar onset of both FRET yields and ZAP70-GFP recruitment immediately after the cells had been exposed to their cognate peptide. Although the FRET value seemed to increase slightly faster, the amount of data was not sufficient to be tested for significance.

Method Limitations and Problems

KT3 binds both of the CD3ε subunits

Precisely targeting the protein of interest and conjugating the fluorophores in a stoichiometric manner is of high priority. In this approach, underlabeled FRET donor could lead to overestimation of FRET whereas the opposite occurs when underlabeling the acceptor.

KT3 binds to both CD3ε subunits and therefore renders the FRET donor : acceptor ratio as 1:2. This must be taken into account when calculating distances from apparent FRET. Even though it was proposed, that KT3 (mAb) preferably binds to CD3εδ rather than CD3εγ [110], titration profiles and TOCCSL (thinning out clusters while conserving stoichiometric labeling) experiments suggest that both epitopes are occupied in saturation. Given the structural data that the distances of CD3εγ and CD3εδ towards TCRβ is not the same [5,52,57], it is likely that contribution of the FRET acceptors to the signal is also not equal. In the current model, CD3εδ is further away of TCRβ, facing to the other side of the TCR complex whereas CD3εγ is thought to directly contact the TCRβ through its FG-loop which is target of our FRET donor H57-scF$_v$ [66,67]. Labeling with the KT3-scF$_v$, that binds to the CD3ε, led to steric hindrance of H57-scF$_v$ in our hands, which further verifies the close proximity of the epitopes. Kuhns and Davis observed reduced CD3ε binding of the CD3ε binding 2C11 Ab after H57 antibody incubation [126]. Here, half of 2C11 binding was retained, speaking for a skewed labeling towards CD3εγ. This fact could be exploited as one might be able to specifically label CD3εγ only.

Repeating FRET experiments under these conditions would allow us to dissect apparent FRET contributions of the two subunits. Epitope specific binding of KJ25-scF$_v$, which should be created in order to control activation at the site of peptide encounter as well as for implementing a second TCRβ binding FRET partner, could not be retained in the truncated version of the antibody even though the complete sequence was obtained from RACE PCR. Adjusting linker length domain composition or even sequence length can be a strategy to target troubleshooting[127].

Proximity FRET

FRET radii of the different fluorophore pairs and inter-dye distances of the probes should be of consideration in order to achieve proper output without risking distortion of the signal by bystander/proximity FRET. This effect can be caused by nearby acceptors and its contribution to overall FRET is dependent on acceptor concentration. The magnitude of this error within the confines of a plasma membrane was calculated by Wolber and Hudson [128,129] and a simulation based on their concept was carried out by King[130]. The model estimates the likelihood of random encounters at a certain concentration of membrane proteins using Monte Carlo simulation. Yet, experimentally evaluating the transient concentrations of acceptors during accumulation of TCR complexes is elaborate. Because of the rapid decay of the evanescent field wave in z direction, excitation and therefore intensity of a fluorophore near z=0 is not the same as one a few nanometers into the sample. Comparison of mean intensities in between fluorophore surface densities are only legitimate, because all of the fluorophores applied are restricted to the plasma membrane. However, reported endocytosis of TCR complexes in the central SMAC[37] could have led to intensity loss in that area due to the alternated z position in TIR field.

Another factor that influences both, excitation by the evanescent field and FRET is the geometrical orientation of the transition dipole moment of the fluorophore. This orientation factor (κ^2) describes configuration of the dyes towards each other and could be affected by a restricted angle of movement. In the case of our probes, free dye rotation for both fluorophores, was verified by anisotropy measurements[1].

Brameshuber and colleagues as well conducted Monte Carlo simulation and complementing SLB experiments for the TCR molecule. Singe molecule intensities that were used to estimate surface concentrations were obtained by sub stochiometric labeling and TOCCSL [20,131].

Those experiments showed the number of TCRs found on inactivated 5C.C7 transgenic T-cells to be 75±24 molecules/µm. This contradicts the previously proposed the 140 molecules/µm^2 TCR surface density for unstimulated cells, calculated from single molecule intensity averaging as well as the 190 molecules/µm^2 for activating cells with enrichment up to 1200 TCRs per µm^2 in microclusters proposed by Lilemeyer[88]. Of

note, even though no FRET events could be observed between two neighboring TCRαβ dimers when using a 8.3 nm Förster radius, both of the CD3ε subunits probed with KT3-scF$_v$ conjugated FRET fluorophores resulted in around 15% FRET for a 1:3 donor: acceptor ratio[20] . As TCR surface density measurements on the cell membrane were not undertaken in context of this project, I correlated measured initial MFIs to already proposed values and roughly estimated the concentrations from intensity fold-increase. However, one has to take into account that the occurrence of FRET is quenching the donor fluorophore intensity used for those calculations to a certain extent. DRAAPB measurement on NVOC activating bilayers indicated this to be less than 10% in our case, rendering major underestimations of TCR densities unlikely. Our data showed 2-fold increase of FRET in accumulated areas 40 and up to 420 seconds post pMHC exposure and around 4-fold increase in DRAAPB experiments in comparison with the unstimulated bilayer control. These results mirror the outcomes of Brameshuber et al. where TCR densities were approximated to be 300 molecules per µm^2 within the microclusters. With a donor : acceptor stoichiometry of 1:2, the number of acceptors on the cell surface doubles up to 600 mol/µm^2. Unfortunately, simulations undertaken by Brameshuber et al. for 5C.C7 transgenic T-cells did not exceed a density of 200 mol/µm^2. In these experiments the bystander FRET was calculated to be 1% for AF555 and AF647[87]. The predicted contribution of bystander FRET for monomers without considering restrictive angles is in the range of 5% for these acceptor densities and for a Förster radius of 53nm [128]. However, surface densities for KT3-scF$_v$ labeled CD3ε molecules must be determined and computational simulation adapted to the parameters of TCR-CD3 complex before making any further conclusions.

DRAAPB experiments on activating bilayers showed significantly higher FRET values than the ones conducted on NVOC caged SLBs as well as SEm calculated indices. If accumulation of TCRs during activation would be the reason for the observed increase of FRET, those values should be reproducible on an NVOC bilayer despite incomplete uncaging 7 minutes after exposure. If engagement with pMHC leads to a conformational or structural rearrangement that is reflected by FRET increase, incomplete NVOC uncaging or diffusion of unaffected, caged molecules from outside the ROI could be responsible for the lower FRET indices.

TCRβ conjugated fluorophore intensities compared to the cell´s respective FRET yields in DRAAPB did not show significant correlation in most of the experiments. The linear regression indicates that major proximity effects can be ruled out in synaptic areas of high TCR densities. As it was shown that TCR engagement is not necessarily reflected by high TCR densities[132] , I generated heatmaps of the FRET values in DRAAPB images in order to correlate FRET and TCR abundance spatially. Unfortunately, one cannot rely

on individual FRET values derived from pixelwise calculations, because minimal movement of the molecules during acquisitions could lead to over- or underestimation.

Nevertheless, we can compare the overall FRET distribution in regards to prominent surface structures like microclusters or the cSMAC, where high TCR density areas transpire as regions of high FRET activity (Figure 23, a), as was also observed when calculating apparent FRET from DRAAPB in the microclusters (Figure 17, d). The images showed inhomogeneous distribution of FRET signal-generating probes within one cell that did only reflect the areas of high TCR density to a certain extent. Additionally, the responsiveness of the cells varied greatly within the cell population.

Perspectives

The attempt of painting a picture

To understand the contribution of the TCR´s various features to this complex signaling machinery, one must not only understand their structure, but also their purpose. This might be easier when looking at the αβ TCRs closest relative the γδ TCR. This simpler relative can be found on intraepithelial lymphocytes (IELs) in gut epithelia and is thought to recognize phosphorylated and lipid antigens. The γδ TCR does not necessarily need MHC for activation[133]. It´s mechanism of activation is quite different from that of the αβ TCRs but besides the fact that most γδ TCRs assemble with two CD3εγ heterodimers instead of one CD3εγ and one CD3εδ many structural features are conserved[134]. The γδ TCR CDRs are germline encoded and therefore less variable leading to a limited number of recognized antigens. The advanced αβ TCR evolved to precisely distinguish between almost similar antigenic sources, still affinities of αβ TCR-pMHC interactions were shown to be two orders of magnitude below of those measured for the γδ TCR in average (K_D≈ 10nM and K_D≈ 100nM respectively) [3,41,133]. One could speculate that the underlying mechanism is a kinetic proofreading model where mechanistic switches present intermediate steps that are needed to overcome a high-energy transition state. Only agonist in contrast to antagonist peptide ligands are proposed to fulfil requirements in order to cross the point of no return and initiate phosphorylation of ITAMs[135,136].

The FG-loop on αβ T-cells evolved at the same time as the γ and δ CD3 subunits diverged from the same progenitor CD3. Due to its adjacency to CD3εγ, it might act like an off-centered torque, adding polarity to the CD3ε subunits. A certain docking geometry seems to be of importance in antigen recognition[2,58,59] and forces are speculated to induce T-cell activation[71]. The FG-loop is also thought to exert pushing or pulling motion onto the CD3 in order to relay stimuli, maybe leading to stretching of TCRα transmembrane helices

and dissociation [93] followed by apposition of the ζ chains[137]. This might be the path the information takes on its way to the insides of the cell and could be represented by the findings presented in this work . Where exactly the critical point of no return manages to set a cutoff- between stimulating and unimportant ligands is yet to be shown.

Lateral pushing and pulling forces, acted out by the T-cell upon encounter with its cognate pMHC that were as well detected using a biomechanical force probe (BFP)[138], supporting a "permissive geometry" model where the CD3 heterodimers are thought to rotate in respect to the αβ TCR[139,140]. This would out rule the piston-like vertical displacement model of activation [64,141].

Taken together the results indicate that some kind of movement between the CD3 and TCR subunits of the receptor complex plays a role in productive signaling that might be the cause of FRET increase upon engagement. The extent of movement as well as whether the source is TCR cooperativity, subunit displacement or conformational change cannot be deciphered yet.

An effective single molecule FRET yield, which can be translated to actual distance, together with a structural model would provide many insights regarding the source of these dynamics. In combination with site-specific probe conjugation, the direction of the transition can be evaluated and incorporated into the model of T-cell activation mechanism.

Outlook

This work provides a glimpse into TCR-CD3 dynamics on a population level and even though results point towards changes in the receptors structure or arrangement, further investigation need to be undertaken to generate information about the origin of FRET increase upon TCR pMHC engagement.

To evaluate the uncaging efficiency of the pMHC-NVOC, an UV-pulse can be applied to a labeled pMHC-NVOC molecule in solution, uncaging can be verified via HPLC and correlated to fluorophore bleaching. FRET efficiency can be measured as a means of pMHC-TCR binding as shown in Huppa 2010[41]. Here, SLB harboring pMHC-NVOC conjugated to a FRET acceptor was uncaged in the presence of H57-scF$_v$ donor conjugated lymphocytes. This FRET system can be alternatively used to evaluate the uncaging efficiency of a NVOC-pMHC SLB upon UV-exposure. If FRET efficiency does not recede when replacing a certain amount of pMHC on an SLB with pMHC-NVOC and applying an UV-uncaging pulse prior to T-cell exposure, epitopes should be accessible for binding. However, rebinding events should be excluded. A functional KJ25-scF$_v$ could help to investigate those events, as it is small enough to enter the IS and could occupy the TCRβ binding cleft. Next, one should undertake single molecule FRET experiment using a FRET pair with a slightly larger R_0 to evaluate the effect of FRET derived from molecular crowding. Here specific labeling of

the CD3ε would have the advantage of minimize heterogeneity of signal generating partners. Overall, the presented method can provide spatiotemporal information to characterize dynamic movements in nm range on a single cell basis. However, more computational effort must be undertaken to analyze great number of obtained data in a qualitative way.

Once a working platform for sensitized emission time track experiments is established, one could investigate the permanence of the altered TCR complex state. This could be achieved by adding an agent or force that disrupts TCR-pMHC engagement. This way we might be able to answer the question of whether a possible switch reflects movement within the TCR CD3 complex during activation or resembles an inactivated state of the receptor.

To conclude, there is more work necessary before unravelling the signaling mechanistic behind one of the immune systems most important receptor and the interplay of its constituents. In the era of targeted immuno- and gene therapy, understanding molecular and cellular interplay of adaptive immunity is substantial for medical progress.

ABBREVATIONS

ACE – acceptor cross excitation
AF – Alexa Fluor fluorescent dye (Thermo Scientific)
AIRE – Autoimmune regulator
APC – antigen presenting cell
β2m – β2-microglobulin, light chain of MHC class I molecules
B7 – co-stimulatory molecule
BG – background
Cα/Cβ - TCR extracellular constant domain α /β
CD – cluster of differentiation, classification determinant for cell surface molecules
CDR – complementary determining region
cTEC – cortical thymic epithelial cell
CTLA-4 – cytotoxic T-lymphocyte-associated protein 4, co-inhibitory molecule
DBT – donor bleed through
DC – dendritic cell
ddH_2O – doubly distilled water
DEPC – diethylpyrocarbonat, used to inactivate RNases (Quality Biological)
DMEM – Dulbecco`s modified Eagle`s medium (Sigma)
DNA – deoxyribonucleic acid
DOL - degree of labeling
DRAAPB - donor recovery after acceptor photobleaching
E – absorption ad maximum measured by spectrophotometry
ECD – extracellular domains
E. coli – *Escherichia coli*
EDTA – ethylenediaminetetraacetic acid (Roth)
EM – electron microscopy
ER – endoplasmic reticulum
FACS – fluorescence-activate cell sorting
FCS – fetal calf serum (Sigma)
FPLC – fast performance liquid chromatography
FRET – Förster resonance energy transfer
GFP – green fluorescent protein
GuHCl – Guanidiniumhydrochloride (AppliChem)
GSP – gene specific primer
GSSG – glutathione disulfide (Thermo Scientific)
HBSS – Hank´s Balanced Salt Solution (Gibco)
HEPES – 4-(2-hydroxyethyl)-1-piperazineethanesulfonic acid
HPLC – high performance liquid chromatography
IB – inclusion bodies
ICAM-1 – intercellular adhesion molecule 1
IEL – intraepithelial lymphocyte
Ig – immunoglobulin
IL-2 – interleukin-2, cytokine
IPTG – isopropyl β-D-1-thiogalactopyranoside (Thermo Scientific)
IP_3 – messenger Inositol (1,4,5) triphosphate
IS – immunological synapse
ITAM – immunoreceptor tyrosine-based activation motif
K_D – dissociation constant
LAT – linker for the activation of T-cells
LB – lysogeny broth, standard medium for bacteria
Lck – lymphocyte-specific protein kinase
LPS – lipopolysaccharides
mAb – monoclonal antibody
MAPK – mitogen-activated protein kinase
MCC – moth cytochrome C peptide (amino acids 88-103)
MDA – Multi-Dimensional Acquisition
MFI - mean fluorescent intensity (quantification unit of fluorescent parameter)
MHC – main histocompatibility complex
mTEC – medullar thymic epithelial cell
MWCO – molecular weight cutoff
NFAT – nuclear factor of activated T-cells
NF-kB – nuclear factor kappa β
NHS – succinimidyl
Ni-DOGS NTA - 1,2-dioleoyl-sn-glycero-3-(N(5-amino-1-carboxypenyl)iminodiacetic acid) succinyl nickel salt (Avanti Polar Lipids)
NSOM – near-field scanning optical microscopy
NVOC – Nitroveratryloxycarbonyl
OD – optical density
PALM – photoactivated localization microscopy
PAMPR – pathogen associated molecular pattern receptor
PBS – phosphate-buffered saline
PIP_2 – Phosphoinositol (4,5) bisphosphate
PKCΘ – protein kinase C theta
PLCγ – phosphoinositide phospholipase phospholipase C isoenzyme γ
pMHC – peptide presented via the MHC complex
POPC – 1-palmitoyl-2-oleoyl-sn-glycero-3-phosphocholine (Avanti Polar Lipids)
ROI – region of interest
PRR – pattern-recognition receptors
PRS – a proline rich sequence of the CD3ε subunits
PSG – Penicillin-Streptomycin glutamine (Gibco)
RACE – rapid amplification of cDNA Ends with polymerase chain reaction
RAG – recombination-activating genes
RT – room temperature
scF_v – single-chain variable fragment
SDS-PAGE – Sodiumdodecylsulfate Polyacrylamidegel
SEm – sensitized emission imaging
SIM – structured illumination microscopy
SLB – supported lipid bilayer
SMAC – supramolecular activation cluster
SN – supernatant
SOP – step-out primer
SPR – surface plasmon resonance
STORM – stochastic optical reconstruction microscopy
TCEP – tris(2-carboxyethyl) phosphine hydrochloride (Roth)
TCR – T-cell antigen receptor
TFA – trifluoroacetic acid
TGF-β1 – transforming growth factor beta 1
TIR – total internal reflection
TMD – transmembrane domain
TNF-α – tumor necrosis factor alpha
TOCCSL – thinning out clusters while conserving stoichiometric labeling
TOFMS – Time-of-flight mass spectrometry
Treg – regulatory T-cell
TRIS – tris(hydroxymethyl)aminomethane buffer (Roth)
TSO – template switch oligo
$t_{1/2}$ – half-life binding time
Vα /Vβ – TCR extracellular variable domain α /β
v/v – volume for volume percentage
ZAP70 – zeta-chain-associated protein of 70kD

KJ25- single chain fragment

T7 Promoter, **NdeI**,START, Heavy Chain, Linker, Light Chain, **BamHI**, stop, stop, **HindIII**, T7 Terminator

TAATACGACTCACTATAGGG**a**catATG
CAGGTGCAGCTGAAGGAGTCAGGACCTGGCCTGGTGCAGCCCTCACAAACCCTGTCTCTGACCTGCACTGT
CTCTGGGTTCGCATTAACTGACCATGCTGTACACTGGGTCCGCCAGCCTTCAGGAAAAGGTCTGGAGTGGA
TGGGAATAATATGGAGTGATGGAAGCACTGATTATAATTCACCTCTGAAATCCCGTGTCACCATCAGCCGT
GACACCTCCATGAGCCAAGTTTCCTTAAAACTGAACAATCTGCAAACCGAGGACACAGCCATGTATTACTG
TGCCCGTCGTCATAGCGGATATCGTTACTTCGATTTCTGGGGCCAGGGGACCCAGGTCACCGTCTCCTCAG
CCGGTGGAGGCGGTTCTGGTGGCGGAGGTTCTGGAGGTGGCGGTTCTGACATCATGATGACCCAGTCTCCA
TCAAGCCTGAGTGTGTCAGCAGGAGAGAAAGCCACTATTACTTGCAAGTCCAGTCAGAGTCTTTTCCACAG
TAACACCAACAAGAACTACCTGAACTGGTACCTGCAGAAGCCAGGCCAGTCTCCTAAACTGCTGATCTATT
ATGCATCCACTCGTCATAATGGCGTCCCTGATCGCTTCATAGGCAGTGGATCTGGGACAGATTTCACTCTG
ACCATCAGCAGTGTCCAGGAGGAAGACCTGGCAGATTATTACTGTCAGCAGTGGCATACCTACCCATACAC
GTTCGGAGGTGGCACCAAACTGGAGATCAAACGGGCT**ggatcc**taataa**aagctt**ACCGCTGAGCAATAAC
TAGC

H57- J5/J3 single chain fragment

start, Heavy Chain, Linker, Light Chain, stop,

```
60  atg tct gaa gtt tac ctg gtg gag tca ggg gga gat tta gtg cag cct gga agt tcc ctg
      M   S   E   V   Y   L   V   E   S   G   G   D   L   V   Q   P   G   S   S   L
120 aaa gtc tcc tgt gca gcc tct gga ttc acc ttc*agt*gac ttc tgg atg tac tgg gtc cgc
      K   V   S   C   A   A   S   G   F   T   F   C   D   F   W   M   Y   W   V   R
180 cag gct cca ggg aag ggg ctg gag tgg gtt ggt aga att aaa aac ata cct aat aat tat
      Q   A   P   G   K   G   L   E   W   V   G   R   I   K   N   I   P   N   N   Y
240 gca aca gaa tat gcg gat tcc gtg aga ggc aga ttc acc atc tca aga gac gac tca aga
      A   T   E   Y   A   D   S   V   R   G   R   F   T   I   S   R   D   D   S   R
300 aac agc atc tat ctg caa atg aat agg tta aga gtc gat gac aca gcc att tat tac tgt
      N   S   I   Y   L   Q   M   N   R   L   R   V   D   D   T   A   I   Y   Y   C
360 act aga gcc ggg agg ttc gac cac ttc gat tac tgg ggc caa gga acc atg gtc acc gtc
      T   R   A   G   R   F   D   H   F   D   Y   W   G   Q   G   T   M   V   T   V
420 tcc*tgt*gcc ggc gga ggc gga tcc ggt ggt ggc gga tct gga ggt ggc gga agc tat gag
      S   C   A   G   G   G   G   S   G   G   G   G   S   G   G   G   G   S   Y   E
480 ctg atc caa cca tct tca gca tca gtc act gta gga gag acg gtc aaa atc act tgc tct
      L   I   Q   P   S   S   A   S   V   T   V   G   E   T   V   K   I   T   C   S
540 ggg gac cag ttg cca aaa aat ttt gct tat tgg ttt cag caa aag tca gac aag aac att
      G   D   Q   L   P   K   N   F   A   Y   W   F   Q   Q   K   S   D   K   N   I
600 tta cta cta ata tac atg gat aat aag cga cca tca ggg atc cca gaa cga ttc tgt ggg
      L   L   L   I   Y   M   D   N   K   R   P   S   G   I   P   E   R   F   C   G
660 tcc act tca ggt aca aca gcc acc ttg acc atc agt gga gcc cag cct gag gat gag gct
      S   T   S   G   T   T   A   T   L   T   I   S   G   A   Q   P   E   D   E   A
720 gcc tat tac tgt ttg tct tca tat ggt gat aat aac gat tta gtt ttt ggc agc gga acc
      A   Y   Y   C   L   S   S   Y   G   D   N   N   D   L   V   F   G   S   G   T
780 cag ctc acc gtc cta cgt gga taa
      Q   L   T   V   L   R   G   -
```

KT3- J5/J1/J4 single chain fragment

start, Heavy Chain, Linker, Light Chain, stop,

```
60  atg gag gtg tac ctg gta gag tct ggg ggc ggt tta gtg cag cct ggc ggg tcc gtg aaa
      M   E   V   Y   L   V   E   S   G   G   G   L   V   Q   P   G   G   S   V   K
120 ctc tcc tgt tca gcc tca gga ttc act ttc*tgt*acc ttt cca atg gcc tgg gtc cgc cag
      L   S   C   S   A   S   G   F   T   F   C   T   F   P   M   A   W   V   R   Q
180 gct cca acg cag ggt ctg cag tgg gtc gca acc ctt agt cct agt ggt gat agc act tac
      A   P   T   Q   G   L   Q   W   V   A   T   L   S   P   S   G   D   S   T   Y
240 tat cgc gat tcc gtg aag ggc cgc ttc act atc tcc cgc gat aat gta ctg aac acc ctg
      Y   R   D   S   V   K   G   R   F   T   I   S   R   D   N   V   L   N   T   L
300 tac ctc cac atg gac att ctg cgc tct gag gac acg gcc act tat tac tgt aca aaa gtc
      Y   L   H   M   D   I   L   R   S   E   D   T   A   T   Y   Y   C   T   K   V
360 gga ttt acc acc ttc tat ttt gat tcc tgg ggc caa gga gtc atg gtc gca gtc tcc tca
      G   F   T   T   F   Y   F   D   S   W   G   Q   G   V   M   V   A   V   S   S
420 gct ggt gga ggc ggt tct ggt ggc gga ggt tct gga ggt ggc ggt tct gac atc cag atg
      A   G   G   G   G   S   G   G   G   G   S   G   G   G   G   S   D   I   Q   M
480 acc cag tct cct tca ttc ctg tct gca tct gtg gga gac cgc gta act atc aac tgc aaa
      T   Q   S   P   S   F   L   S   A   S   V   G   D   R   V   T   I   N   C   K
540 gca agt cag aat att aac aag tac ttg gac tgg tat cag caa aag ttt ggt gag act ccg
      A   S   Q   N   I   N   K   Y   L   D   W   Y   Q   Q   K   F   G   E   T   P
600 aaa ctc ctg atc tat aat att aac aat ttg cat tca gga gtc cca tca cgc ttc agt ggc
      K   L   L   I   Y   N   I   N   N   L   H   S   G   V   P   S   R   F   S   G
620 agt gga*tgt*ggt cct gat ttc aca ctt acc atc agc agc ctg cag cct gaa gat gtt gcc
      S   G   C   G   P   D   F   T   L   T   I   S   S   L   Q   P   E   D   V   A
680 aca tat ttc tgc ctt caa cat cgc act ggg tgg acg ttc ggt gga ggc acc aag gtg gaa
      T   Y   F   C   L   Q   H   R   T   G   W   T   F   G   G   G   T   K   V   E
740 ttg cgt cgc gct*tgt*taa
      L   R   R   A   C   -
```

ACKNOLEDGEMENTS

I want to thank everyone that was physically or mentally involved in the making of this thesis. I want to thank Johannes Huppa for giving me the opportunity to work on this fascinating project and for having an unerring eye to find not only the most enigmatic questions of immunology but also the most amazing crowd of scientists to work together to answer those with such dedication and joy. Thank you to all of the members of the lab and Lara <3 , that made my time at the Institute for Hygiene and Applied Immunology an unforgettable memory. I especially want to mention Fluorian, my supervisor, that managed the difficult task to guide my mind along the way of this project and Iago DP in which I found not only an exceptional scientific consultant but more importantly a friend that I do not want to miss in my life. Finally, I want to thank my parents for providing all the love and all the money and sci.hub for providing all the knowledge.

Authorship statement

I herewith declare that I am the author of this thesis and the presented work and that all experiments and analysis were done while in candidature for a master´s degree at the University of Vienna. Further I can confirm that all parts of this thesis that have previously been published are clearly attributed and the source of such or/and quotes of other publications are always stated. I have acknowledged all main sources of help.

Ethical compliance statement

All animal experimentation (related to breeding, sacrifice for T-cell isolation) was evaluated by the ethics committee of the Medical University of Vienna and approved by the Federal Ministry of Science, Research and Economy, BMWFW (BMWFW-66.009/0378-WF/V/3b/2016). Animal husbandry and experimentation were performed under national laws (Federal Ministry of Science, Research and Economy, Vienna, Austria) and the ethics committee of the Medical University of Vienna and according to the guidelines of the Federation of Laboratory Animal Science Associations (FELASA).

REFERENCES

1. Huppa, J. B. & Davis, M. M. The Interdisciplinary Science of T-cell Recognition. in *Advances in Immunology* vol. 119 1–50 (Elsevier, 2013).
2. Rossjohn, J. *et al.* T Cell Antigen Receptor Recognition of Antigen-Presenting Molecules. *Annu. Rev. Immunol.* **33**, 169–200 (2015).
3. Hayes, S. M. & Love, P. E. Distinct structure and signaling potential of the gamma delta TCR complex. *Immunity* **16**, 827–838 (2002).
4. Nielsen, M. M., Witherden, D. A. & Havran, W. L. γδ T cells in homeostasis and host defence of epithelial barrier tissues. *Nat. Rev. Immunol.* **17**, 733–745 (2017).
5. Birnbaum, M. E. *et al.* Molecular architecture of the αβ T cell receptor–CD3 complex. *Proc. Natl. Acad. Sci.* **111**, 17576–17581 (2014).
6. Rock, K. L., Reits, E. & Neefjes, J. Present Yourself! By MHC Class I and MHC Class II Molecules. *Trends Immunol.* **37**, 724–737 (2016).
7. Embgenbroich, M. & Burgdorf, S. Current Concepts of Antigen Cross-Presentation. *Front. Immunol.* **9**, 1643 (2018).
8. Jones, E. Y., Fugger, L., Strominger, J. L. & Siebold, C. MHC class II proteins and disease: a structural perspective. *Nat. Rev. Immunol.* **6**, 271–282 (2006).
9. Roche, P. A. & Furuta, K. The ins and outs of MHC class II-mediated antigen processing and presentation. *Nat. Rev. Immunol.* **15**, 203–216 (2015).
10. Hewitt, E. W. The MHC class I antigen presentation pathway: strategies for viral immune evasion. *Immunology* **110**, 163–169 (2003).
11. Skapenko, A., Leipe, J., Lipsky, P. E. & Schulze-Koops, H. The role of the T cell in autoimmune inflammation. *Arthritis Res. Ther.* **7**, S4 (2005).

12. Hirahara, K. & Nakayama, T. CD4 $^{+}$ T-cell subsets in inflammatory diseases: beyond the T $_{h}$ 1/T $_{h}$ 2 paradigm. *Int. Immunol.* **28**, 163–171 (2016).

13. Montoya, J. G. *et al.* Cytokine signature associated with disease severity in chronic fatigue syndrome patients. *Proc. Natl. Acad. Sci.* **114**, E7150–E7158 (2017).

14. Roep, B. O. The role of T-cells in the pathogenesis of Type 1 diabetes: From cause to cure. *Diabetologia* **46**, 305–321 (2003).

15. Shevach, E. M. Regulatory T Cells in Autoimmmunity. *Annu. Rev. Immunol.* **18**, 423–449 (2000).

16. Abbas, A. K., Lichtman, A. H., Pillai, S., Baker, D. L. & Baker, A. *Cellular and molecular immunology*. (Elsevier, 2018).

17. de Greef, P. C. *et al.* The naive T-cell receptor repertoire has an extremely broad distribution of clone sizes. *eLife* **9**, e49900 (2020).

18. Morris, G. P. & Allen, P. M. How the TCR balances sensitivity and specificity for the recognition of self and pathogens. *Nat. Immunol.* **13**, 121–128 (2012).

19. Vicente, R. *et al.* Molecular and cellular basis of T cell lineage commitment. *Semin. Immunol.* **22**, 270–275 (2010).

20. Brameshuber, M. *et al.* Monomeric TCRs drive T cell antigen recognition. *Nat. Immunol.* **19**, 487–496 (2018).

21. Wiest, D. L. & Carleton, M. Control of early thymocyte development by the pre-T cell receptor complex: A receptor without a ligand? *Semin. Immunol.* **11**, 251–262 (1999).

22. Starr, T. K., Jameson, S. C. & Hogquist, K. A. Positive And Negative Selection Of T Cells. *Annu. Rev. Immunol.* **21**, 139–176 (2003).

23. Klein, L., Kyewski, B., Allen, P. M. & Hogquist, K. A. Positive and negative selection of the T cell repertoire: what thymocytes see (and don't see). *Nat. Rev. Immunol.* **14**, 377–391 (2014).

24. Zerrahn, J., Held, W. & Raulet, D. H. The MHC Reactivity of the T Cell Repertoire Prior to Positive and Negative Selection. *Cell* **88**, 627–636 (1997).

25. Singer, A., Adoro, S. & Park, J.-H. Lineage fate and intense debate: myths, models and mechanisms of CD4- versus CD8-lineage choice. *Nat. Rev. Immunol.* **8**, 788–801 (2008).

26. Abramson, J., Giraud, M., Benoist, C. & Mathis, D. Aire's Partners in the Molecular Control of Immunological Tolerance. *Cell* **140**, 123–135 (2010).

27. Hsieh, C.-S. Selection of regulatory T cells in the thymus. 12 (2012).

28. Davey, G. M. *et al.* Preselection Thymocytes Are More Sensitive to T Cell Receptor Stimulation Than Mature T Cells. *J. Exp. Med.* **188**, 1867–1874 (1998).

29. Li, Q.-J. *et al.* miR-181a Is an Intrinsic Modulator of T Cell Sensitivity and Selection. *Cell* **129**, 147–161 (2007).

30. Gaud, G., Lesourne, R. & Love, P. E. Regulatory mechanisms in T cell receptor signalling. *Nat. Rev. Immunol.* **18**, 485–497 (2018).

31. Zhu, J., Yamane, H. & Paul, W. E. Differentiation of Effector CD4 T Cell Populations. *Annu. Rev. Immunol.* **28**, 445–489 (2010).

32. Davis, S. J. & van der Merwe, P. A. The kinetic-segregation model: TCR triggering and beyond. *Nat. Immunol.* **7**, 803–809 (2006).

33. Yokosuka, T. & Saito, T. The Immunological Synapse, TCR Microclusters, and T Cell Activation. in *Immunological Synapse* (eds. Saito, T. & Batista, F. D.) vol. 340 81–107 (Springer Berlin Heidelberg, 2010).

34. Huppa, J. B., Gleimer, M., Sumen, C. & Davis, M. M. Continuous T cell receptor signaling required for synapse maintenance and full effector potential. *Nat. Immunol.* **4**, 749–755 (2003).

35. Dustin, M. L., Chakraborty, A. K. & Shaw, A. S. Understanding the Structure and Function of the Immunological Synapse. *Cold Spring Harb. Perspect. Biol.* **2**, a002311–a002311 (2010).

36. Varma, R., Campi, G., Yokosuka, T., Saito, T. & Dustin, M. L. T Cell Receptor-Proximal Signals Are Sustained in Peripheral Microclusters and Terminated in the Central Supramolecular Activation Cluster. *Immunity* **25**, 117–127 (2006).

37. Martínez-Martín, N. *et al.* T Cell Receptor Internalization from the Immunological Synapse Is Mediated by TC21 and RhoG GTPase-Dependent Phagocytosis. *Immunity* **35**, 208–222 (2011).

38. Choudhuri, K. *et al.* Polarized release of T-cell-receptor-enriched microvesicles at the immunological synapse. *Nature* **507**, 118–123 (2014).

39. Chen, L. & Flies, D. B. Molecular mechanisms of T cell co-stimulation and co-inhibition. *Nat. Rev. Immunol.* **13**, 227–242 (2013).

40. Jönsson, P. *et al.* Remarkably low affinity of CD4/peptide-major histocompatibility complex class II protein interactions. *Proc. Natl. Acad. Sci.* **113**, 5682–5687 (2016).

41. Huppa, J. B. *et al.* TCR–peptide–MHC interactions in situ show accelerated kinetics and increased affinity. *Nature* **463**, 963–967 (2010).

42. Purbhoo, M. A., Irvine, D. J., Huppa, J. B. & Davis, M. M. T cell killing does not require the formation of a stable mature immunological synapse. *Nat. Immunol.* **5**, 524–530 (2004).

43. Davis, M. M. *et al.* Dynamics of Cell Surface Molecules During T Cell Recognition. *Annu. Rev. Biochem.* **72**, 717–742 (2003).

44. Isakov, N. Immunoreceptor tyrosine-based activation motif (ITAM), a unique module linking antigen and Fc receptors to their signaling cascades. *J. Leukoc. Biol.* **61**, 6–16 (1997).

45. Palacios, E. H. & Weiss, A. Function of the Src-family kinases, Lck and Fyn, in T-cell development and activation. *Oncogene* **23**, 7990–8000 (2004).

46. Love, P. E. & Hayes, S. M. ITAM-mediated Signaling by the T-Cell Antigen Receptor. *Cold Spring Harb. Perspect. Biol.* **2**, a002485–a002485 (2010).

47. Lo, W.-L. *et al.* Lck promotes Zap70-dependent LAT phosphorylation by bridging Zap70 to LAT. *Nat. Immunol.* **19**, 733–741 (2018).

48. Macian, F. NFAT proteins: key regulators of T-cell development and function. *Nat. Rev. Immunol.* **5**, 472–484 (2005).

49. Feske, S., Giltnane, J., Dolmetsch, R., Staudt, L. M. & Rao, A. Gene regulation mediated by calcium signals in T lymphocytes. *Nat. Immunol.* **2**, 316–324 (2001).

50. *The molecular probes handbook: a guide to fluorescent probes and labeling technologies*. (Life Technologies, 2010).

51. Call, M. E., Pyrdol, J., Wiedmann, M. & Wucherpfennig, K. W. The Organizing Principle in the Formation of the T Cell Receptor-CD3 Complex. *Cell* **111**, 967–979 (2002).

52. Dong, D. *et al.* Structural basis of assembly of the human TCR–CD3 complex. *Nature* (2019) doi:10.1038/s41586-019-1537-0.

53. Mallaun, M. *et al.* The T Cell Receptor's -Chain Connecting Peptide Motif Promotes Close Approximation of the CD8 Coreceptor Allowing Efficient Signal Initiation. *J. Immunol.* **180**, 8211–8221 (2008).

54. Sasada, T. *et al.* Involvement of the TCR Cβ FG Loop in Thymic Selection and T Cell Function. *J. Exp. Med.* **195**, 1419–1431 (2002).

55. Kim, S. T. *et al.* The αβ T Cell Receptor Is an Anisotropic Mechanosensor. *J. Biol. Chem.* **284**, 31028–31037 (2009).

56. Mazza, C. *et al.* How much can a T-cell antigen receptor adapt to structurally distinct antigenic peptides? *EMBO J.* **26**, 1972–1983 (2007).

57. Natarajan, A. *et al.* Structural Model of the Extracellular Assembly of the TCR-CD3 Complex. *Cell Rep.* **14**, 2833–2845 (2016).

58. Christopher Garcia, K., Adams, J. J., Feng, D. & Ely, L. K. The molecular basis of TCR germline bias for MHC is surprisingly simple. *Nat. Immunol.* **10**, 143–147 (2009).

59. Adams, J. J. *et al.* T Cell Receptor Signaling Is Limited by Docking Geometry to Peptide-Major Histocompatibility Complex. *Immunity* **35**, 681–693 (2011).

60. Kuhns, M. S. *et al.* Evidence for a functional sidedness to the αβTCR. 6 (2010).

61. Kuhns, M. S. & Davis, M. M. TCR Signaling Emerges from the Sum of Many Parts. *Front. Immunol.* **3**, (2012).

62. He, Y. *et al.* Identification of the Docking Site for CD3 on the T Cell Receptor β Chain by Solution NMR. *J. Biol. Chem.* **290**, 19796–19805 (2015).

63. Krshnan, L., Park, S., Im, W., Call, M. J. & Call, M. E. A conserved αβ transmembrane interface forms the core of a compact T-cell receptor–CD3 structure within the membrane. *Proc. Natl. Acad. Sci.* **113**, E6649–E6658 (2016).

64. Sun, Z.-Y. J., Kim, K. S., Wagner, G. & Reinherz, E. L. Mechanisms Contributing to T Cell Receptor Signaling and Assembly Revealed by the Solution Structure of an Ectodomain Fragment of the CD3□□ Heterodimer. 11 (2001).

65. Wucherpfennig, K. W., Gagnon, E., Call, M. J., Huseby, E. S. & Call, M. E. Structural Biology of the T-cell Receptor: Insights into Receptor Assembly, Ligand Recognition, and Initiation of Signaling. *Cold Spring Harb. Perspect. Biol.* **2**, a005140–a005140 (2010).

66. Ghendler, Y., Smolyar, A., Chang, H.-C. & Reinherz, E. L. One of the CD3□ Subunits within a T Cell Receptor Complex Lies in Close Proximity to the C□ FG Loop. 8 (1998).

67. Kuhns, M. S. & Davis, M. M. Disruption of Extracellular Interactions Impairs T Cell Receptor-CD3 Complex Stability and Signaling. *Immunity* **26**, 357–369 (2007).

68. Kjer-Nielsen, L. *et al.* The 1.5 Å Crystal Structure of a Highly Selected Antiviral T Cell Receptor Provides Evidence for a Structural Basis of Immunodominance. *Structure* **10**, 1521–1532 (2002).

69. Beddoe, T. *et al.* Antigen Ligation Triggers a Conformational Change within the Constant Domain of the αβ T Cell Receptor. *Immunity* **30**, 777–788 (2009).

70. Lee, M. S. *et al.* A Mechanical Switch Couples T Cell Receptor Triggering to the Cytoplasmic Juxtamembrane Regions of CD3ζζ. *Immunity* **43**, 227–239 (2015).

71. Brazin, K. N. *et al.* The T Cell Antigen Receptor α Transmembrane Domain Coordinates Triggering through Regulation of Bilayer Immersion and CD3 Subunit Associations. *Immunity* **49**, 829-841.e6 (2018).

72. Xu, C. *et al.* Regulation of T Cell Receptor Activation by Dynamic Membrane Binding of the CD3ε Cytoplasmic Tyrosine-Based Motif. *Cell* **135**, 702–713 (2008).

73. Zhang, H., Cordoba, S.-P. & Dushek, O. Basic residues in the T-cell receptor ζ cytoplasmic domain mediate membrane association and modulate signaling. 6.

74. Kim, S. T. *et al.* Distinctive CD3 Heterodimeric Ectodomain Topologies Maximize Antigen-Triggered Activation of T Cell Receptors. *J. Immunol.* **185**, 2951–2959 (2010).

75. Das, D. K. *et al.* Force-dependent transition in the T-cell receptor β-subunit allosterically regulates peptide discrimination and pMHC bond lifetime. *Proc. Natl. Acad. Sci.* **112**, 1517–1522 (2015).

76. Touma, M. *et al.* The TCR C FG Loop Regulates T Cell Development. *J. Immunol.* **176**, 6812–6823 (2006).

77. Gil, D., Schamel, W. W. A. & Montoya, M. Recruitment of Nck by CD3 Reveals a Ligand- Induced Conformational Change Essential for T Cell Receptor Signaling and Synapse Formation. 12 (2002).

78. Borroto, A. *et al.* Relevance of Nck-CD3 Interaction for T Cell Activation In Vivo. *J. Immunol.* **192**, 2042–2053 (2014).

79. Mingueneau, M. *et al.* The proline-rich sequence of CD3epsilon controls T cell antigen receptor expression on and signaling potency in preselection CD4+CD8+ thymocytes. *Nat. Immunol.* **9**, 522–532 (2008).

80. Risueno, R. M. Ligand-induced conformational change in the T-cell receptor associated with productive immune synapses. *Blood* **106**, 601–608 (2005).

81. Minguet, S., Swamy, M., Alarcón, B., Luescher, I. F. & Schamel, W. W. A. Full Activation of the T Cell Receptor Requires Both Clustering and Conformational Changes at CD3. *Immunity* **26**, 43–54 (2007).

82. Liu, B., Chen, W., Evavold, B. D. & Zhu, C. Accumulation of Dynamic Catch Bonds between TCR and Agonist Peptide-MHC Triggers T Cell Signaling. *Cell* **157**, 357–368 (2014).

83. Hong, J. *et al.* Force-Regulated In Situ TCR–Peptide-Bound MHC Class II Kinetics Determine Functions of CD4 $^{+}$ T Cells. *J. Immunol.* **195**, 3557–3564 (2015).

84. Hertig, S. & Vogel, V. Catch bonds. *Curr. Biol.* **22**, R823–R825 (2012).

85. Schamel, W. W. A. *et al.* Coexistence of multivalent and monovalent TCRs explains high sensitivity and wide range of response. *J. Exp. Med.* **202**, 493–503 (2005).

86. Kumar, R. *et al.* Increased Sensitivity of Antigen-Experienced T Cells through the Enrichment of Oligomeric T Cell Receptor Complexes. *Immunity* **35**, 375–387 (2011).

87. Yokosuka, T. & Saito, T. Dynamic regulation of T-cell costimulation through TCR-CD28 microclusters. *Immunol. Rev.* **229**, 27–40 (2009).

88. Lillemeier, B. F. *et al.* TCR and Lat are expressed on separate protein islands on T cell membranes and concatenate during activation. *Nat. Immunol.* **11**, 90–96 (2010).

89. Martínez-Martín, N. *et al.* Cooperativity Between T Cell Receptor Complexes Revealed by Conformational Mutants of CD3e. 13 (2009).

90. Martin-Blanco, N. *et al.* A window of opportunity for cooperativity in the T Cell Receptor. *Nat. Commun.* **9**, 2618 (2018).

91. Lin, J. J. Y. *et al.* Mapping the stochastic sequence of individual ligand-receptor binding events to cellular activation: T cells act on the rare events. *Sci. Signal.* **12**, eaat8715 (2019).

92. Axmann, M., Huppa, J. B., Davis, M. M. & Schütz, G. J. Determination of Interaction Kinetics between the T Cell Receptor and Peptide-Loaded MHC Class II via Single-Molecule Diffusion Measurements. *Biophys. J.* **103**, L17–L19 (2012).

93. Sibener, L. V. *et al.* Isolation of a Structural Mechanism for Uncoupling T Cell Receptor Signaling from Peptide-MHC Binding. *Cell* **174**, 672-687.e27 (2018).

94. Valitutti, S. The Serial Engagement Model 17 Years After: From TCR Triggering to Immunotherapy. *Front. Immunol.* **3**, (2012).

95. Silfies, J., Schwartz, S. & Davidson, M. MicroscopyU- The source for microscopy Education, Title: Nikons MicroscopyU, 2019 Nikon Instruments Inc.; (2019).

96. Ambrose, E. J. A Surface Contact Microscope for the study of Cell Movements. *Nature* **178**, 1194–1194 (1956).

97. Mattheyses, A. L., Simon, S. M. & Rappoport, J. Z. Imaging with total internal reflection fluorescence microscopy for the cell biologist. *J. Cell Sci.* **123**, 3621–3628 (2010).

98. Axelrod, D. Total Internal Reflection Fluorescence Microscopy in Cell Biology. 11 (2001).

99. Heintzmann, R. A Appendix: Practical Guide to Optical Alignment. in *Fluorescence Microscopy* (ed. Kubitscheck, U.) 393–401 (Wiley-VCH Verlag GmbH & Co. KGaA, 2013). doi:10.1002/9783527671595.app1.

100. *Fluorescence microscopy: from principles to biological applications*. (Wiley-VCH, 2017).

101. Burghardt, T. P. Measuring incidence angle for through-the-objective total internal reflection fluorescence microscopy. *J. Biomed. Opt.* **17**, 126007 (2012).

102. Patterson, G., Davidson, M., Manley, S. & Lippincott-Schwartz, J. Superresolution Imaging using Single-Molecule Localization. *Annu. Rev. Phys. Chem.* **61**, 345–367 (2010).

103. Biteen, J. S. & Moerner, W. E. Single-Molecule and Superresolution Imaging in Live Bacteria Cells. *Cold Spring Harb. Perspect. Biol.* **2**, a000448–a000448 (2010).

104. Thorley, J. A., Pike, J. & Rappoport, J. Z. Super-resolution Microscopy. in *Fluorescence Microscopy* 199–212 (Elsevier, 2014). doi:10.1016/B978-0-12-409513-7.00014-2.

105. Bajar, B., Wang, E., Zhang, S., Lin, M. & Chu, J. A Guide to Fluorescent Protein FRET Pairs. *Sensors* **16**, 1488 (2016).

106. Zeug, A., Woehler, A., Neher, E. & Ponimaskin, E. G. Quantitative Intensity-Based FRET Approaches—A Comparative Snapshot. *Biophys. J.* **103**, 1821–1827 (2012).

107. Kubo, R. & Born, W. Characterization of a monoclonal antibody which detects all murine alpha beta T cell receptors. *J Immunol* **142**, 2736–42 (1989).

108. GrFgoire, C. *et al.* Engineered secreted T-cell receptor a4i heterodimers. *Proc Natl Acad Sci USA* 5 (1991).

109. Wang, J. -h. Atomic structure of an alpha beta T cell receptor (TCR) heterodimer in complex with an anti-TCR Fab fragment derived from a mitogenic antibody. *EMBO J.* **17**, 10–26 (1998).

110. Rossi, N. E. *et al.* Differential antibody binding to the surface TCR{middle dot}CD3 complex of CD4+ and CD8+ T lymphocytes is conserved in mammals and associated with differential glycosylation. *Int. Immunol.* **20**, 1247–1258 (2008).

111. Pullen, A. M., Marrack, P. & Kappler, J. W. The T-cell repertoire is heavily influenced by tolerance to polymorphic self-antigens. *Nature* **335**, 796–801 (1988).

112. Kim, S. T. *et al.* The αβ T Cell Receptor Is an Anisotropic Mechanosensor. *J. Biol. Chem.* **284**, 31028–31037 (2009).

113. Pinto, F. L. & Lindblad, P. A guide for in-house design of template-switch-based 5′ rapid amplification of cDNA ends systems. *Anal. Biochem.* **397**, 227–232 (2010).

114. Matz, M. Amplification of cDNA ends based on template-switching effect and step- out PCR. *Nucleic Acids Res.* **27**, 1558–1560 (1999).

115. Bower, N. I. & Johnston, I. A. Targeted rapid amplification of cDNA ends (T-RACE)--an improved RACE reaction through degradation of non-target sequences. *Nucleic Acids Res.* **38**, e194–e194 (2010).

116. Yamaguchi, H. & Miyazaki, M. Refolding Techniques for Recovering Biologically Active Recombinant Proteins from Inclusion Bodies. *Biomolecules* **4**, 235–251 (2014).

117. Tsumoto, K. *et al.* Role of Arginine in Protein Refolding, Solubilization, and Purification. *Biotechnol. Prog.* **20**, 1301–1308 (2004).

118. Chen, J., Liu, Y., Wang, Y., Ding, H. & Su, Z. Different effects of L-arginine on protein refolding: Suppressing aggregates of hydrophobic interaction, not covalent binding. *Biotechnol. Prog.* **24**, 1365–1372 (2008).

119. Gery, Ph.D. Nolan. https://web.stanford.edu. (2019).

120. Savarino, A., Boelaert, J. R., Cassone, A., Majori, G. & Cauda, R. Effects of chloroquine on viral infections: an old drug against today's diseases. *Lancet Infect. Dis.* **3**, 722–727 (2003).

121. Guo, L. *et al.* Optimizing conditions for calcium phosphate mediated transient transfection. *Saudi J. Biol. Sci.* **24**, 622–629 (2017).

122. Bundesamt für Verbraucherschutz und Lebensmittelsicherheit. Allgemeine Stellungnahme der ZKBS zu häufig durchgeführten gentechnischen Arbeiten mit den zugrunde liegenden Kriterien der Vergleichbarkeit: Gentransfer mit Hilfe retroviraler Vektoren; www.bvl.bund.de. (2011).

123. Seder, R. A., Paul, W. E., Davis, M. M. & Fazekas de St Groth, B. The presence of interleukin 4 during in vitro priming determines the lymphokine-producing potential of CD4+ T cells from T cell receptor transgenic mice. *J. Exp. Med.* **176**, 1091–1098 (1992).

124. Grakoui, A. The Immunological Synapse: A Molecular Machine Controlling T Cell Activation. *Science* **285**, 221–227 (1999).

125. *The immune synapse: methods and protocols*. (Humana Press, 2017).

126. Kuhns, M. S., Davis, M. M. & Garcia, K. C. Deconstructing the Form and Function of the TCR/CD3 Complex. *Immunity* **24**, 133–139 (2006).

127. Ahmad, Z. A. *et al.* scFv Antibody: Principles and Clinical Application. *Clin. Dev. Immunol.* **2012**, 1–15 (2012).

128. Wolber, P. K. & Hudson, B. S. An analytic solution to the Förster energy transfer problem in two dimensions. *Biophys. J.* **28**, 197–210 (1979).

129. Chattopadhyay, A. Taking Care of Bystander FRET in a Crowded Cell Membrane Environment. *Biophys. J.* **106**, 1227–1228 (2014).

130. King, C., Sarabipour, S., Byrne, P., Leahy, D. J. & Hristova, K. The FRET Signatures of Noninteracting Proteins in Membranes: Simulations and Experiments. *Biophys. J.* **106**, 1309–1317 (2014).

131. Brameshuber, M. & Schütz, G. J. Detection and Quantification of Biomolecular Association in Living Cells using Single-Molecule Microscopy. in *Methods in Enzymology* vol. 505 159–186 (Elsevier, 2012).

132. Klein, L. Imaging Initial Events in T-cell Activation: Ligand Binding and Signaling. 171.

133. Willcox, B. E. & Willcox, C. R. γδ TCR ligands: the quest to solve a 500-million-year-old mystery. *Nat. Immunol.* **20**, 121–128 (2019).

134. Hayes, S. M. & Love, P. E. Distinct Structure and Signaling Potential of the □□TCR Complex. 12.

135. McKeithan, T. W. Kinetic proofreading in T-cell receptor signal transduction. *Proc. Natl. Acad. Sci.* **92**, 5042–5046 (1995).

136. Coombs, D. & Goldstein, B. T cell activation: Kinetic proofreading, serial engagement and cell adhesion. *J. Comput. Appl. Math.* **184**, 121–139 (2005).

137. Lee, M. S. *et al.* A Mechanical Switch Couples T Cell Receptor Triggering to the Cytoplasmic Juxtamembrane Regions of CD3ζζ. *Immunity* **43**, 227–239 (2015).

138. Husson, J., Chemin, K., Bohineust, A., Hivroz, C. & Henry, N. Force Generation upon T Cell Receptor Engagement. *PLoS ONE* **6**, e19680 (2011).

139. Kjer-Nielsen, L. *et al.* Crystal structure of the human T cell receptor CD3 heterodimer complexed to the therapeutic mAb OKT3. *Proc. Natl. Acad. Sci.* **101**, 7675–7680 (2004).

140. Minguet, S. & Schamel, W. W. A. Permissive Geometry Model. in *Multichain Immune Recognition Receptor Signaling* (ed. Sigalov, A. B.) vol. 640 113–120 (Springer New York, 2008).

141. Davis, M. M. A New Trigger for T Cells. *Cell* **110**, 285–287 (2002).